

**UCSF**

**UC San Francisco Electronic Theses and Dissertations**

**Title**

Discovery and development of dual PI3Kdelta/gamma inhibitors for use as novel anti-inflammatory agents

**Permalink**

<https://escholarship.org/uc/item/0vr1d8sv>

**Author**

Williams, Olusegun

**Publication Date**

2011

Peer reviewed|Thesis/dissertation

**Discovery and development of dual PI3K $\delta/\gamma$  inhibitors for use as  
novel anti-inflammatory agents.**

by

**Olusegun Williams**

DISSERTATION

Submitted in partial satisfaction of the requirements for the degree of

DOCTOR OF PHILOSOPHY

in

Chemistry and Chemical Biology

in the

GRADUATE DIVISION

of the

UNIVERSITY OF CALIFORNIA, SAN FRANCISCO

Copyright 2011  
by  
Olusegun Williams

## **DEDICATION**

I would like to dedicate my thesis to all of my immediate and extended family members with advanced degrees who have helped me pursue my Ph.D. and spurred me on to pursue excellence; and to my wife whose constant encouragement and support brightened my last few years of graduate school. Thank You.

## ACKNOWLEDGMENTS

Science is no longer a lone effort, and I would like to thank all the people who have had an impact on my scientific career. This includes scientists at Johnson & Johnson and Merck, where I interned and Dr. Veronika A. Szalai my undergraduate research mentor at University of Maryland Baltimore County. I would also like to thank Valerie Ohman for all of her hard work and lab administration duties, and the past and present members of Dr. Kevan M. Shokat's lab who I overlapped with for general scientific discussion and help.

Chapters 2 and 3 of this thesis contain material previously published as *Discovery of dual inhibitors of the immune cell PI3Ks p110delta and p110gamma: a prototype for new anti-inflammatory drugs*. Chem Biol, 2010. **17**(2): p. 123-34.

Specifically for the work outlined in this thesis, I would like to thank my mentor Dr. Kevan M. Shokat and Dr. Zachary A. Knight who helped start this project. I would also like to thank:

Dr. Benjamin T. Houseman who helped me with the THP-1 experiments, and conducted the neutrophils experiments was a key mover in the initial sepsis experiments.

Dr. Eric J. Kunkel, formerly of BioSeek who conducted the BioMAP experiments.

Dr. Paul Wolters and Dr. Eric Seeley, for their help conducting the mouse sepsis studies. The scientists at Invitrogen (Dr. Randy Hoffman, Dr. Brian Aizenstein, & Dr. Kurt Vogel) who performed the kinase screening with SW18, DL01, DL06, and DL07.

Dr. Alex Berndt and Dr. Roger Williams for the work they did in solving the PI3K $\delta$  crystal structure and their structural insights.

Daniel D. Le, for the initial synthesis of many of the members of the DL series and for whom the DL series of molecules is named.

Gregory Ducker for assaying DL07's ability to kill cancer cell lines.

Dr. Ernesto Diaz-Flores for his help with the western blots in mouse bone marrow macrophages, and for culturing the macrophages.

Dr. Yi Liu and Dr. Christian Rommel of Intellikine for useful discussion, ideas and comments on my work and manuscripts.

I would also like to thank my thesis committee, Dr. Arthur Weiss, Dr. James W. Wells, Dr. Brian K. Shoichet and Dr. Kevan M. Shokat, for their encouragement and scientific guidance throughout the course of my graduate work.

For funding I would like to thank the National Science Foundation Predoctoral Fellowship, the UCBREP GREAT training grant and the UNCF/Merck Graduate Dissertation Fellowship, and for encouragement and support, I would like to thank my parents, my sister and my lastly, but by no means least, my wife.

## ABSTRACT

PI3K $\delta$  and PI3K $\gamma$  regulate immune cell signaling, while the related PI3K $\alpha$  and PI3K $\beta$  regulate cell survival and metabolism. Selective dual inhibitors of PI3K $\delta$  and PI3K $\gamma$  represent a potential class of anti-inflammatory agents lacking the anti-proliferative effects associated with PI3K $\alpha$  and PI3K $\beta$  inhibition. Here we outline the discovery and synthesis of PI3K $\delta$  and PI3K $\delta/\gamma$  dual inhibitors that display up to 1,000-fold selectivity over PI3K $\alpha$  and PI3K $\beta$ . We explain the criteria for selectivity for PI3K $\delta$  and PI3K $\gamma$  and evaluate the selective compounds in a high-content inflammation assay using mixtures of primary human cells. We find selective inhibition of only PI3K $\delta$  is weakly anti-inflammatory, but PI3K $\delta/\gamma$  inhibitors show superior inflammatory marker suppression through suppression of LPS-induced TNF $\alpha$  production and T cell activation. Moreover, PI3K $\delta/\gamma$  inhibition yields an anti-inflammatory signature distinct from pan-PI3K inhibition and known anti-inflammatory drugs, yet bears striking similarities to glucocorticoid receptor agonists. These results highlight the potential of selectively designing drugs that target kinases with shared biological function. We also outline the discovery and synthesis of a new set of PI3K inhibitors in which a small change in structure yields an extremely promiscuous molecule in contrast to the much more selective members of the set. We explain the principles behind the extreme selectivity achieved with the PI3K $\delta/\gamma$  and PI3K $\delta$  inhibitors and hypothesize what led to the extreme promiscuity displayed by one molecule.

# TABLE OF CONTENTS

CHAPTER	TITLE	PAGE
	List of Tables.....	vi
	List of Figures.....	vii
<b>1</b>	<b>Introduction.....</b>	<b>1</b>
	Shortcomings of genetic disruption.....	1
	When genetic knockouts and pharmacological knockdown disagree.....	4
<b>2</b>	<b>Design, Rationale, Synthesis, and Biochemical Characterization of PI3K<math>\delta</math>/<math>\gamma</math> dual inhibitors.....</b>	<b>10</b>
	Rationale for differential effects on PI3K $\gamma$ and PI3K $\delta$ .....	31
	Stereochemical evidence for a distinct conserved binding mode.....	32
	Varying Flexibility in Met804 region between PI3K isoforms.....	35
	Comparison of tolyl quinazolinone series to common PI3K scaffolds.....	38
	Insights from the crystal structure.....	40
<b>3</b>	<b>Cellular Characterization of Selected PI3K<math>\delta</math>/<math>\gamma</math> dual inhibitors.....</b>	<b>42</b>
	Cellular $\gamma$ / $\delta$ ratios of selected compounds.....	46
	Effects of pan-PI3K inhibition.....	51
	Comparison of Selective PI3K $\delta$ and Selective PI3K $\delta$ /PI3K $\gamma$ inhibition...	52
	Biological Activity of PI3K Inhibitors Relative to Other Agents.....	54
	Identifying roles for PI3K $\delta$ and PI3K $\gamma$ .....	57
	Using PI3K $\delta$ / $\gamma$ inhibitors to elucidate fine points of PI3K signaling.....	67
<b>4</b>	<b>The Design, Rationale, Synthesis, Biochemical, and Cellular Characterization of a new series of PI3K inhibitors.....</b>	<b>71</b>
	Testing the DL series outside the PI3K family.....	78
	Insights from the crystal structure of DL06 and DL07 with PI3K $\delta$ .....	81
	Application of DL07 toward an AML disease model.....	84
	Investigating the unusual promiscuity of DL07.....	88
	Lessons from the DL series.....	93
<b>5</b>	<b>Summary, Future Work and Clinical Implications.....</b>	<b>95</b>
	Further investigation with the SW series.....	95
	Further investigation with the DL series.....	98
	Using PI3K $\delta$ and PI3K $\delta$ / $\gamma$ inhibitors in the clinic.....	100
	Using PI3K $\delta$ , PI3K $\delta$ / $\gamma$ and PI3K $\gamma$ inhibitors to treat cancer.....	106
	Drawbacks to the use of PI3K $\delta$ and PI3K $\delta$ / $\gamma$ inhibitors.....	110
	Conclusion.....	113
	<b>References.....</b>	<b>115</b>
	<b>Appendix.....</b>	<b>126</b>
	Invitrogen Kinase Profiling Data (SW18).....	126
	Invitrogen Kinase Profiling Data (DL01).....	132
	Invitrogen Kinase Profiling Data (DL06).....	139
	Invitrogen Kinase Profiling Data (DL07).....	145
	BioMAP Profiles of PI3K Inhibitors.....	151
	Synthetic Data and Characterization.....	156

## LIST OF TABLES

Table 2.1 Structures and Biochemical IC <sub>50</sub> s for Series 1, tested at 10μM ATP.....	28
Table 2.2 Structures and Biochemical IC <sub>50</sub> s for Series 2, tested at 10μM ATP.....	29
Table 4.1 Structures and Biochemical IC <sub>50</sub> s for DL Series against Class I PI3Ks.....	75
Table 4.2 Structures and Biochemical IC <sub>50</sub> s for DL Series against other kinases.....	80



## LIST OF FIGURES

Figure 2.1 Met 804 “down” conformation precludes ATP binding.....	14
Figure 2.2 Basis of selectivity and potency for aryl quinazolinones.....	15
Figure 2.3 ATP-Binding site Sequence Identity among human Class I PI3-Ks.....	19
Figure 2.4 Diversification of Toly Quinazolinone Series.....	22
Synthetic Schemes.....	23
Figure 2.5 Model for PI3K $\delta$ selectivity of SW series 2.....	34
Figure 2.6 Comparison of SW series to other PI3K inhibitors.....	36
Figure 3.1 Effect of selected compounds on THP-1 monocyte signaling.....	45
Figure 3.2 Effect of selected compounds on neutrophil adhesion, migration and endothelial cell proliferation.....	50
Figure 3.3 BioMAP Analysis of PI3K Inhibitors.....	55
Figure 3.4 BioMAP Analysis of SW14, SW18, and Prednisolone.....	56
Figure 3.5 Function Similarity Map of PI3K inhibitors and other compounds.....	60
Figure 3.6 Function Similarity Map of PI3K pathway inhibitors.....	61
Figure 4.1 Pyrazolopyrimidines as multifaceted kinase inhibitors.....	73
Scheme 4.1 Alkynyl-substituted isopropyl & cyclopentyl pyrazolopyrimidines.....	74
Figure 4.2 Size of R1 substituent on pyrazolopyrimidines correlates with PI3K IC <sub>50</sub> s.....	79
Figure 4.3 Crystal Structure of DL06 and DL07 with PI3K $\delta$ .....	83
Figure 4.4 Effect of selected compounds on ERK phosphorylation in macrophages.....	86
Figure 4.5 Kinome inhibition of DL06 and DL07.....	87
Figure 4.6 DL07 does not potently inhibit cell proliferation.....	92

## Chapter 1 – Introduction

### *Shortcomings of genetic disruption*

The central dogma in biochemistry for many years was that one gene led to the production of one protein. Complexities aside, this paradigm led to the molecular biology revolution, and played an integral role in the birth of the fields of gene therapy, and was instrumental in the development of knockout mice. Genetic disruption is based on the premise that the appropriate disruption of a gene will lead to ablation of the protein produced by the disrupted gene. Then the key question is in what ways the disrupted gene and subsequent loss of protein will affect the organism. The values of the conclusions that can be drawn from the answer to this question depend on the areas that are analyzed. For example, it is quite difficult and can require biological acrobatics to assess the role of a protein in an adult organism, when loss of the corresponding gene results in embryonic lethality. Additionally, proteins can play different roles in development and in the adult animal; and, separating the effects of the two roles can be quite challenging.

Nevertheless, genetic disruption (in particular knockout mouse models) is an extremely valuable tool in biology, and when used properly can be a powerful tool in target validation and drug discovery. Still, due to the nature of the technique it fails to capture some of the special complexities that arise when considering protein targets for small molecule antagonist/agonist discovery. Of greatest significance are the problems of time scale, developmental compensation, and that of dual catalytic and non-catalytic roles of the protein target.

Standard knockout mice live without the disrupted gene for their entire life, which presents several problems. Firstly, a gene essential to development cannot be properly studied because it would lead to death of the organism. This problem has been partially solved with the advent of conditional knockouts with the Cre-Lox system, which allows for gene knockout in adult animals and in specific tissues<sup>1-2</sup>. Secondly, there is the problem of time in relation to drug discovery. In general, drugs work on a time scale of minutes to hours, and depending on the disorder, could be used in single dose treatments or for years. Since in knockout mice, protein activity is generally ablated since conception, a knockout mouse could very well represent a lifetime (from conception onward) of a high-dose of a drug, however in reality very few drugs are dosed in such a manner. In addition, because the targeted protein is absent during development, the organism can often compensate for its loss, often showing a less severe phenotype, or in some cases no phenotype at all<sup>3</sup>. These problems are further confounded when the protein target exists as a series of isoforms, which can compensate for each other despite the varying roles each isoform plays<sup>3-4</sup>.

One of the more subtle dangers of relying too heavily on knockout mouse data is based on the assumption that the protein target only plays one role in the body, and the knockout phenotype faithfully mimics a drug-treated state. Several proteins play both scaffolding and catalytic roles in the body. While most small molecule agonists would be predicted to only affect the catalytic activity and not to interfere with the expression of the target protein, in the knockout, as a result of complete protein ablation, any phenotypic effects could reflect a combination of the catalytic, scaffolding, or any other roles of the target protein. Generally, scaffolding effects are not disrupted by small

molecules, though specific interactions are more likely to be inhibited by antibody drugs, allosteric drugs, or drugs that inhibit protein-protein interactions. Additionally, the knockout phenotype could easily be due to the compounding effects of a lifetime without the protein, or to the alternative roles the target protein plays in development, roles that may no longer be relevant in the fully developed adult.

Ultimately, as our society seeks to improve healthcare by providing better drugs for more diseases, we need to ask if genetic disruption in mice or other species is truly translatable to human disease, or if there are other complementary ways to validate drug targets. While a good start to validating drug targets, genetic disruption does not always provide an accurate or complete picture, and the appropriate precautions must be taken when analyzing knockout data and drawing conclusions.

Several steps have been taken to address the shortcomings of standard genetic knockout studies. Conditional knockouts, which allow for knocking a gene out in a tissue specific manner or in response to an inducer like tetracycline, are one method of compensating for deficits in standard genetic methods<sup>5-6</sup>. Also, knock-ins, which involve substituting the targeted gene with a different version with higher or lower activity, and RNA interference are capable of better predicting the effects of a drug selective to the relevant protein target<sup>5-6</sup>. Still, all methods can present significant disadvantages, and it is paramount to remember that while mice and humans do share extensive genetic similarity, a mouse is not a human, and there are scores of documented cases in which mouse and human genetics differ.

Recently, pharmacological intervention, in the form of relatively drug-like small molecules, has been used as a tool to study protein function and as a drug target

validation aid. Small molecules work quickly and reversibly, and can generally be applied across various organisms. Although they do not possess the perfect specificity of some genetic tools, as small molecules, they bear a closer resemblance to actual drugs. Additionally, their use is not only limited to interfering with the catalytic activity of enzymes or blocking receptor function either, now there are small molecules being developed that inhibit specific protein-protein interactions.

Drug target validation is always complex, but it is more straightforward when both the genetic knockout and pharmacological knockdown phenotypes agree. For the past several years, genetic methods have been the gold standard for drug target validation, and the resultant phenotypes were considered the most significant, with any differences between genetic and pharmacological perturbations assumed to be due to pharmacological promiscuity. However, recent evidence suggests that genetic knockouts may not always fully represent the effect of a drug, and when there are differences between pharmacological knockdown and genetic knockouts, it may be due to the inadequacy of the genetic knockout<sup>3</sup>.

#### *When genetic knockouts and pharmacological knockdown disagree*

The differences between small molecule and genetic perturbation of protein function are of special interest generally within drug discovery, and specifically within protein and lipid kinase drug discovery and target validation. In 2007, Knight and Shokat analyzed the differences between small molecule kinase inhibition and their corresponding knockout models. The majority of the phenotypic discrepancies could be

explained by allosteric drug binding, cellular compensation, or disrupted protein complexes<sup>3</sup>.

The case of the kinase Ire1 provides an interesting example of a genetic vs. pharmacological phenotypic discrepancy explained by allosteric binding. Ire1, an endoplasmic reticulum transmembrane kinase, controls the unfolded protein response. When it is knocked out, the unfolded protein response is blocked<sup>7</sup>. Ire1 also contains an RNase domain that is activated when unfolded proteins induce dimerization of Ire1, thereby activating the kinase domains which subsequently activate the RNase domains, triggering the unfolded protein response<sup>8</sup>. Since Ire1 is an active kinase, it was originally thought that the kinase activity of Ire1 led to the activation of the RNase domains and the unfolded protein response<sup>9-10</sup>. This model was initially supported by the genetic disruption of Ire1 and the Ire1 kinase domains. However, a specifically engineered ATP-competitive inhibitor of Ire1 didn't block the unfolded protein response<sup>3, 11</sup>. Although Ire1 has an active kinase domain, its catalytic kinase activity is irrelevant to its function; instead, its ability to dimerize and subsequently induce the unfolded protein response is controlled by occupation of the ATP-binding site, and the 'substrate' ATP can be replaced by an 'inhibitor' that, despite inhibiting the unnecessary kinase activity, activates dimerization thereby preserving the unfolded protein response, and acting as an allosteric drug activator<sup>3, 11</sup>. In this case, genetic disruption of Ire1 yielded an incomplete picture of its true mechanism of action which was only revealed with the use of pharmacological intervention.

Genetically disrupted cells can also compensate for the lack of the disrupted protein, confounding the results of many experiments, and leading to phenotypic

discrepancies. A recent example of this involves the roles of c-Jun N-terminal Kinases (JNKs) 1 and 2. JNKs are kinases that phosphorylate the c-Jun transcription factor on its N-terminus, activating it and ultimately leading to increased cellular proliferation<sup>12</sup>. JNK1 and JNK2 are expressed in all cells, and when either is knocked out, there is no significant change in phenotype<sup>3</sup>. Embryonic fibroblasts from JNK1 knockout mice display markedly lower levels of c-Jun phosphorylation and slightly decreased proliferation, while MEFs from JNK2 knockouts show slightly increased proliferation and exhibit normal levels of c-Jun phosphorylation<sup>4</sup>. These data led to the conclusion that JNK1 was a positive regulator of c-Jun while JNK2 was a negative regulator. This conclusion was not completely satisfying since JNK2 was shown to activate c-Jun in vitro<sup>12</sup>. When JNK2 activity was specifically blocked using small molecules, a different picture emerged. Pharmacological disruption of JNK2 activity, using the chemical genetic approach pioneered by Shokat and colleagues, blocked cellular proliferation and c-Jun phosphorylation, an effect exactly opposite that of the JNK2 knockout<sup>4</sup>. Further investigation showed that in the JNK2 knockouts, JNK1 activity was increased as a means to compensate for the lack of JNK activity<sup>4</sup>. It was this increase in the activity of JNK1 in the JNK2 knockouts which led to the slightly increased proliferation and normal levels of c-Jun phosphorylation.

Genetic disruption can also lead to disrupted protein complexes which are generally not present with pharmacological interference. These disrupted protein complexes, examples of which are seen in the phosphoinositide-3-kinase (PI3K) family, often lead to divergent phenotypes which also highlight the differences between small molecule and genetic perturbation. The first example involves the ubiquitously expressed

PI3K p110 $\alpha$  that transduces growth-factor signals. The p110 $\alpha$  knockout was embryonic lethal<sup>13</sup>, but the heterozygote deletion displayed a relatively normal phenotype<sup>14</sup>. Knocking out the p85 subunit of PI3K $\alpha$ , the binding partner and putative activator of p110 $\alpha$  caused an increase in insulin signaling<sup>15</sup>, yet inhibition of p110 $\alpha$  with selective inhibitors displayed the opposite phenotype of decreased insulin signaling<sup>16</sup>. Closer study revealed that p85 expression was decreased, compensating for the decreased p110 $\alpha$  present in the heterozygote. The ability of the regulatory p85 subunit to negatively regulate p110 $\alpha$  activity, led to increased unbound p110 $\alpha$  activity which increased insulin signaling<sup>14</sup>.

In the case of the PI3K p110 $\gamma$  initial knockout studies suggested p110 $\gamma$  was responsible for many immune functions leading to inflammation<sup>17-18</sup>. This evidence led to the closer scrutiny and further analysis of p110 $\gamma$  as an anti-inflammatory drug target. Subsequent investigation showed that p110 $\gamma$  knockouts displayed increased cardiac contractility, and were more likely to suffer from heart damage<sup>19</sup>, temporarily decreasing interest in p110 $\gamma$  as a drug target. If p110 $\gamma$  inhibitors mimicked the knockout phenotype and caused myocardial damage, their utility as anti-inflammatories would be severely compromised. The p110 $\gamma$ -myocardial damage link was further complicated by a study showing that overexpression of a catalytically inactive form of p110 $\gamma$  protected mice from heart damage<sup>20</sup>. To resolve this dilemma, Patrucco and coworkers examined the heart tissue of mice which expressed a catalytically inactive p110 $\gamma$  in order to determine if the cardiac phenotype was due to loss of the catalytic activity of p110 $\gamma$  or loss of the entire protein<sup>21</sup>. It was eventually discovered that in addition to its PI3K activity, p110 $\gamma$  also allosterically activated phosphodiesterase 3B (PDE3B) through p87, one of its



regulatory subunits<sup>21</sup>. PDE3B catalyzed the conversion of cyclic AMP (cAMP), thus loss of p110 $\gamma$  led to lowered PDE3B catalytic activity, leading to an increase in cAMP concentrations and increased cardiac contractility<sup>21</sup>. Since the myocardial damage seen in the p110 $\gamma$  knockout was due to loss of protein, this left pharmaceutical companies free to pursue selective p110 $\gamma$  inhibitors as anti-inflammatories without fear of dangerous cardiac side-effects.

The incongruities that arise when comparing results of genetic disruption and pharmacological interference should initiate close scrutiny of genetic disruption data before drug target validation. The PI3K family has already provided two examples of these inconsistencies. Concurrent with the nascent interest in p110 $\gamma$  inhibitors was a similar assessment of inhibitors for the PI3K p110 $\delta$  and dual p110 $\gamma$ /p110 $\delta$  inhibitors as novel anti-inflammatories. The genetic evidence did suggest that loss of p110 $\delta$  was generally anti-inflammatory and tolerated well<sup>22-24</sup>, and although the dual p110 $\gamma$ /p110 $\delta$  knockout was viable, it displayed defects in T-cell development and decreased thymocyte survival<sup>25-26</sup>. Though the problem of heart contractility was exposed as an artifact of gene disruption, there was no way to adequately assess the effects of an inhibitor targeting the catalytic activity of both p110 $\gamma$  and p110 $\delta$ .

We have been interested in drug discovery and target validation in our lab, and seek to approach these problems through the use of synthetic organic chemistry. We sought to validate PI3K $\delta$ / $\gamma$  as a drug target, by constructing inhibitors from first principles using crystal structure data and protein and lipid kinase SAR information we had compiled over years of research. However, in order to draw conclusions from pharmacological inhibition of protein function, it is important that the pharmacological

agent be exquisitely specific for its protein, not only among closely related isoforms, but within the larger family, and more distantly related enzymes. This is more easily accomplished with protein kinases because the chemical genetic method pioneered by Shokat with protein kinases is not possible to use with PI3K because it cannot tolerate the space-creating mutations in the ATP pocket<sup>27</sup>. Therefore, it was also necessary that our inhibitors, in addition to possessing exquisite selectivity, were also potent, so that they could be used at concentrations where they only inhibited the target enzyme. This allowed us to conclude with certainty that the phenotypic effects were due to the disruption of the catalytic activity of a single protein. The design of such a set of inhibitors would be a significant achievement in target validation within the PI3K family.

## Chapter 2 – Design Rationale, Synthesis and Biochemical

### Characterization of PI3K $\delta/\gamma$ dual inhibitors

Selective inhibitors of protein and lipid kinases are potential drugs, and can be used as valuable tools to dissect signaling networks. The key challenge in the discovery of selective kinase inhibitors is obtaining the necessary potency for the kinase of interest without inhibiting the over 500 closely-related kinases. Generally, it is quite difficult to discover exquisitely specific kinase inhibitors because all kinases bind the same co-factor, ATP, and share relatively conserved features including similar catalytic domains that allow them to be distinguished from other ATP utilizing/hydrolyzing enzymes<sup>28-30</sup>. However, two exceptions to this general situation exist. The first involves discovery of inhibitors which exploit differences in amino acid identity between different classes of kinases, particularly differences in the gatekeeper residue which controls access to a variable sized hydrophobic pocket in the kinase active site<sup>31-33</sup>. The second, involves design of inhibitors which bind to an inactive conformation of the protein kinase, which not only differ between kinases<sup>34-36</sup>, but are also dissimilar to active protein kinase conformations<sup>34-36</sup>. The prime example of this is Gleevec, which inhibits Bcr-Abl, without inhibiting Src, two kinases with identical amino acids in their ATP binding sites. Structural studies by Kuriyan and coworkers have shown that Gleevec binds to an inactive (DFG-out) conformation of Bcr-Abl that is somehow energetically less favored in the closely related Src kinase<sup>34-36</sup>. The “inactive” binders have been quite successful as drugs, making up the majority of FDA approved protein kinase inhibitors.

Phosphoinositide 3-kinases (PI3Ks), a family of ATP dependent phosphotransferases, first discovered almost 10 years after protein kinases, lag behind the

protein kinases in inhibitor drug discovery. Recently, targeted inhibitors of the phosphoinositide-3-kinase (PI3K) pathway have been suggested as immunomodulatory agents.<sup>37-38</sup> This interest stems from the fact that the PI3K pathway serves multiple functions in immune cell signaling, primarily through the generation of phosphatidylinositol (3,4,5)-trisphosphate (PIP<sub>3</sub>), a membrane-bound second messenger.<sup>37, 39-41</sup> PIP<sub>3</sub> recruits proteins to the cytoplasmic side of the lipid bilayer, including protein kinases and GTPases<sup>37, 39, 41</sup>, initiating a complex network of downstream signaling cascades important in the regulation of immune cell adhesion, migration, and cell-cell communication.

The four class I PI3K isoforms differ significantly in their tissue distribution. PI3K $\alpha$  and PI3K $\beta$  are ubiquitous and activated downstream of receptor tyrosine kinases (RTK)<sup>37, 41</sup>, while PI3K $\delta$  and PI3K $\gamma$  are primarily limited to hematopoietic<sup>38, 40</sup> and endothelial cells<sup>24, 42</sup>, and are activated downstream of RTKs, and G-protein coupled receptors (GPCR) respectively<sup>41</sup>. Mouse genetic studies have revealed that PI3K $\alpha/\beta$  are essential for normal development<sup>43</sup>, while loss of PI3K $\delta$  and/or PI3K $\gamma$  yields viable offspring with selective immune deficits<sup>25-26, 43-44</sup>. The expression pattern and functions of PI3K $\delta$  and PI3K $\gamma$  have generated much interest in developing PI3K $\delta/\gamma$  inhibitors as agents for many diseases, including rheumatoid arthritis, allergies, asthma, chronic obstructive pulmonary disease and multiple sclerosis<sup>37-38, 45-46</sup>. Studies using both pharmacologic and genetic methods have shown these two isoforms often demonstrate synergistic interactions with each other<sup>47-48</sup>. In mast cells, for example, PI3K $\delta$  is essential for degranulation in response to IgE crosslinking of Fc-receptors<sup>49-50</sup>, but PI3K $\gamma$  plays an important role in amplifying the response<sup>48</sup>. Similar effects have been seen in

other cellular functions, including lymphocyte homing<sup>51</sup> and the neutrophil respiratory burst<sup>52</sup>, where PI3K $\gamma$  plays a critical role and PI3K $\delta$  amplifies or enhances each process.

There are not clearly defined means to achieve isoform-specific inhibition and perhaps as a result there are no PI3K inhibitor approved drugs. The key challenge in developing isoform selective PI3K inhibitors is that all Class I PI3Ks share nearly identical ATP binding pockets<sup>53</sup>. However, we and others reported that a quinazolinone-based chemical scaffold binds PI3K $\delta$  with high selectivity<sup>16, 24</sup>. This chemotype exploits a unique, non-catalytically active conformation of PI3K $\delta$  (and PI3K $\gamma$ ) that is not easily adopted by PI3K $\alpha$  and PI3K $\beta$ <sup>16, 54</sup>. The inactive conformation is characterized by the movement of Methionine 804 into the space normally occupied by ATP (Fig 2.1), resulting in a “Met-down” conformation that is not observed in any of the other PI3K crystal structures (Fig 2.2A). The kinases within the PI3K family that are capable of accessing this “Met-down” conformation are PI3K $\gamma$ , in which the conformation was originally captured in a crystal structure, and PI3K $\delta$ , the original target of the tolyl quinazolinone chemotype, in which the “Met-down” conformation has been recently confirmed<sup>54</sup>. Our data suggest that PI3K $\alpha$  and PI3K $\beta$  are not susceptible to adopting this conformation, and thus the tolyl quinazolinone series acts as a PI3K $\gamma$  and PI3K $\delta$  selective scaffold.

Since PI3K $\gamma$  and PI3K $\delta$  are selectively expressed in the cells of the immune system<sup>38, 41, 46</sup>, the tolyl quinazolinone provides an ideal chemical tool to explore the immune cell function of these isozymes, while not disrupting the ubiquitous PI3K $\alpha$  and PI3K $\beta$ , which are involved in growth factor signal transduction, and have been shown to be essential to embryonic development<sup>43, 55</sup>. PI3K $\gamma$  and PI3K $\delta$  have distinct binding

cofactors, which allow them to couple to different families of receptors. PI3K $\delta$ , a Class IA PI3K, obligatorily associates with the dual-SH2 domain containing protein p85, which binds activated receptor tyrosine kinases and subsequently increases the catalytic activity of PI3K $\delta$  by 100-fold. PI3K $\gamma$ , in contrast, associates with the GPCR-activated regulatory protein p101<sup>38, 41, 46</sup>.

Figure 2.1

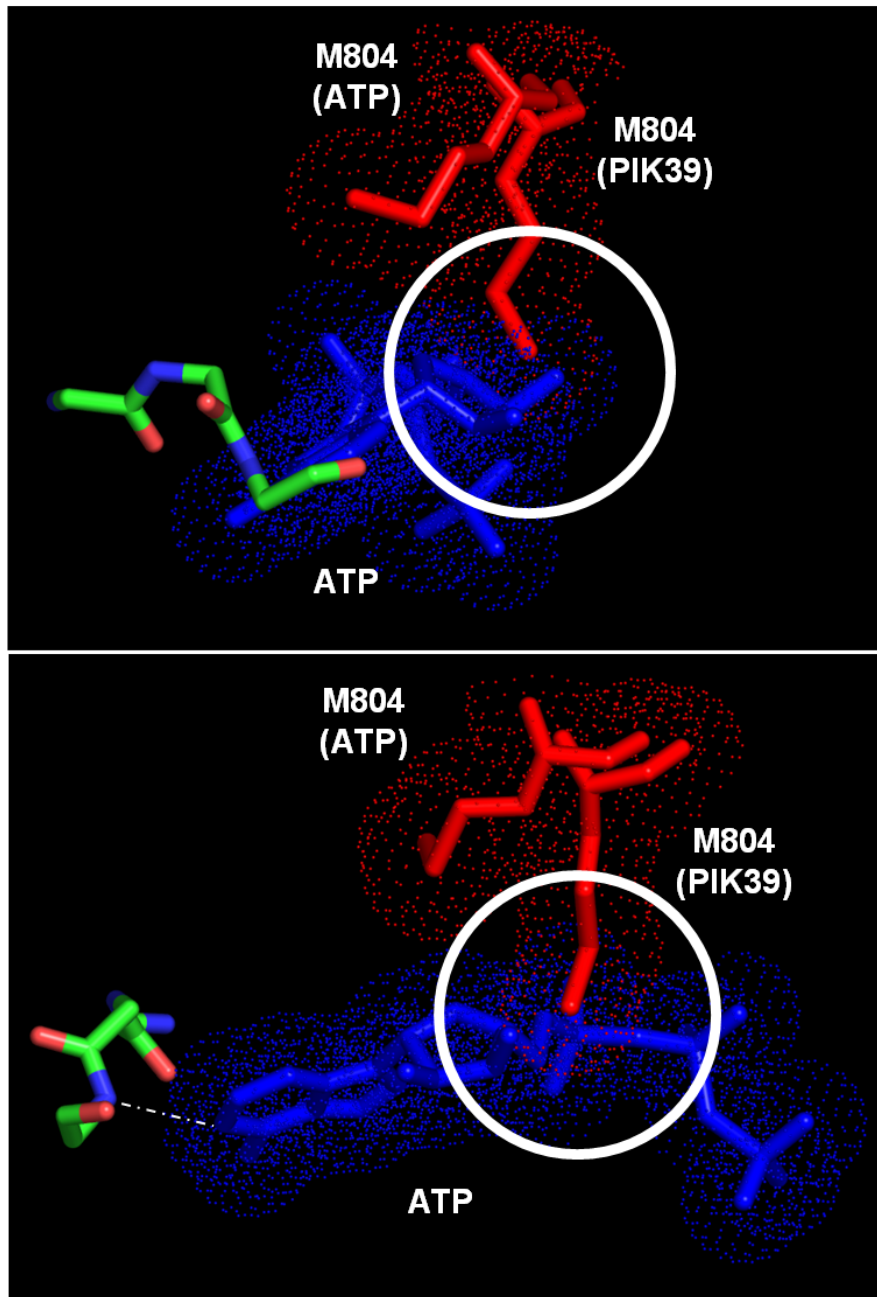


**Figure 2.1 – Met 804 “down” conformation precludes ATP binding.**

(Top) There is no steric clash with Met804 (red) in the ATP (blue) bound structure (PDB accession code : 1E8X ), yet with Met 804 in the “down” (PIK-39 bound) conformation(PDB accession code : 2CHW) it occupies a portion (circled in white) of the same space that ATP does.

(Bottom) 90° rotation around vertical axis of left panel.

Figure 2.2

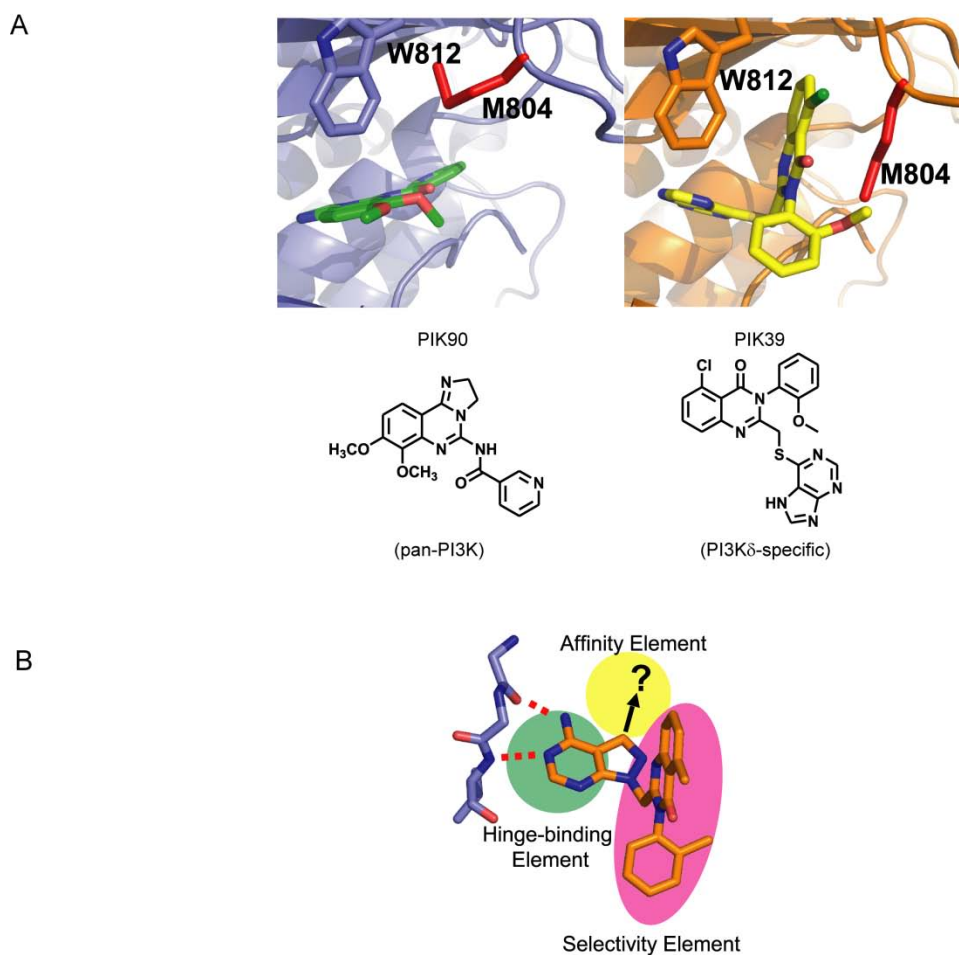


**Figure 2.2 - Basis of selectivity and potency for aryl quinazolinones**

A. Crystal structure of PI3K $\gamma$  with PIK90, a pan-PI3K inhibitor (Left) and PIK39, a PI3K $\delta$  inhibitor (Right)<sup>16</sup>. The bi-planar binding mode of PIK39 and alternate positioning of Met804 (red) are illustrated. Chemical compound structures are shown below.

B. Compounds in this study introduce affinity elements (yellow) onto selective tolyl quinazolinone (red) scaffold maintaining selectivity for PI3K $\gamma$  and PI3K $\delta$ .



The non-redundant but related roles of PI3K $\delta$  and PI3K $\gamma$  have made it difficult to determine which of the two isoforms (alone or in combination) is best targeted in a particular inflammatory disorder. Studies using mice that lack PI3K $\delta$  and/or PI3K $\gamma$  or express kinase-dead variants of PI3K $\delta$  and PI3K $\gamma$  have been valuable tools in understanding their roles. For example, PI3K $\delta$  knockout mice demonstrated diminished neutrophil chemotaxis<sup>24</sup>, diminished antibody production (both T-cell dependent and independent)<sup>23</sup>, and lower numbers of mature B-cells<sup>22-23</sup>, and a decrease in their proliferation in response to anti-IgM<sup>23</sup>. This phenotype was replicated in the PI3K $\delta$  kinase-dead variant<sup>56</sup>, and with PI3K $\delta$  selective inhibitors<sup>24, 49, 57</sup>, along with decreased numbers of and proliferation of mast cells, and an attenuated allergic response<sup>49</sup>. The PI3K $\gamma$  knockout contained higher numbers of, but less responsive neutrophils<sup>18</sup>, lower numbers of and less responsive macrophages<sup>18</sup> and dendritic cells<sup>58</sup>, displayed decreased mast cell degranulation<sup>48</sup>, a higher ratio of CD4<sup>+</sup> to CD8<sup>+</sup> T-cells<sup>59</sup>, increased thymocyte apoptosis<sup>17</sup>, diminished induction of CXCR3 on activated T cells<sup>60</sup>, and decreased cardiac contractility<sup>19</sup>. This latter effect on cardiac tissue was a concern for chronic dosing of patients with PI3K $\gamma$  inhibitors. However, this concern was largely mitigated when the PI3K $\gamma$  kinase-dead variant (which better mimics inhibition of the kinase rather than loss of the protein) showed similar immune cell phenotypes, but importantly had no cardiac defects<sup>21</sup>. The cardiac effect was later shown to be due to scaffolding effects rather than the catalytic activity of PI3K $\gamma$ . The dual PI3K $\delta$  /PI3K $\gamma$  knockout was viable but exhibited serious defects in T-cell development<sup>25</sup> and thymocyte survival<sup>26</sup>. The PI3K $\gamma$  knockout/PI3K $\delta$  kinase-dead combination produced a similar phenotype

suggesting that at least within the immune system, the role of PI3K $\delta$  is likely only a catalytic one<sup>61</sup>.

The primary difficulty with studies using knockout and kinase-dead mice is that they provide only a steady-state picture of the immune system, lack temporal and dose control, and do not permit a full understanding of how a dynamic immune response will react to reversible inhibition. Selective inhibitors with varying profiles (PI3K $\delta$ , PI3K $\gamma$ , and PI3K $\delta/\gamma$ ) are necessary for studies of leukocyte signaling in order to assess the relative contributions of each PI3K to immune cell activation.

It is widely held that a PI3K inhibitor which targets PI3K $\delta$  and/or PI3K $\gamma$  but not PI3K $\alpha$  or PI3K $\beta$  may be beneficial for the treatment of inflammatory diseases including rheumatoid arthritis, lupus, and asthma. Although the selectivity for PI3K $\delta/\gamma$  over PI3K $\alpha/\beta$  is agreed upon, it is not known whether a purely PI3K $\delta$ -selective, purely PI3K $\gamma$ -selective or a dual inhibitor is optimal for treatment of certain immune disorders. Rommel and colleagues have suggested that only a dual inhibitor would be sufficient to shut down signaling from both the RTK and GPCR sides of immune signaling thus providing an effective treatment<sup>38, 46</sup>. A purely PI3K $\delta$ -selective or purely PI3K $\gamma$ -selective inhibitor would be unable to do so alone. Guided by the PI3K $\gamma$  crystal structure and our own chemical intuition, we designed highly potent PI3K $\delta$  inhibitors and PI3K $\delta/\gamma$  dual inhibitors.

#### *Design Rationale for PI3K $\delta/\gamma$ dual inhibitors*

The ATP binding pocket of the four class I PI3K isoforms is extremely conserved<sup>53</sup>. All the residues within the ATP-binding site whose side chains possess a

rotamer that can extend to within 4 Å of the adenine core of ATP are identical (Fig 2.3)<sup>53</sup>. This makes the design of ATP-competitive isoform-selective compounds quite challenging. The binding pocket of the class I PI3Ks ( $\alpha$ ,  $\beta$ ,  $\delta$ ,  $\gamma$ ) also contains three distinct binding elements: a hinge region with two hydrogen bonding contacts, a hydrophobic pocket deep in the protein which is not occupied by ATP, and a conformationally-mobile methionine residue above the plane of the adenine ring of ATP<sup>16, 62</sup>. The first two binding elements are common to all PI3Ks while the third appears to be unique to PI3K $\delta$  and PI3K $\gamma$ <sup>16, 54</sup>. The hinge region, common to all PI3Ks, connects the N- and C- terminal sub-domains of the kinase providing key interactions anchoring the adenosine of ATP between the two sub-domains<sup>62</sup>. The vast majority of both protein and lipid kinase inhibitors make hydrogen bonds with backbone amide and carbonyl groups of the hinge region<sup>62-63</sup>. Interaction with this region thus provides specificity for the kinases compared to other ATP-dependent enzymes. The deeper hydrophobic pocket is best complemented by aromatic substituents often bearing a hydroxyl, aromatic amine, or halogen<sup>16</sup> (Fig. 2.2A, left panel). These inhibitor binding elements provide van der Waals contacts with the hydrophobic amino acids lining this pocket and provide an affinity enhancement over the substrate, ATP<sup>16, 54</sup>. Although some differences in affinity between PI3K isoforms due to differential binding in the hydrophobic pocket have been achieved<sup>16, 45</sup>, these differences are typically minor (2-10 fold) and do not afford the 30-100 fold or greater levels of differential binding desirable in a selective inhibitor useful for chronic therapy of immune disorders. Additionally, most of these inhibitors were multi-targeted, with a slight bias towards inhibiting either PI3K $\alpha/\gamma$  or PI3K $\beta/\delta$  isoforms<sup>16, 45</sup>.

Figure 2.3

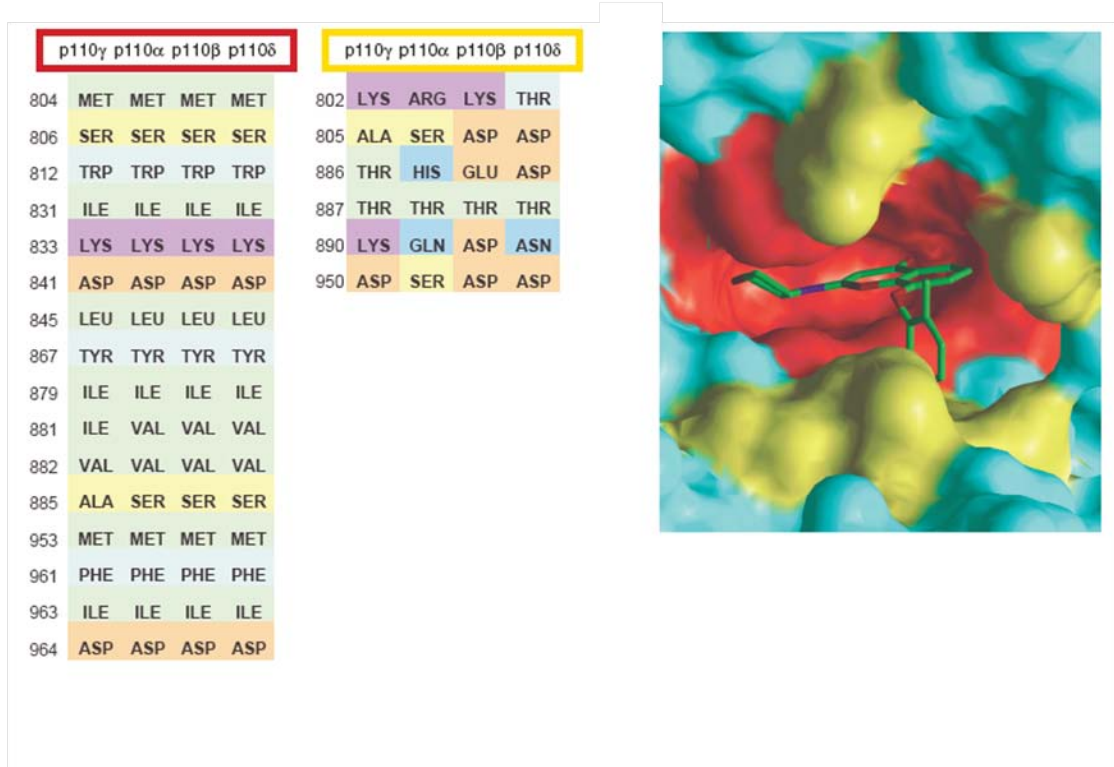


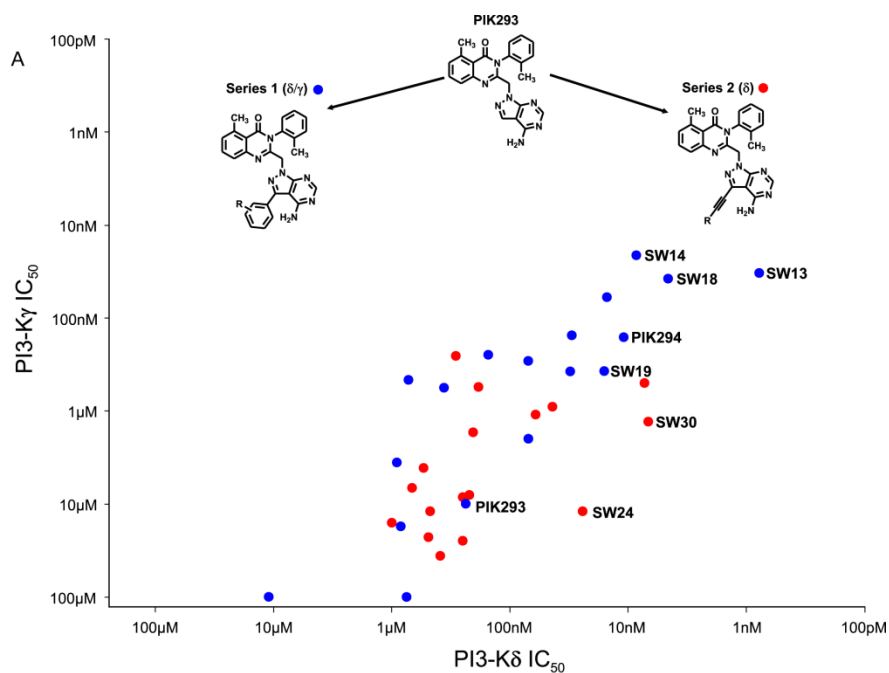
**Figure 2.3 – ATP-Binding site Sequence Identity among human Class I PI3-Ks.** Sequence alignment of residues in the interior (red) of the ATP binding pocket (residues whose side chains possess a rotamer that can extend within 5 Å of the adenine core. From reference <sup>53</sup>.

In order to achieve maximal differential binding to PI3K $\delta$  or PI3K $\gamma$  compared to PI3K $\alpha$  and PI3K $\beta$  we exploited the lessons learned from the binding mode of PIK-39. We had previously determined the unique binding mode and basis of selectivity for PIK-39, one of the most selective PI3K $\delta$  inhibitors reported in collaboration with Roger Williams<sup>16</sup>. The anisole quinazolinone of PIK-39 is positioned orthogonally to the mercaptopurine which satisfies the hinge-hydrogen bonds necessary for kinase inhibitor potency. This bi-planar conformation is not seen in any of the other classes of PI3K inhibitors, which tend to adopt a uniplanar conformation (Fig 2.2A), in line with the hinge hydrogen bonds. For successful binding in the proper orientation, the vertical plane (quinazolinone) requires a rearrangement of Methionine 804 in the PI3K $\gamma$  crystal structure. In all other crystal structures, Met804 adopts an “up” position, forming the roof of the binding pocket (Fig 2.2A). However, with PIK-39 and with other selective PI3K inhibitors containing both an aryl quinazolinone and a hinge-binding element, Met804, exists in the “down” conformation<sup>16, 54</sup>. This rearrangement reveals a new pocket, not found in any ATP bound forms of PI3Ks<sup>16</sup>. The aryl quinazolinone inhibitor PIK39 (Fig 2.2A, right panel) exists in a conformation which projects the quinazolinone moiety deep into the pocket produced by the Met804 movement, burying  $\sim 180 \text{ \AA}^2$  of inhibitor<sup>16</sup> and affording highly selective binding of this inhibitor chemotype to PI3K $\delta$  and PI3K $\gamma$ <sup>16, 54</sup>. Very recently, the first x-ray crystal structure of PI3K $\delta$  by Roger Williams and colleagues<sup>54</sup> revealed that PIK39 engages the methionine switch in PI3K $\delta$  as well. The ease with which PI3K $\delta$  and PI3K $\gamma$  isoforms adopt the “Met-down” conformation when compared to the relative inability of PI3K $\alpha$  and PI3K $\beta$  as revealed by the isoform selectivity profile of the aryl quinazolinone PI3K inhibitors, provides a

critical difference between the ATP pockets of the inflammatory PI3Ks (PI3K $\delta$  and PI3K $\gamma$ ) compared to the ubiquitously expressed PI3K $\alpha$  and PI3K $\beta$  isoforms.

PIK39, the inhibitor which revealed the unanticipated “Met-down” binding mode, and a related molecule we synthesized PIK293, form hydrogen bonds with the hinge region of PI3Ks, but do not contain binding elements which project into the hydrophobic pocket (Fig 2.2B) As a result of this incomplete site occupancy, we explored the effects of adding two classes of substituents to PIK293, (Fig 2.4A) with the goal of increasing potency against PI3K $\delta$  and PI3K $\gamma$ . Despite the isoform similarities in the hydrophobic binding pocket, we reasoned that it might be possible to discriminate between PI3K $\delta$  and PI3K $\gamma$  with the appropriate binding elements. Importantly, we required that in achieving these goals we did not lose the large differential binding between the inflammatory PI3Ks (PI3K $\delta$  and PI3K $\gamma$ ) and the ubiquitous PI3K $\alpha$  and PI3K $\beta$ . An early study of the feasibility of appending hydrophobic pocket binders to a tolyl-quinazolinone scaffold suggested this approach would be successful. PIK294, a meta-phenol derivative of a pyrazolopyrimidine PIK293 demonstrated a 24-fold increase in potency against PI3K $\delta$  and a 62-fold increase in activity against PI3K $\gamma$  without diminishing the selectivity between PI3K $\alpha$  and PI3K $\beta$  (Fig 2.4B) <sup>16</sup>. This result demonstrated the ability to prepare selective, potent inhibitors of PI3K $\gamma$  and PI3K $\delta$  and provided evidence that the affinity pocket may also modulate selectivity toward PI3K $\gamma$ .

Figure 2.4



B

IC<sub>50</sub> (nM)

Compound	Group	$\alpha$	$\beta$	$\delta$	$\gamma$	$\gamma/\delta$ ratio
PIK293	H	>90,000	>90,000	237	10,000	42
PIK294		>90,000	486	11	162	15
SW13		1,240	221	0.7	33	47
SW14		8,910	697	9	21	2.3
SW18		6,700	2,400	5	38	7.6
SW19		>90,000	7,900	16	376	23
SW30		85,000	740	7	1,300	186
PIK90	N/A	11	350	58	18	0.31
AS605240	N/A	60	270	300	8	0.026

Series 1

Series 2

Benchmark Compounds

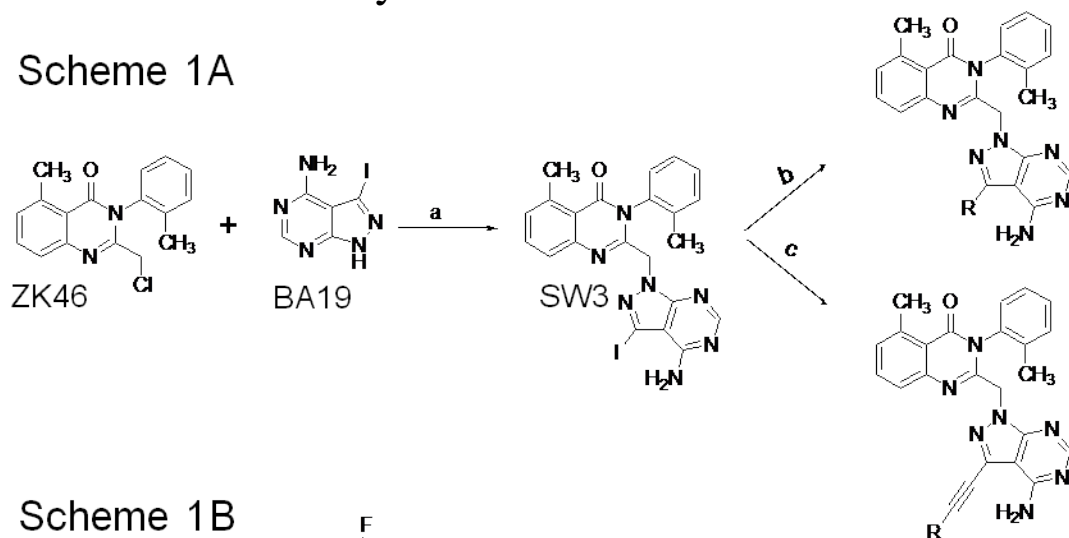
**Figure 2.4 - Diversification of Tolylyl Quinazolinone Series**

A. Introduction of affinity elements to PIK293. Series 1 (PI3K $\delta/\gamma$ ) introduces aryl groups and Series 2 (PI3K $\delta$ ) introduces alkynyl-linked groups. IC<sub>50</sub>s of both Series 1 (blue) and Series 2 (red) were graphed.

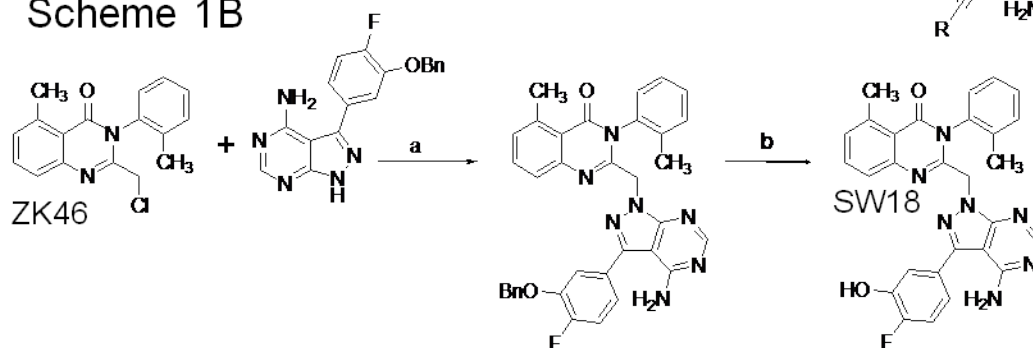
B. Biochemical IC<sub>50</sub>s and  $\gamma/\delta$  ratios for Series 1 and 2 along with benchmark compounds. All compounds were tested at 10 $\mu$ M ATP.

## Synthetic Schemes

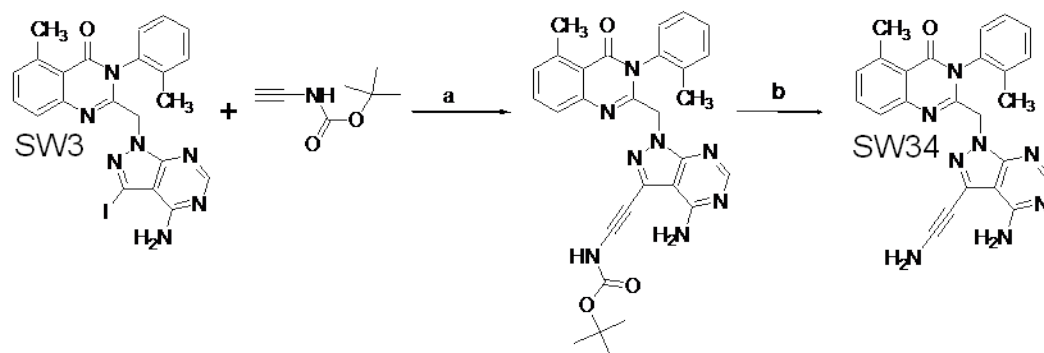
### Scheme 1A



### Scheme 1B



### Scheme 1C



#### Scheme 1A - Synthesis of substituted tolyl quinazolinone pyrazolopyrimidines<sup>a</sup>

<sup>a</sup>Reagents and Conditions: (a) K<sub>2</sub>CO<sub>3</sub>, DMF; (b) Pd(PPh<sub>3</sub>)<sub>4</sub>, EtOH, Na<sub>2</sub>CO<sub>3</sub>, aryl boronic acid, DME, Δ; (c) Pd(PPh<sub>3</sub>)<sub>4</sub>, CuI, (iPr)<sub>2</sub>NH, terminal alkyne, THF.

#### Scheme 1B - Synthesis and deprotection of SW18<sup>a</sup>

<sup>a</sup>Reagents and Conditions: (a) K<sub>2</sub>CO<sub>3</sub>, DMF; (b) 90% formic acid, 10% conc. HCl.

#### Scheme 1C - Synthesis and deprotection of SW34<sup>a</sup>

<sup>a</sup>Reagents and Conditions: (a) Pd(PPh<sub>3</sub>)<sub>4</sub>, CuI, (iPr)<sub>2</sub>NH, THF; (b) CH<sub>2</sub>Cl<sub>2</sub>:TFA:0.2% H<sub>2</sub>O.



### *Synthesis of PI3K $\delta$ / $\gamma$ dual inhibitors*

The series of compounds we synthesized can be divided into three segments (Fig 2.2B). The first segment, (highlighted in red) the selectivity element is a tolyl quinazolinone the synthesis of which was previously described<sup>16</sup>. The joining of the second element, an iodo-pyrazolopyrimidine, (BA19), the synthesis of which was also previously described<sup>64</sup>, to the tolyl quinazolinone was accomplished in the presence of K<sub>2</sub>CO<sub>3</sub> to yield SW3, a fairly potent PI3K inhibitor in its own right (Scheme 1 A). The series was then diversified through the addition of the third element (affinity element) with standard palladium catalyzed chemistries (Scheme 1A). The first series (Table 2.1) was synthesized through a standard Suzuki-Miyaura coupling with aryl boronic acids. For the most part, we avoided substituents on the 2 and 6 positions because we had previously seen that substituents in those positions hindered the Suzuki reactions because of their proximity to the reaction center, thus resulting in lower yields. Originally, the affinity element we were attempting to mimic was the meta-phenol of PI-103; as a result, the majority of the first group of molecules synthesized contained oxygen in the 3 or 4 position. We tested all molecules synthesized against all Class I PI3K isoforms as previously described<sup>65</sup>, and the increased potency of SW4 (also reported in the literature as PIK294) against PI3K $\gamma$ , led us to calculate PI3K $\gamma$ /PI3K $\delta$  IC<sub>50</sub> ratios ( $\gamma/\delta$  ratio) (Tables 2.1&2.2) for all our compounds, in the hope of discovering substituent patterns that could increase potency against PI3K $\gamma$ . Because our compounds inhibit PI3K $\delta$  most potently, and often inhibits PI3K $\gamma$  with the next lowest IC<sub>50</sub>, the  $\gamma/\delta$  ratio represents the lower limit of selectivity for these molecules.

### *Biochemical Characterization of Series 1*

Compounds SW11, SW15, and SW47 demonstrated that substituents in the 4 position decreased the  $\gamma/\delta$  ratio, which was an indication that despite their lower potency they were behaving more like PI3K $\gamma/\delta$  dual inhibitors than strict PI3K $\delta$  inhibitors. The 3,4 meta- para- substituent pattern present in SW10, SW14, SW17 and SW18 quickly emerged as the best candidate for a dual-specificity PI3K $\gamma$ /PI3K $\delta$  inhibitor. For reasons that will be discussed later, it appears that this substituent pattern in the affinity element increases the potency against PI3K $\gamma$  much more than it does against PI3K $\delta$  when compared to the parent compounds PIK293 and SW3. SW18, one of the most potent PI3K $\delta$  and PI3K $\gamma$  inhibitors in the series, was screened against 219 protein kinases at a concentration of 10 $\mu$ M. 218 kinases in the panel retained at least 75% activity, and only one, macrophage stimulating 1 receptor (MST1R) kinase, was inhibited to less than 60% activity (See Invitrogen Data in Appendix). These data demonstrate that the tolyl quinazolinone moiety responsible for selectivity within the PI3K family also confers selectivity against protein kinases.

Of all the compounds synthesized and reported in the literature SW13 was the most potent PI3K $\delta$  inhibitor, with an IC<sub>50</sub> under 1nM, so low it was difficult to measure accurately. Both SW4 and SW46 were relatively potent, and nothing would immediately suggest that combination of their substituents into one molecule would result in an order of magnitude increase in potency. Although alterations of this substituent pattern still yielded potent molecules, the next most potent molecule was SW18 with an IC<sub>50</sub> of 5nM (a 7-fold drop in potency). The 3,5 -fluoro-hydroxy affinity element of SW13 for reasons that we still do not understand seems to be the perfect affinity element. Addition

of that affinity element drastically increases the potency of other related scaffolds designed to specifically inhibit PI3K $\delta$  by engaging the methionine switch.

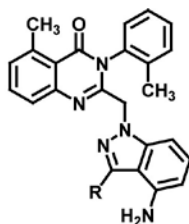
We attempted to test the boundaries of the pocket by synthesizing several compounds with bicyclic affinity elements. These compounds (SW6, SW11, and SW12) were of considerable less potency than the unicyclic affinity elements, suggesting that the affinity pocket preferred smaller substitutions, limited to just one aryl group. While there is considerable precedent for hydroxyl groups in the hydrophobic affinity pocket of PI3Ks<sup>66-68</sup>, phenolic substituents are often subject to first pass metabolism, limiting their oral bioavailability. We therefore explored groups that would preserve hydrogen-bonding interactions but would not contain a phenol. The indole, a classic phenol bioisostere, was an obvious choice and has been used before with success<sup>69</sup>. We knew that the pocket did not tolerate large bicyclic substituents well, but in an attempt to design metabolically stable inhibitors, we constructed indoles with different connectivities, but only SW19 was able to retain significant PI3K $\delta$  potency and some activity against PI3K $\gamma$  while eliminating the presence of a hydroxyl group.

We also attempted to incorporate trifluoromethyl, a group with established pharmacological activity<sup>70-72</sup>, into our series, but the resultant compound (SW23) was inactive, and even less potent than the molecules with bicyclic affinity elements. Replacement of the trifluoromethyl units with fluorine, afforded a slightly more potent compound (SW50). Still, in light of the extreme potency of SW13 (obtained by replacement of one of the fluorines of SW50 with a hydroxyl), and other members of the series, SW50 was quite disappointing.

The tolyl quinazolinone scaffold's bias toward PI3K $\delta$  and PI3K $\gamma$  allowed us to focus our efforts on altering selectivity between PI3K $\gamma$  and PI3K $\delta$  by only altering the substitution pattern on the affinity element. Selectivity between PI3K $\gamma$  and PI3K $\delta$  was controlled primarily by substituents in the four position. Substitution in the four position lowers PI3K $\delta$  activity, but leaves PI3K $\gamma$  potency relatively unchanged, thus lowering selectivity between PI3K $\gamma$  and PI3K $\delta$  (compare SW13 and SW18). This results in 3,4 substituted compounds being better PI3K $\gamma$ / PI3K $\delta$  dual inhibitors than any other substituent pattern we explored. All 3,4 substituted compounds have PI3K $\gamma$ /PI3K $\delta$  ratios under 10, and SW49 actually reverses the selectivity trend, being slightly more potent on PI3K $\gamma$  than on PI3K $\delta$ .

The increased PI3K $\gamma$  activity of SW10, SW14, SW15, SW17, and SW18 suggested that the affinity pocket controlled more than just potency, and may perhaps be termed "affinity/selectivity" pocket. For this sub-series (Table 2.1), selectivity can now be controlled by two portions of the molecule; in addition to the quinazolinone which directed the selectivity toward PI3K $\delta$ , the aryl group that extended to interact in the "affinity pocket" could alter selectivity between PI3K $\gamma$  and PI3K $\delta$ . In order to determine if this held true for another chemotype, we synthesized another series of compounds with a different coupling reaction. We also realized that coupling to alkynes would change the trajectory of the affinity element, and may also modify the relative rotation of the three sections of the series (around the pyrazolopyrimidine to affinity element bond), so we decided to couple to terminal alkynes with the palladium catalyzed Sonogashira reaction for the next set of molecules (Scheme 1A).

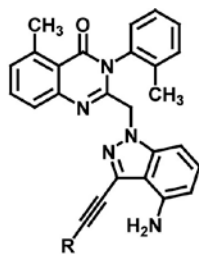
Table 2.1



Cpd	R	IC <sub>50</sub> (nM)				γ/δ ratio
		PI3Kα	PI3Kβ	PI3Kδ	PI3Kγ	
PIK293	H	**	**	237	10000	42
SW3	I	10000	1260	7	279	40
SW4		**	486	11	162	15
SW10		**	4500	15	60	4
SW11		**	4600	906	3600	4
SW13		1240	221	0.7	33	47
SW14		8910	697	9	21	2.3
SW15		18200	12860	30	154	5.1
SW18		6700	2400	5	38	7.6
SW23		**	**	**	11000	N.C.
SW46		N.D.	N.D.	31	377	12.2
SW47		N.D.	N.D.	360	567	1.58
SW49		N.D.	N.D.	725	462	<b>0.63</b>
SW50		N.D.	N.D.	750	**	N.C.
SW19		**	7900	16	376	23.5
SW20		25000	9500	70	2000	28.6
SW29		12000	13000	153	250	1.6

Table 2.1 - Structures and Biochemical IC<sub>50</sub>s for Series 1, tested at 10μM ATP.\*\* = IC<sub>50</sub> greater than 100μM. N.D. = not determined N.C. = not calculated

Table 2.2



Cpd	R	IC <sub>50</sub> (nM)				γ/δ ratio
		PI3Kα	PI3Kβ	PI3Kδ	PI3Kγ	
SW25		20500	25000	287	256	0.9
SW26		**	23700	472	12000	25.4
SW27		**	25000	205	1100	5.4
SW28		**	17000	185	548	3
SW43		**	30000	250	25000	100
SW44		**	26000	250	8500	34
SW24		**	25000	24	12000	500
SW34		**	21000	389	3600	9.3
SW31		22000	30000	489	23000	47
SW35		1700	19000	1000	1600	1.6
SW30		85000	740	7	1300	186
SW36		**	7540	61	1100	18
SW37		3800	956	7	505	72
SW40		**	14000	44	896	20.4
SW41		**	**	220	8000	36
SW38		69000	50000	538	4100	7.6

Table 2.1 - Structures and Biochemical IC<sub>50</sub>s for Series 2, tested at 10μM ATP.\*\* = IC<sub>50</sub> greater than 100μM. N.D. = not determined N.C. = not calculated

### *Biochemical Characterization of Series 2*

The second series of molecules, (Table 2.2) was synthesized with the palladium-catalyzed Sonogashira reaction with commercially available terminal alkynes. The first subset of these, SW25-SW28 contained an aryl group at other end of the terminal alkyne. These compounds were of similar potency (on PI3K $\delta$ ) to the overly large bicyclic compounds (SW11-12 and SW21-22, 20-22) (Table 2.1), indicating that the affinity element was most likely too large to appropriately occupy the hydrophobic affinity pocket created by residues isoleucine 831, lysine 833, aspartate 836, leucine 838, aspartate 841, tyrosine 867, isoleucine 879, isoleucine 963, aspartate 964, and phenylalanine 965 in the PI3K $\gamma$  structure. In order to test that hypothesis, alkynes with smaller groups were coupled to the starting material (SW3). The resulting compounds were quite interesting. SW43 with a hydroxyl cyclopentyl and SW44 with a cyclopentyl were not much more potent than the previous aryl group compounds, however the smallest of the group, SW24, with a cyclopropyl affinity element confirmed our hypothesis that smaller substituents were preferred with the alkynes, most probably because the alkyne provides a straight long bond which would place the terminal affinity element deeper into the pocket, thus a smaller substituent would be tolerated better. Since we knew from the crystal structure<sup>16</sup> that there was a possibility for various hydrogen bonding interactions in the affinity pocket, we next attempted to add polar/hydrogen bonding groups while maintaining the small size of the affinity elements.

The amines (SW31 and SW34-35) were not very potent. They were most likely positively charged at the pH of the assay, and we know from crystal structures that the catalytic lysine (Lys833) is known to make interactions in the affinity pocket and is most likely positively charged as well<sup>16, 66</sup>. The low activity of the amines is consistent with

electrostatic repulsion of the two positively charged groups and suggested that there needed to be a hydrogen bond acceptor in the affinity pocket (as the protonated amines cannot act as acceptors). The compounds with alkynyl alcohol affinity elements (SW30 and SW36-37) were quite potent on PI3K $\delta$ . Interestingly, these compounds also had considerably less PI3K $\gamma$  activity. This trend was carried through most of this alkynyl series, and was especially evident with the smaller compounds (SW24, SW30, SW36, and SW37). It is possible that this reflects a difference in the shape of the affinity pocket (Fig 2.5)

#### *Rationale for differential effects on PI3K $\gamma$ and PI3K $\delta$*

The effects of the affinity element could not be simply attributed to specific interactions with the residues lining that pocket, because those residues were conserved throughout the isoforms<sup>73</sup>; yet we saw differential isoform response to the same affinity element. The aryl substituted series (Table 2.1) showed increased PI3K $\gamma$  activity, and a lower  $\gamma/\delta$  ratio when a substituent in the para (or 4) position was present. Movement of the 3-hydroxyl in SW13 to the 4-position (SW14) increased PI3K $\gamma$  activity and decreased PI3K $\delta$  activity resulting in a balanced dual PI3K $\delta/\gamma$  inhibitor, additionally, movement of the methoxy group in the 3-position of SW21 to the 4-position (SW22) also increased PI3K $\gamma$  potency.

Para-substituted molecules are predicted to extend deeper into the affinity pocket than those with substituents on the 3 and 5 positions, which could result in a broader/wider group (Fig 2.5). If the PI3K $\delta$  affinity pocket is shallower (and potentially broader), while the PI3K $\gamma$  affinity/selectivity pocket is deeper, then a “shorter”



compound, such as SW24, or SW30 (the most PI3K $\delta$  selective compounds of the entire series) would retain their PI3K $\delta$  activity and lose PI3K $\gamma$  activity due to the presence of unsatisfied van der waals interactions that only exist within PI3K $\gamma$ . Based on this reasoning, larger compounds may lose activity against PI3K $\delta$ , but not be penalized as much in PI3K $\gamma$ , because the deeper pocket in PI3K $\gamma$  may be able to accommodate the affinity element, and thus PI3K $\delta$  favors smaller compounds, while PI3K $\gamma$  can handle and in some cases favor larger compounds. This principle is evident with SW24, SW30, and SW37 which contained small selectivity elements and were potent PI3K $\delta$  inhibitors, but did not inhibit PI3K $\gamma$  very well (Table 2.2). Additionally, large compounds SW25, SW27, and SW29 demonstrated more PI3K $\gamma$  potency than expected when considering the trends evident in the aryl-substituted compounds (Tables 2.1&2.2).

*Stereochemical evidence for a distinct conserved binding mode*

SW36 and SW37 make a stereochemical case for a very distinct binding mode conserved within members of this class. They are enantiomers, and only differ in the exact position their methyl group will occupy in the affinity pocket (assuming, both hydroxyl groups attempt to make the same hydrogen bond.) SW30 and SW37 behaved identically against PI3K $\delta$ , suggesting that SW37 can assume the binding mode of SW30, and place the methyl group in an area of the pocket where it does not detract from binding. This orientation seems to be impossible with SW36, which was nearly 10-fold less potent against PI3K $\delta$ . Since the hydroxyl group present in all three compounds was found to interact with Asp787 and Asp911 in PI3K $\delta$ <sup>54</sup> then there would be more space for the methyl group in SW37, than for SW36, which would explain the difference in IC<sub>50</sub>.

When we capped the hydroxyl with a methyl group (SW40) we found that some potency was lost, but the PI3K $\delta$  IC<sub>50</sub> remained under 50nM suggesting that the hydroxyl group in the affinity pocket likely acts as a hydrogen bond acceptor. We were able to confirm this when solution of the crystal structure showed that the oxygen was both a hydrogen bond donor and acceptor, making interactions with two aspartates 787 and 911<sup>54</sup>. Extending the hydroxyl deeper (SW41) into the pocket resulted in a much more significant loss of potency, suggesting unfavorable interactions deeper in the “affinity/selectivity” pocket and a possible disruption of the optimal binding geometry.

Figure 2.5

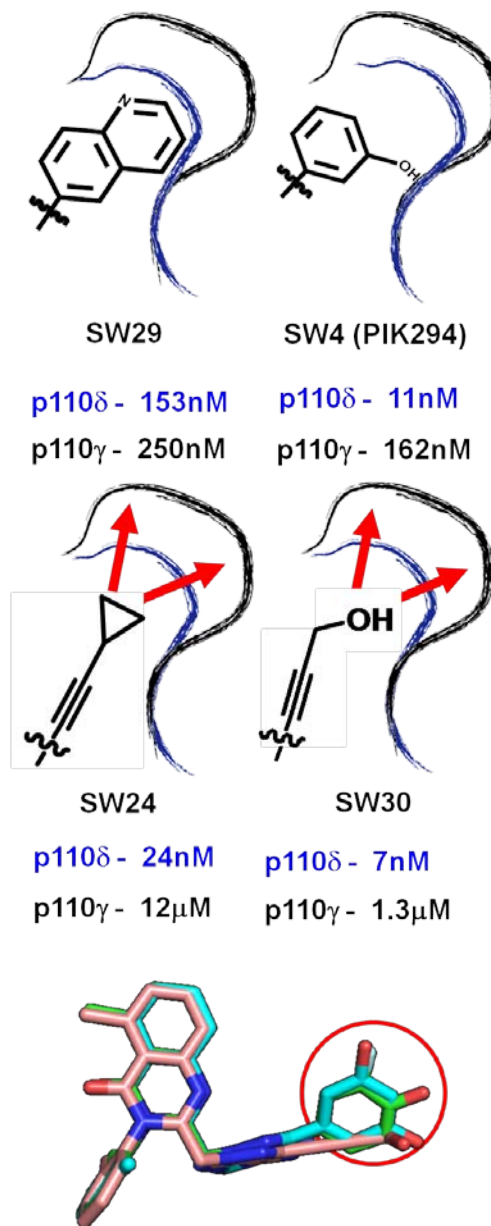


**Figure 2.5 – Model for PI3K $\delta$  selectivity of SW series 2.**

Top Panel – Substituents in series 1 adequately fill the pocket of both PI3K $\delta$  (blue) and PI3K $\gamma$  (black)

Middle panel – Substituents in series 2 adequately fill the pocket of PI3K $\delta$ , but cannot completely establish interactions with PI3K $\gamma$ , resulting in unsatisfied interactions in the pocket of PI3K $\gamma$ , diminishing the potency of series 2 against PI3K $\gamma$

Bottom panel – Crystal structure of SW13, SW14, and SW30<sup>74</sup>, showing the additional space occupied by the series 1 molecules that is not occupied by the more PI3K $\delta$ -selective series 2 representative.

### *Varying Flexibility in Met804 region between PI3K isoforms*

We had previously proposed that the isoform selectivity was specifically due to Met 804 flexibility and the exploitation of that flexibility by the quinazolinone moiety<sup>16</sup>. It then follows from this proposal that the relative potency of quinazolinone containing compounds between isoforms should be due to the Met 804 flexibility in isoforms. In other words, the potency of the quinazolinone compounds should be correlated with the Met 804 flexibility between isoforms. This series of compounds is most potent against PI3K $\delta$ , followed by PI3K $\gamma$ . Even in the most potent compounds, there is usually a large jump between the PI3K $\gamma$  and the PI3K $\beta$  IC<sub>50</sub>s. From the IC<sub>50</sub> data we generated we can then infer that in PI3K $\gamma$  Met 804 is also flexible, but not equal to the degree of flexibility in PI3K $\delta$ , and in PI3K $\alpha$  and PI3K $\beta$ , Met 804 is not very flexible at all. Met 804's moderate flexibility in PI3K $\gamma$  may also be evidenced by the fact that we were able to capture a relevant alternate conformation PI3K $\gamma$  in the crystal structure with PIK-39. This idea was also supported by some theoretical simulations conducted on PI3K $\delta$  and PI3K $\gamma$  suggesting that the methionine movement is more favorable in PI3K $\delta$  than in PI3K $\gamma$ <sup>54</sup>.

Figure 2.6

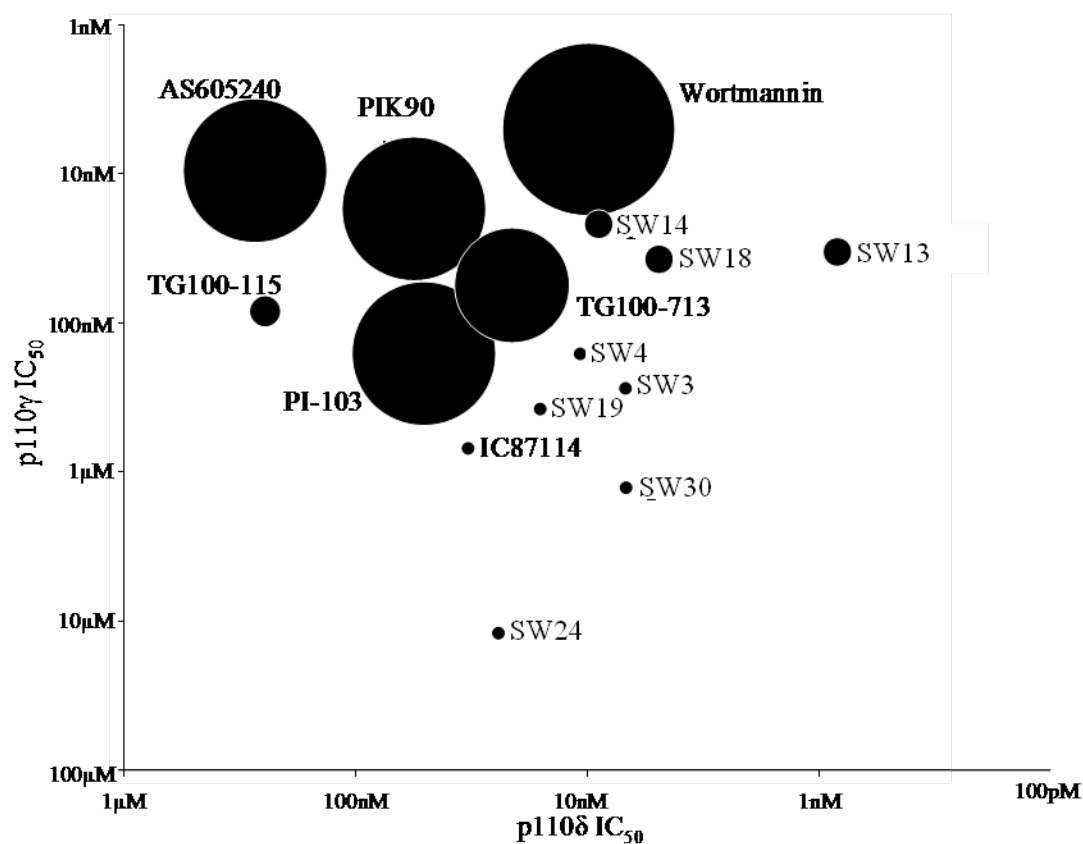


**Figure 2.6 – Comparison of SW series to other PI3K inhibitors.**

IC<sub>50</sub>s against PI3-K $\delta$ <sup>16, 66-67, 75-77</sup> were plotted on the X-axis and IC<sub>50</sub>s against PI3-K $\gamma$ <sup>16, 66-67, 75-77</sup> were plotted on the Y-axis. The IC<sub>50</sub> against PI3-K $\alpha$ <sup>16, 66-67, 75-77</sup> was translated into a circle with a diameter that scaled according to the IC<sub>50</sub>.

Diameter Scaling Key: IC<sub>50</sub> = 1-20nM, circle diameter = 1.5 units; IC<sub>50</sub> = 20-100nM, circle diameter = 1.25 units; IC<sub>50</sub> = 100-500nM, circle diameter = 1.0 units; IC<sub>50</sub> = 500nM-1 $\mu$ M, circle diameter = 0.75 units; IC<sub>50</sub> = 1 $\mu$ M-10 $\mu$ M, circle diameter = 0.5 units; IC<sub>50</sub> = 10-50 $\mu$ M units, circle diameter = 0.25 units; IC<sub>50</sub> >50 $\mu$ M, circle diameter = 0.1 units.

Still, it appears that PI3K $\gamma$  and PI3K $\delta$  group together because they can both adopt the ‘Met down’ conformation and PI3K $\alpha$  and PI3K $\beta$  group together also. While this grouping reflects the expression patterns of the Class I PI3K isoforms, it is in direct opposition to the pattern we had previously seen with other PI3K directed chemotypes which correlated with genetic (as opposed to expression) similarity. Before we had expanded on this class of inhibitors, we had noticed that compounds that inhibit PI3K $\beta$  strongly tend to inhibit PI3K $\delta$  strongly also, and that compounds that inhibit PI3K $\gamma$  tend to inhibit PI3K $\alpha$ <sup>16</sup>. This is quite evident in the PI3K $\beta$ /PI3K $\delta$  inhibitor TGX221<sup>78</sup>, and Serono’s furan-2-yl-methylene thiazolidinedione series that inhibit PI3K $\gamma$  but also have activity against PI3K $\alpha$ <sup>66</sup>. We called these enzyme pairs (PI3K $\beta$ /PI3K $\delta$  and PI3K $\alpha$ /PI3K $\gamma$ ) “pharmalogs,”<sup>16</sup> and they reflected the overall sequence identity between the PI3Ks, with PI3K $\beta$  and PI3K $\delta$  being the most closely related<sup>79</sup>. However, since these tolyl quinazolinone pyrazolopyrimidines have a different binding mode, which is dependent on the flexibility of a particular residue, it seems that flexibility is the deciding factor, and not general sequence identity.

#### *The Ideal PI3K Inhibitor for Immune Disorders*

Certain members of the alkynyl substituted series showed improved potency against PI3K $\delta$  when compared to the parent compounds SW3 and PIK293. In addition these compounds also demonstrated a different selectivity profile than did the aryl substituted tolyl quinazolinone pyrazolopyrimidines confirming our suspicion that the affinity pocket is a gateway to controlling isoform selectivity in addition to potency. As a whole, the tolyl quinazolinone pyrazolopyrimidine series is now quite special when

compared to the other standard molecules in the field as shown in figure 2.6. This series is simultaneously more potent and more selective and represents a significant step towards an ideal PI3K inhibitor for immune disorders.

Since both PI3K $\delta$  and PI3K $\gamma$  play essential non redundant roles in the majority of immune cells<sup>37-38, 46</sup>, it has been proposed that a dual PI3K $\delta$  and PI3K $\gamma$  inhibitor would be necessary to silence both “partners in crime in inflammation”<sup>37-38, 46</sup>. The first attempt at constructing a dual inhibitor, TG100-115 has already shown efficacy in a myocardial infarction injury model, and was introduced into clinical trials<sup>67, 76</sup>. In recent reviews, both Rommel and Hirsch have noted the need for a potent, and selective dual PI3K $\delta$  and PI3K $\gamma$  inhibitor that can be used to test they hypothesized synergy between PI3K $\delta$  and PI3K $\gamma$  in immune system disorders<sup>37-38, 46</sup>. Biochemically, SW14 (also SW17 and SW18) represents the realization of this goal in both potency and in selectivity for PI3K $\delta$  and PI3K $\gamma$  over PI3K $\alpha$  and PI3K $\beta$  and other lipid and protein kinases.

#### *Comparison of tolyl quinazolinone series to common PI3K scaffolds*

Presented in figure 2.6 are selected compounds representing various  $\gamma/\delta$  ratios. The strength of our compound series is due to two factors which are represented in figure 2.6. Firstly, the vast majority of the series, are extremely potent PI3K $\delta$  inhibitors, and they range from the very specific PI3K $\delta$  inhibitors SW24, SW30, to the PI3K $\delta$  and PI3K $\gamma$  dual inhibitors, SW14 and SW18 to the most potent PI3K $\delta$  inhibitor in SW13. Secondly, other compounds that inhibit PI3K $\delta$  are not nearly as specific (Fig 2.6). Inhibition of ubiquitously expressed PI3K $\alpha$  may be desirable in cancer treatments<sup>16, 37</sup>, but should be avoided, especially if a treatment for a chronic disorder is being investigated. Other

reported compounds with nanomolar  $IC_{50}$ s against PI3K $\delta$  or PI3K $\gamma$ , (AS605240<sup>75</sup>, Wortmannin<sup>75</sup>, PIK90<sup>16</sup>, and PI-103<sup>16</sup>) also have considerable activity against PI3K $\alpha$  (represented by the radius of the circle in Fig 2.6). SW13, SW14, SW19, and SW30, maintain extreme PI3K $\delta$  potency (due to affinity elements), but show varied selectivity between PI3K $\delta$  and PI3K $\gamma$  (due to differing affinity elements), yet extremely limited activity against PI3K $\alpha$  as demonstrated by the size of the circle. We believe this level of selectivity is due to the tolyl-quinazolinone selectivity element, present throughout the series. The only compounds without considerable activity against PI3K $\alpha$  are TG100-115<sup>76</sup>, and IC87114<sup>16</sup>. TG100-115, though selective, lacks potency on both PI3K $\gamma$  and PI3K $\delta$ , and our series represents a significant improvement over IC87114 in terms of PI3K $\delta$  potency, SW13 and SW30, selectivity for PI3K $\delta$  over PI3K $\gamma$ , SW30 and SW24, and inclusion of PI3K $\gamma$  inhibition SW4, SW14, and SW18. These selected compounds now represent the most potent and selective PI3K $\delta$  inhibitors reported, and the most potent and selective PI3K $\gamma$ / PI3K $\delta$  dual inhibitors

Approaching the problem of developing selective molecules by identifying and taking advantage of an inactive conformation was successful in this case<sup>16, 54, 77</sup>, and has already been shown to be successful<sup>34-36</sup>. The tolyl quinazolinone has been very useful in determining the structure of PI3K $\delta$ , and in general understanding the interplay between PI3K $\delta$  and PI3K $\gamma$  in primary human cells<sup>77</sup>. Our strategy of dividing the molecule into its constituent parts and assigning a role/activity to each one and then attempting to vary the pieces that would influence the properties we were interested in modulating also proved successful. In our attempts to increase potency and probe the properties of the pocket we made several interesting discoveries and chemical advances, all centered on the affinity



element. We discovered that substituents in the 4 position increased PI3K $\gamma$  activity, and the 3,4 (meta,para) substituent pattern increased resulted in PI3K $\delta/\gamma$  dual inhibitors, while the 3,5 fluoro-hydroxy affinity element resulted in extreme potency. These structure-activity relationships suggest that potency against PI3K $\delta$  requires the presence of a properly positioned hydrogen bond donor/acceptor and that the additional bulk provided by aryl groups in Series 1 affords activity against PI3K $\gamma$ . In general, however, large substituents were not tolerated in the affinity pocket of any of the PI3Ks. Importantly, we were also able to move away from the metabolically labile phenol in both in the PI3K $\delta$  selective with the cyclopropyl containing SW24 and in the PI3K  $\delta/\gamma$  selective series with the indole SW19. Although we lost some potency with both compounds, they maintained selectivity and were still potent enough to have effects in cells.

*Insights from the crystal structure.*

As a result of the high potency of our molecules they were used to help stabilize some crystals of PI3K $\delta$ , and were instrumental in solving the inhibitor-bound “Met-down” structure of PI3K $\delta$ , and provided direct evidence that PI3K $\delta$  does engage the methionine switch and is capable of adopting both “Met-up” and “Met-down” conformations. Although the crystal structure was unable to give us insight into the extreme potency conferred by the 3,5- fluorohydroxy affinity element, we did discover that the fluorine (and halogen) interaction with the catalytic lysine 779 was an important interaction and explained the high potency of the compounds that placed a halogen in the affinity pocket.

Close examination of the crystal structure also helped explain the precedent for hydroxyl groups in the affinity pocket of the PI3Ks. One of our collaborators from Intellikine, Yi Liu, noticed a conserved water molecule in the structure of PIK39 with PI3K $\delta$ . This conserved water molecule occupied the hydrophobic pocket, making hydrogen bonds with Asp911 and Tyr813. In the structures with the other inhibitors that project groups into the hydrophobic pocket, that water is displaced, and the hydroxyl groups on the affinity elements make the same (or a very similar) set of hydrogen bonds. Since the hydrogen bonds from the displaced water molecule are maintained, the enthalpic cost of displacement should be negligible, but the entropic gain from removing the constraints on the degrees of freedom of the water molecule probably plays a large part in the affinity gained by the addition of the appropriate affinity elements. Hydroxyl-containing affinity elements are naturally predisposed to maintaining the same set of hydrogen bonds that the water possessed, allowing water-displacement to be thermodynamically favorable.

## Chapter 3 –Cellular Characterization of Selected PI3K $\delta$ / $\gamma$ dual inhibitors

### *Confirmation of Biochemical Selectivity in THP-1 Monocytes*

The PI3K $\gamma$ / $\delta$  ratio of the compounds we synthesized covered a wide range of biochemical activity against PI3K $\gamma$  while preserving potency against PI3K $\delta$ . Out of nearly fifty compounds, SW13, SW14, SW19, and SW30 (Fig. 2.4, 2.6) were selected for characterization in cellular assays based on their potency for PI3K $\delta$  and PI3K $\gamma$  and their range of selectivity between the two targets. In order to confirm these biochemical selectivity differences in cellular signaling we sought to compare our molecules to AS605240 an established PI3K $\gamma$  inhibitor with cellular activity and extensive biochemical characterization<sup>75</sup>. We also characterized these compounds using primary human leukocytes stimulated in co-culture with different cytokine and chemokine ligands in order to determine if targeting PI3K $\gamma$  and PI3K $\delta$ , either alone or in combination, resulted in a distinct anti-inflammatory fingerprint. Subsequently, we compared selective PI3K $\delta$ / $\gamma$  inhibitors to other kinase inhibitors and clinical anti-inflammatory therapeutics.

We assessed the inhibition of PI3K $\delta$  and PI3K $\gamma$  in a cell model with a single readout by stimulating THP-1 monocytes with different ligands to activate either PI3K $\delta$  or PI3K $\gamma$ . Macrophage colony stimulating factor (M-CSF, also known as CSF-1) is a cytokine that binds to the M-CSF receptor activating RTK-linked PI3Ks<sup>80</sup> (including PI3K $\delta$ ) while the chemokine, monocyte chemoattractant protein-1 (MCP-1) activates PI3K $\gamma$  in a GPCR-mediated fashion<sup>81</sup>. Both stimuli result in phosphorylation of Akt at Ser473<sup>66, 75, 81</sup>, which was monitored by fluorescence activated cell sorter analysis (Fig.

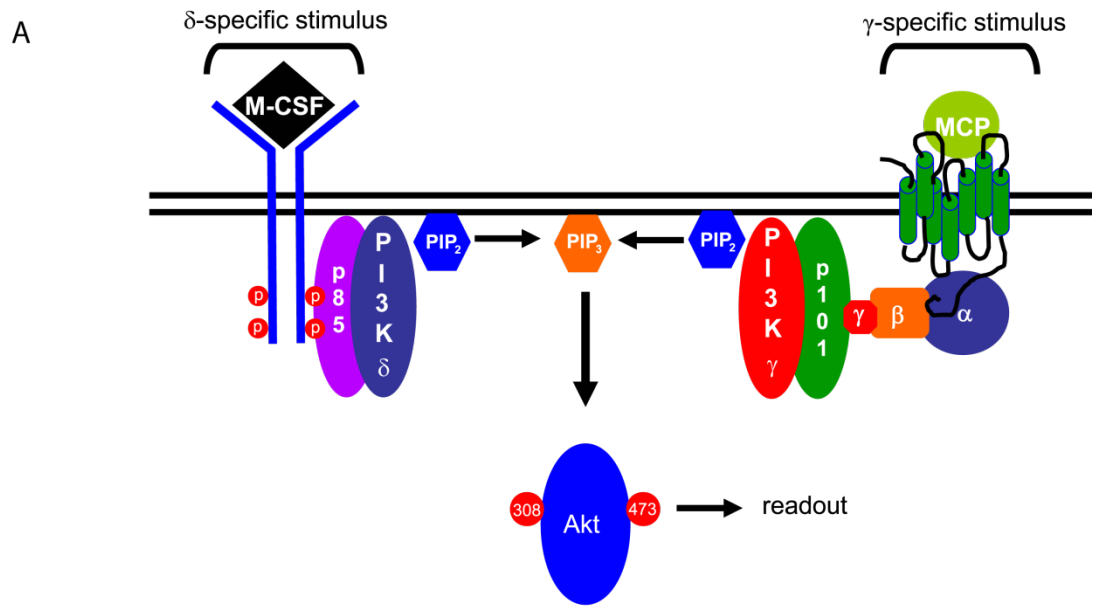
3.1A). We also included both a literature benchmark compound and a negative control compound in our analysis. AS605240, a well-characterized inhibitor of PI3K $\gamma$  that had been evaluated in a similar assay format<sup>66, 75, 82</sup>, provided a good benchmark for PI3K $\gamma$  inhibition. As a negative control, we used SW23 (Table 2.1), which had the same scaffold as the potent members of the SW series but exhibited negligible activity against any PI3K isoform.

M-CSF stimulated Ser473 p-Akt production was potently blocked by SW13, SW14, SW19 and SW30, but not by SW23 or AS605240 (Fig. 3.1B). We attribute these effects to PI3K $\delta$  inhibition because SW23 and AS605240, which did not significantly inhibit PI3K $\delta$  at the doses tested, were ineffective. Only the compounds with biochemical IC<sub>50</sub> values under 25 nM against PI3K $\delta$  were able to inhibit Ser473 p-Akt production in this assay. Further support for the role of PI3K $\delta$  in this assay came from the consistent rank order (biochemical IC<sub>50</sub> vs. cellular EC<sub>50</sub>). SW13 was most potent in the biochemical assay and was the most potent in the cellular M-CSF assay as well.

SW13, the most potent in the biochemical assays also stood out as extremely potent in this assay, and we attribute this to the potential that SW13 has to be a slow tight binding inhibitor. Compounds of this nature generally take advantage of an alternative non-catalytically active conformation in order to bind, and because of that, we believe that the more potent the SW series becomes, the less they are affected by the ATP concentration. Although part of the molecule does occupy the ATP binding site, the quinazolinone occupies another induced-fit pocket (Fig 2.2). This pocket is only seen when the quinazolinone is bound, and when Met 804 is in the down position, there is a steric clash with the ribose ring of ATP precluding ATP binding and catalytic activity

(Fig 2.1). AS605240, a compound of a different structural class and binding mode shows the expected drop in  $IC_{50}$  from biochemical data to the cellular assay<sup>63</sup>. It is also likely that SW13 was much more potent than we could actually test biochemically. We repeatedly obtained  $IC_{50}$ s under 1nM, and it was challenging to accurately determine an exact  $IC_{50}$  with our kinase assay for such a potent compound; the best we could actually do was set an upper limit on the potency. Thus, the combination of cellular potency on PI3K $\delta$  being very close to biochemical potency, and the overestimation of the  $IC_{50}$ s of our most potent compounds may serve to explain the potency shown by SW series 1 in this assay. Nevertheless, it was encouraging to see that the cellular data basically reflected the biochemical data. It is also important to note that we can conclude that the inhibition of phosphorylation of Akt is not due to the inhibition of PI3K $\alpha$  or PI3K $\beta$  because AS605240 (which routinely tested over 1 $\mu$ M in this assay), has an  $IC_{50}$  against PI3K $\alpha$  of 60nM and 270nM against PI3K $\beta$ . All of our compounds were less potent on PI3K $\alpha$  and PI3K $\beta$ , yet more potently inhibited formation of p-Akt (Fig 3.1) so we can conclude that the effect we see is solely due to their potency on PI3K $\delta$ .

Figure 3.1



B

Compound	IC <sub>50</sub> (nM)		$(\gamma/\delta)$ Ratio	
	MCP( $\gamma$ )	CSF( $\delta$ )	Cellular	Biochemical <sup>a</sup>
SW13	515	0.7	735	47
SW14	132	4.5	29.3	2.3
SW19	395	35	11.2	23
SW30	2,700	16	168	186
AS605240	117	1,400	0.083	0.026

**Figure 3.1 - Effect of selected compounds on THP-1 monocyte signaling.**

A. THP-1 monocyte signaling pathway leads to phosphorylation of Akt through either RTK-linked Macrophage Colony Stimulating Factor (M-CSF) or GPCR-linked Monocyte chemoattractant protein 1 (MCP-1).

B. pAkt was measured by FACS using fluorescent pSer473 Akt antibodies. Quantitated fluorescence was used to determine an EC<sub>50</sub> for selected compounds. Biochemical  $\gamma/\delta$  ratios are provided for comparison.

MCP-1 stimulated Ser473 p-Akt production was blocked by AS605240 and SW14, but not by SW30 or SW23. SW13 and SW19 blocked MCP-1 stimulated Ser473 p-Akt production but only at somewhat higher concentrations, in a manner consistent with the biochemical IC<sub>50</sub> values (Fig. 3.1B). SW14, the most potent tolyl quinazolinone PI3K $\gamma$  inhibitor in the biochemical assays was of equal potency with AS605240, the most potent PI3K $\gamma$  inhibitor included in our studies. The selectivity of SW30 for PI3K $\delta$  is highlighted by its lack of activity in this assay, while the inability of SW23 to inhibit p-Akt formation suggests that the activity in this assay is due to inhibition of PI3K rather than chemotype/scaffold-dependent effects. Similar to the M-CSF assay, this rank order is consistent with the biochemical potency of these compounds against PI3K $\gamma$ . Generally, the IC<sub>50</sub>s of the SW series in this assay showed the expected drop in potency<sup>63</sup>. This may signify that the order of steps necessary for inhibition is different between PI3K $\gamma$  and PI3K $\delta$ . It is possible that because PI3K $\delta$  is more flexible, the binding of the SW series to PI3K $\delta$  is regulated by the alternative conformation, and is less sensitive to ATP concentration, but with the less flexible PI3K $\gamma$ , binding is first regulated by access to the ATP pocket, after which the Met804 movement is induced.

#### *Cellular $\gamma/\delta$ ratios of selected compounds*

Whether this class of molecules is used in a therapeutic setting or just as chemical tools, it is important that they maintain their selectivity in cells. One of the more unique attributes of our compounds is the tuning up and down of the PI3K $\gamma$  inhibition, reflected in the  $\gamma/\delta$  ratio (Tables 2.1&2.2). A higher  $\gamma/\delta$  ratio shows a more selective PI3K $\delta$  inhibitor (over PI3K $\gamma$ , usually the next most inhibited PI3K). AS605240, SW19, and SW30 displayed cellular  $\gamma/\delta$  ratios within approximately 3-fold of their biochemical

ratios. On the other hand, SW13 and SW14, showed ratios that would suggest they were much more powerful PI3K $\delta$  inhibitors in cells than might be expected. Again, this may be explained by the idea of PI3K $\gamma$  IC<sub>50</sub>s being more affected by the larger amounts of ATP in the cells, and thus being higher altering the  $\gamma/\delta$  ratio. Currently, the balance of PI3K $\gamma$ /PI3K $\delta$  inhibition that will be the most beneficial is not known, and until now has been very difficult to investigate. The availability of compounds like the SW series will allow the optimal balance of PI3K $\gamma$  to PI3K $\delta$  inhibition in various diseases and disorders to be assessed through administration of a single molecular agent. In addition, this series of compounds demonstrated excellent biochemical potency and selectivity that was carried through in cells. The PI3K $\gamma$ /PI3K $\delta$  dual inhibitor SW14 was of equal PI3K $\gamma$  cellular potency with AS605240 which had already demonstrated efficacy in immune system disease models.

*Effect of PI3K $\gamma$  and PI3K $\delta$  inhibition on Neutrophil-Endothelial cell interactions.*

Neutrophils are integral to the proper function of the immune system, but also play significant roles in many autoimmune diseases<sup>83-85</sup>. Critical to neutrophil function (and neutrophil-mediated autoimmune injury) is their ability to adhere to endothelial cells and migrate through the endothelium toward inflammatory signals<sup>85</sup>.

We wanted to interrogate the entire PI3K pathway with isoform-selective and multi-targeted inhibitors to determine the individual role and combined roles of isoforms in neutrophil-endothelial cell interaction. First, we examined the effect of a set of inhibitors including PW12(PI3K $\alpha$ -directed)<sup>86</sup>, TGX-221(PI3K $\beta$ /PI3K $\delta$ )<sup>78</sup>, SW14 (PI3K $\delta$ /PI3K $\gamma$ )<sup>77</sup>, SW30(PI3K $\delta$ )<sup>77</sup>, AS605240(PI3K $\gamma$ )<sup>66, 75</sup>, PIK90(PI3K $\alpha$ ,  $\beta$ ,  $\delta$ ,  $\gamma$ )<sup>16</sup> and



LY294002(PI3K $\alpha$ ,  $\beta$ ,  $\delta$ )<sup>87</sup> on rat neutrophil adhesion to HUVEC monolayers and their effect on migration toward IL-8, a potent pro-inflammatory cytokine released by macrophages and endothelial cells <sup>88-89</sup>. Figure 3.2A shows that adhesion is primarily affected by compounds with potency against PI3K $\delta$ , while migration is significantly decreased by compounds targeting PI3K $\gamma$  (Figure 3.2B). These results, especially the latter is unsurprising because like most cytokines, IL-8 signals through a GPCR and that signal should be processed by PI3K $\gamma$  and sensitive to PI3K $\gamma$  inhibitors. Moreover, these data show that the dual PI3K $\delta$ / PI3K $\gamma$  inhibitor, SW14, appears to be more effective at reducing adhesion and migration than either AS605240 (PI3K $\gamma$  inhibition) or SW30 (PI3K $\delta$  inhibition) alone.

When these inhibitors were incubated with endothelial cells, it became quite clear that although both PIK90 and SW14 were equally effective in blocking both neutrophil adhesion and migration, PIK90 also severely compromised endothelial cell growth, as did any inhibitors with PI3K $\alpha$  or PI3K $\beta$  activity (Fig 3.2C). On the other hand, inhibition of PI3K $\delta$ , PI3K $\gamma$  or both isoforms together did not significantly affect growth. Again, this is unsurprising because both PI3K $\alpha$  and PI3K $\beta$  can process growth factor signaling in all cell types, while PI3K $\delta$  and PI3K $\gamma$  are only coupled to specific immune cell signaling pathways. This represents a significant step in understanding the confounding results seen with PI3K inhibitors in various experimental settings. Several studies have shown that the entire PI3K pathway is protective<sup>90-93</sup>, and when multi-targeted inhibitors are used, that protective effect is diminished. In actuality, it is more likely that the ubiquitous isoforms PI3K $\alpha$  and PI3K $\beta$  are protective, while inhibiting PI3K $\delta$  and PI3K $\gamma$  can actually be beneficial in limiting injurious immune responses.

*Modulation of Inflammatory Signaling in Human Peripheral Blood Mononuclear Cells (PBMCs) and Umbilical Vein Endothelial Cells (HUVECs)*

The above cellular data motivated us to assess the role of PI3K $\delta$  and PI3K $\gamma$  in inflammatory signaling by use of co-cultures of primary human cells not adapted to long-term growth *in vitro*. There were two advantages of this approach. First, human cells rather than rodent cells were used, permitting an accurate assessment of human PI3K immune signaling. Second, the *in vitro* nature of the assay allowed use of the compounds with highly distinct inhibitory profiles and minimized any pharmacokinetic/pharmacodynamic issues that arose in the transition from cell-based to animal-based models. We compared the activity of selective and pan-PI3K inhibitors using the Biologically Multiplexed Activity Profiling (BioMAP) method<sup>94-95</sup>. This assay utilized primary human cells (HUVECs alone or in combination with PBMCs), stimulated with combinations of inflammatory signals (IL-1 $\beta$ , TNF $\alpha$ , IFN- $\gamma$ , IL-4, Histamine, Lipopolysaccharide, and Superantigen) (Fig. 3.3A). The expression levels of a panel of 20 receptors, cytokines, cell adhesion molecules and second messengers (Fig. 3.3A) – were measured following stimulation and drug treatment.

Figure 3.2

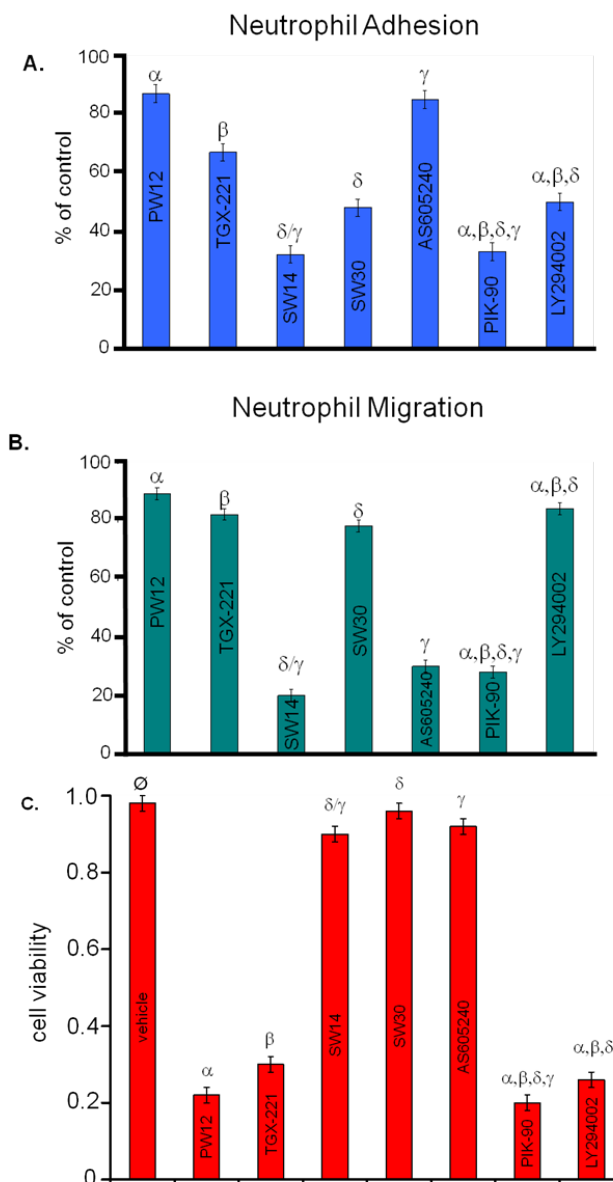


**Figure 3.2 - Effect of selected compounds on neutrophil adhesion, migration and endothelial cell proliferation**

A. HUVEC monolayers were treated with inhibitors (5  $\mu$ M for LY294002, 0.25  $\mu$ M for all others) for two hours, then rat neutrophils (stimulated with 10 ng/mL IL-8) were added. After 30 min, the monolayers were gently washed and adherent cells were counted.

B. HUVEC monolayers were grown to confluence on CoStar Transwell plates and were treated with inhibitors for two hours before neutrophils in serum free medium were added to the top well and IL-8 (10 ng/mL in serum free media) to the bottom well. After 2 hours cells in the bottom chamber were counted.

C. Cells seeded in 96 well plates (5 x 10<sup>4</sup>/well) were treated with or without inhibitors (5  $\mu$ M for LY294002, 0.25  $\mu$ M for all others) for 48 hrs. XTT labeling mixture was added to each well and absorbance was measured after an additional 6 hrs.

We evaluated pan-PI3K ( $\alpha,\beta,\delta,\gamma$ ) inhibition and PI3K $\gamma$  inhibition using PIK90 and AS605240 as benchmark compounds, while PI3K $\delta$  inhibition and dual PI3K $\delta/\gamma$  inhibition were evaluated using SW30 and SW14, respectively. Each compound was tested at a range of concentrations (Fig 3.3B) in order to identify potential off-target activities at higher doses. For each marker analyzed, a  $\log_{10}$  ratio for drug-treated protein levels vs. 0.1% DMSO-treated cells is indicated (Fig 3.3B). A  $\log_{10}$  ratio of -1.0 indicated a ten-fold decrease in protein level upon treatment with drug as compared to the levels with 0.1% DMSO. The 0.1% DMSO measurement, compiled over several donor pools provided a benchmark for the inherent variability of the assay, and was represented by the gray shading surrounding  $\log_{10}$  ratio = 0.0 in Figures 3.3 and 3.4.

#### *Effects of pan-PI3K Inhibition*

The pan-PI3K inhibitor PIK90 elicited both anti-inflammatory and anti-proliferative effects. In conditions designed to mimic T<sub>H</sub>1-driven endothelial cell-based inflammation, (HUVECs stimulated with IFN $\gamma$ , TNF $\alpha$ , and IL1 $\beta$ ) (3C; Fig. 3.3B), pan-PI3-K inhibition showed a moderate effect on human umbilical vein endothelial cell (HUVEC) viability (indicated by a reduction in sulforhodamine B (SRB) protein binding < -0.3 log ratio) and inhibited HUVEC proliferation. PIK90 also strongly inhibited the urokinase receptor (CD87/uPAR), important in tissue remodeling<sup>96</sup> and cell motility<sup>97</sup>, and HLA-DR, a surface receptor important in antigen presentation to T cells<sup>98</sup>. In HUVECs stimulated with Histamine and IL-4 (4H; Fig 3.3B), the effects of PIK90 were more subtle, showing only mild inhibition of CD62/P-selectin, a cell adhesion molecule.

When introduced to a PBMC/HUVEC co-culture stimulated with lipopolysaccharide, PIK90 exhibited little effect on cell viability but significantly reduced CD40 and mildly reduced TNF $\alpha$  production (Fig 3.3B; LPS). In PBMCs and HUVECs stimulated with superantigen, PIK90 showed modest effects on E-selectin (CD62), CCL2/MCP-1 and CD38 production, and a decrease in PBMC (mostly monocytes and T cells) proliferation (Fig 3.3B; SAg). E-selectin is a cell-adhesion molecule expressed by endothelial cells that recognizes sialylated sugars on leukocytes, and is involved in the first stages of leukocyte recruitment<sup>99</sup>. CCL2/MCP-1 is a cytokine that recruits monocytes to sites of injury<sup>100</sup>. Together, these results suggest that pan-PI3K inhibitors reduce some parameters associated with inflammation but exhibit general cytotoxicity and decreased HUVEC proliferation. These effects may significantly limit their utility for chronic conditions requiring frequent administration.

#### *Comparison of Selective PI3K $\delta$ and Selective PI3K $\delta$ /PI3K $\gamma$ Inhibition*

In contrast to the effects of pan-PI3K inhibition (PIK90), specific inhibitors of PI3K $\delta$  (SW30) or PI3K $\delta$ / $\gamma$  (SW14) had effects on inflammatory markers but little anti-proliferative activity. SW30 and SW14 showed little effect on HUVECs stimulated with inflammatory cytokines (Fig. 3.3B; 3C,4H), but were active in suppressing markers of inflammation in co-cultures of HUVEC and PBMCs stimulated with lipopolysaccharide, the bacterial cell wall component which binds Toll-like Receptor 4 (TLR4) or with superantigens, another bacterial product which universally engages the T-cell receptor (TCR) (Fig. 3.3B; LPS, SAg). The principal effect of the PI3K $\delta$  selective compound SW30 occurred under superantigen stimulated conditions (reduction of E-selectin

expression and PBMC proliferation) likely because the TCR, engaged by superantigens, is coupled to PI3K $\delta$ <sup>44, 56</sup>. PBMC proliferation decreased under the same conditions in response to SW30 and SW14, but they did not exhibit a toxic effect as read out by Alamar Blue reduction (PBMC cytotoxicity, Fig 3.3B) indicating that they can inhibit PBMC growth without inducing cell death. Together, these results suggest that PI3K $\delta$  inhibition is more selective in exerting an anti-inflammatory profile than a pan-PI3K inhibitor and may be particularly suited to treatment of disorders with a dominant T cell component.

PI3K $\delta/\gamma$  inhibition (SW14) was largely inactive in the HUVEC-only culture conditions, only slightly decreasing proliferation at the highest (10  $\mu$ M) dose (Fig. 3.3B). In the lipopolysaccharide-stimulated HUVEC/PBMC co-culture, PI3K $\delta/\gamma$  inhibition led to decrease of TNF $\alpha$  production, more so than either PI3K $\delta$  inhibition (SW30) or pan-PI3K inhibition (PIK90). When the HUVEC/PBMC co-culture was stimulated with superantigen, SW14 decreased proliferation and CCL2/MCP-1, CD38, and E-Selectin expression. An enhanced effect of PI3K $\delta/\gamma$  inhibition was observed: decreased monocyte TNF $\alpha$  production (under lipopolysaccharide stimulation) and more efficacious (magnitude) inhibition of T cell activation (E-selectin, PBMC proliferation; under superantigen stimulation). Importantly, although SW14 inhibited PI3K $\beta$  at below 1 $\mu$ M (Fig. 2.4B), related analogs (SW18, 19) with three-fold and ten-fold less PI3K $\beta$  inhibition, respectively (Fig. 2.4B, Table 2.1) exhibited similar enhanced activity. The profile of SW19 (Appendix) also provided evidence that the effects on TNF $\alpha$  were truly due to additional PI3K $\gamma$  activity, and not simply more potent PI3K $\delta$  inhibition. SW19, though less potent on PI3K $\delta$  than SW30 (Fig 2.4B), displayed moderate activity against

PI3K $\gamma$ , which was enough to exhibit the characteristic reduction of TNF $\alpha$  (Appendix) levels and cluster it with SW14, and SW18, other PI3K $\delta/\gamma$  dual inhibitors. The stronger monocyte and T cell inhibition seen with PI3K $\delta/\gamma$  inhibition may make these inhibitors particularly effective in the treatment of inflammatory disorders driven by TNF $\alpha$ .

### *Biological Activity of PI3K Inhibitors Relative to Other Agents*

Having defined a potential role for PI3K $\delta$  (SW30) in treatment of T cell-mediated inflammatory diseases and PI3K $\delta/\gamma$  (SW14) in treatment of TNF $\alpha$ -mediated inflammatory disease, we sought to put these agents in the broader context of approved anti-inflammatory agents. We compared PI3K inhibitors with different isoform selectivities to a panel of clinical and experimental compounds with anti-inflammatory (cyclosporin A, prednisolone) and anti-cancer activities. Included were CDK inhibitors (kenpaullone, olomoucine, roscovitine), microtubule disruptors (vincristine, colchicine), estrogens (17- $\beta$ -estradiol, 2-methoxyestradiol), HSP90 inhibitors (17-AAG, geldanamycin, radicicol), taxanes (epithilone B, paclitaxel), p38 inhibitors (BIRB-796, VX-745), IKK inhibitors (Ro106-9920, SC-514), JNK inhibitors (AS602801), and mTOR inhibitors (everolimus, rapamycin) (Fig. 3.5). The profiles for each compound were analyzed using a Pearson correlation metric and visualized in two dimensions through a multi-dimensional scaling algorithm<sup>95, 101</sup>.

Figure 3.3

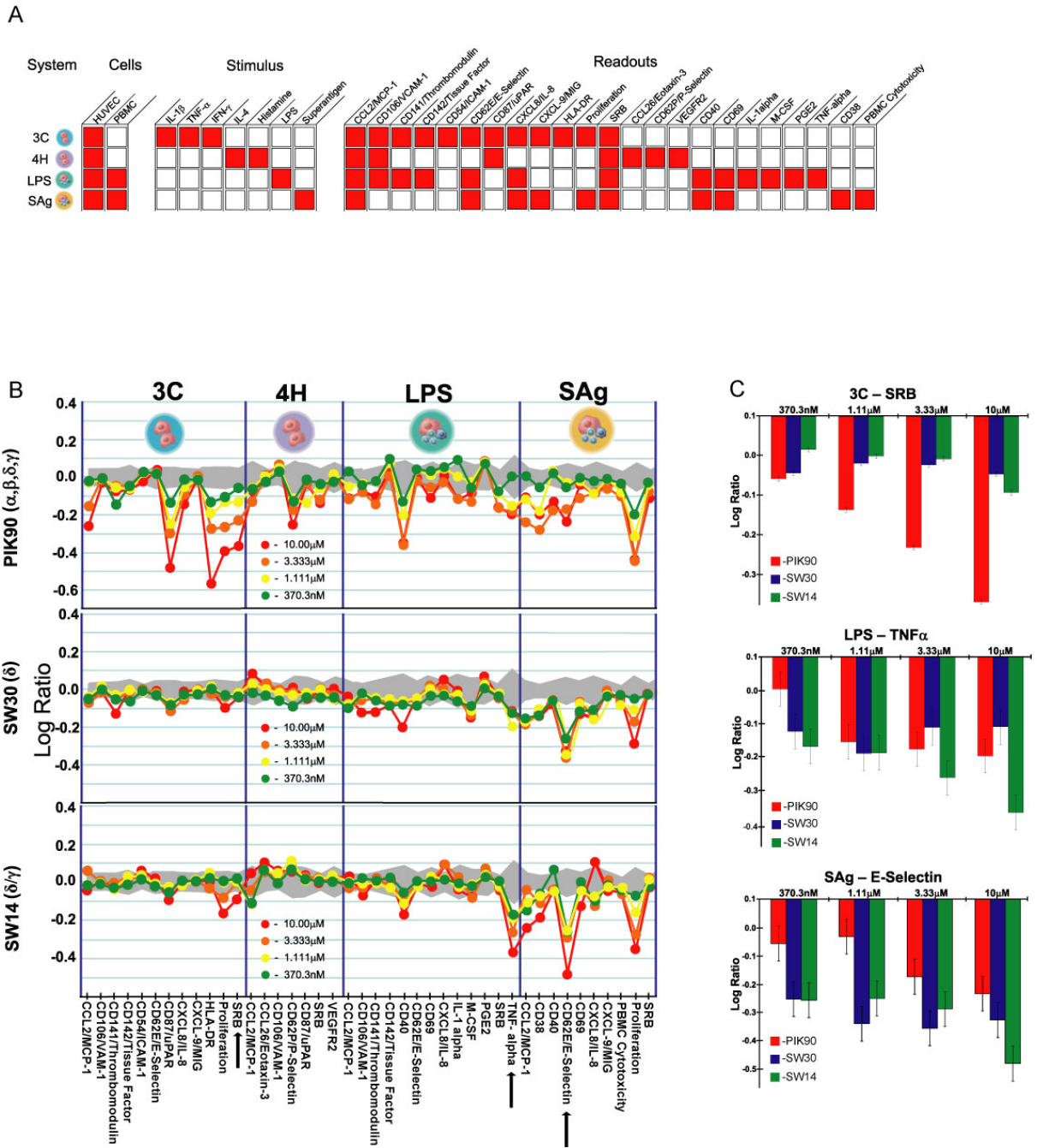


**Figure 3.3 - BioMAP Analysis of PI3K Inhibitors**

A. BioMAP Systems details.

B. BioMAP profiles for PIK90 (pan-PI3K) (top), SW30(PI3K $\delta$ ) (middle), and SW14(PI3K $\delta/\gamma$ ) (bottom). Red dots represent a 10 $\mu$ M dose, orange corresponds to 3.3 $\mu$ M, yellow represents 1.1 $\mu$ M and green represents 370nM. Levels of proteins were measured by ELISA and presented as log expression ratios [ $\log_{10}$ (parameter value with inhibitor/parameter value of 0.1% DMSO)]. The gray area represents the 95% prediction interval of the 0.1% DMSO data.



**Figure 3.4**

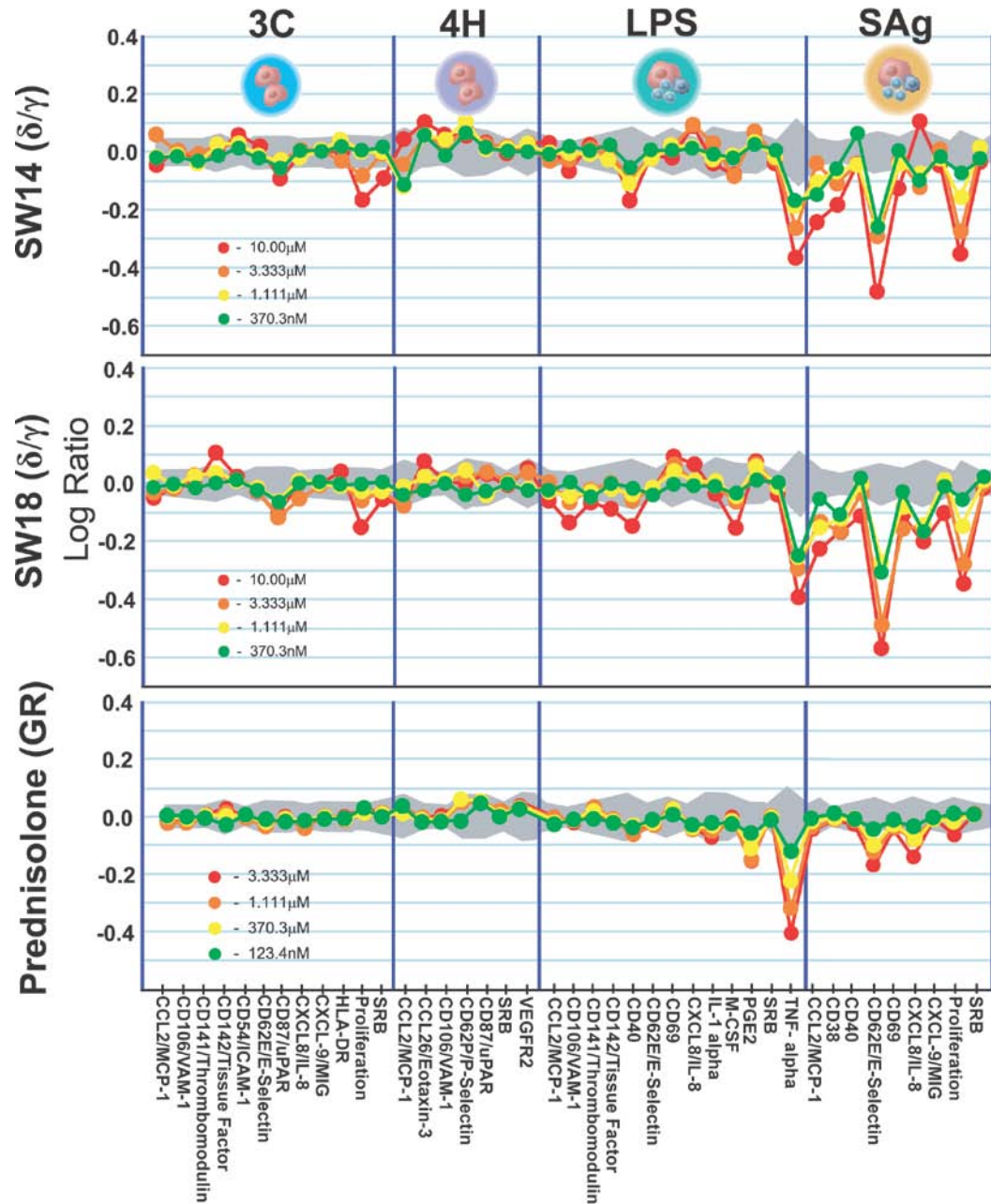


**Figure 3.4 - BioMAP Analysis of SW14, SW18, and Prednisolone**

BioMAP profiles for the PI3K $\delta$ /PI3K $\gamma$  dual inhibitor SW14 (top), the PI3K $\delta$ /PI3K $\gamma$  dual inhibitor SW18 (middle), and glucocorticoid receptor agonist Prednisolone (bottom) tested at multiple concentrations. Red circles represent the highest dose of 10.00  $\mu$ M, orange corresponds to 3.33  $\mu$ M, yellow represents 1.11  $\mu$ M and green represents the lowest dose of 370.3 nM. (For Prednisolone the doses are shifted down one concentration with Red circles corresponding to 3.33  $\mu$ M and the green circle representing a dose of 123.4 nM.) Levels of protein were measured by ELISA (as described in Materials and Methods) and presented as log expression ratios [ $\log_{10}$ (parameter value with inhibitor/parameter value of 0.1% DMSO)]. Gray area represents the 95% prediction interval of the 0.1% DMSO data.

Compounds targeting PI3K $\gamma$  and PI3K $\delta$  (SW14, SW18, SW30) occupied a distinct space in this map. The more PI3K $\delta$  selective compounds (SW30 and IC87114) clustered with lower doses of the PI3K $\delta/\gamma$  compounds, confirming our observations on their specificity. Strikingly, compounds with significant activity against PI3K $\gamma$  (SW14, SW18) were functionally linked to the glucocorticoid prednisolone, the active metabolite of prednisone. This result was supported by direct comparison of the profiles of SW14, SW18, and prednisolone, which showed significant similarities, especially with regard to their effect on TNF $\alpha$  production in the LPS-stimulated HUVEC/PBMC co-culture (Fig. 3.4). Conversely, the pan-PI3K inhibitor (PIK-90), grouped with other pan-PI3K inhibitors in a different region of the similarity map (Fig. 3.5) with inhibitors of their downstream target mTOR, microtubule modulators (another downstream target of PI3K)<sup>102</sup>, and estrogens which have also been linked to PI3Ks<sup>103-104</sup>.

A comparison of compounds that target the PI3K pathway (Fig. 3.6) showed that agents with significant PI3K $\alpha$  activity including AS605240, clustered with mTOR inhibitors. AS605240, often described as a PI3K $\gamma$  directed inhibitor, showed significant similarity to the multi-targeted inhibitors and clustered with them, likely due to its activity against PI3K $\alpha$  (Fig 3.6).

#### *Identifying roles for PI3K $\delta$ and PI3K $\gamma$*

Several PI3K inhibitors with different isoform selectivities were tested in primary human cell models of inflammatory signaling. Pan-PI3K inhibition (PIK90) was highly anti-proliferative to both HUVECs and PMBCs whereas PI3K $\delta$  inhibition (SW30) or PI3K $\delta/\gamma$  inhibition (SW14) resulted in selective T cell inhibition. Selective PI3K $\delta$

inhibition (SW30) blocked T cell cytokine production, resulting in decreased HUVEC E-selectin expression and revealing the potential to elicit a potent anti-inflammatory response without a direct effect on endothelial cells. Interestingly, SW30 and other selective PI3K $\delta$  inhibitors such as IC87114 (Appendix) did not inhibit E-selectin expression in HUVECs directly stimulated with IFN $\gamma$ , TNF $\alpha$ , and IL1 $\beta$  (3C; Fig 3.3B) but only did so in the superantigen-stimulated HUVEC/PMBC co-culture conditions (SAg; Fig 3.3B, Appendix). This result was consistent with these compounds *indirectly* blocking E-selectin expression in HUVECs as a result of lymphocyte TNF $\alpha$  production inhibition (TNF $\alpha$  is known to rapidly upregulate E-selectin expression in HUVECs<sup>105</sup>), and these data clearly illustrated the ability of these assays to capture parts of the intercellular communication integral to inflammatory responses.

When many cell-types are present, context becomes extremely important. For example, Puri and coworkers previously noted that although PI3K $\delta$  inhibition partially blocks neutrophil adhesion to the endothelium<sup>24</sup>, it does so without affecting E-selectin expression<sup>42</sup>. Close inspection reveals that E-selectin expression was only assayed in endothelial cells<sup>42</sup>. We confirmed the ineffectiveness of PI3K inhibition on E-selectin production within the 3C system (consisting only of endothelial cells), but in the multicellular SAg system (endothelial cells and PBMCs), we were able to depress E-selectin expression (SAg; Fig 3.3B, Appendix). This suggests a dual role for PI3K $\delta$  in neutrophil adhesion. Firstly, there is expression of E-selectin which we can affect in a multicellular context, and secondly there is the neutrophil response to E-selectin, which Puri demonstrated is controlled at least partially by PI3-K $\delta$ <sup>42</sup>.

PI3K $\delta/\gamma$  inhibition (SW14) was not cytotoxic to HUVECs and displayed more significant anti-inflammatory effects in the HUVEC/PBMC co-cultures. Dual targeting of PI3K $\delta/\gamma$  resulted in enhanced inhibition of LPS-induced TNF $\alpha$  production and overall T cell activation. The inhibitory effects observed with inhibition of PI3K $\delta/\gamma$  in these assays led us to wonder whether they were due to synergistic inhibition of PI3K $\delta/\gamma$  or whether PI3K $\gamma$  inhibition might be sufficient. Unfortunately, the most commonly used PI3K $\gamma$  compound in the literature, AS605240, inhibited all PI3K isoforms at 300nM<sup>75</sup>, and in the primary human cell assays displayed a profile similar to pan-PI3K compounds (Fig. 3.6; Appendix).

Our studies using both new and benchmark compounds show that of the isoform combinations currently available, the most effective anti-inflammatory PI3K inhibitor is one that inhibits both PI3K $\delta$  and PI3K $\gamma$ . Pan-PI3K inhibitors, on the other hand, demonstrated limited effects on anti-inflammatory markers in T cell and monocyte-driven environments with concurrent anti-proliferative effects. Nevertheless, it remains possible that selectively inhibiting other combinations of PI3K isoforms, for instance PI3K $\delta$  and PI3K $\beta$ , may also show synergistic anti-inflammatory activity.

Figure 3.5

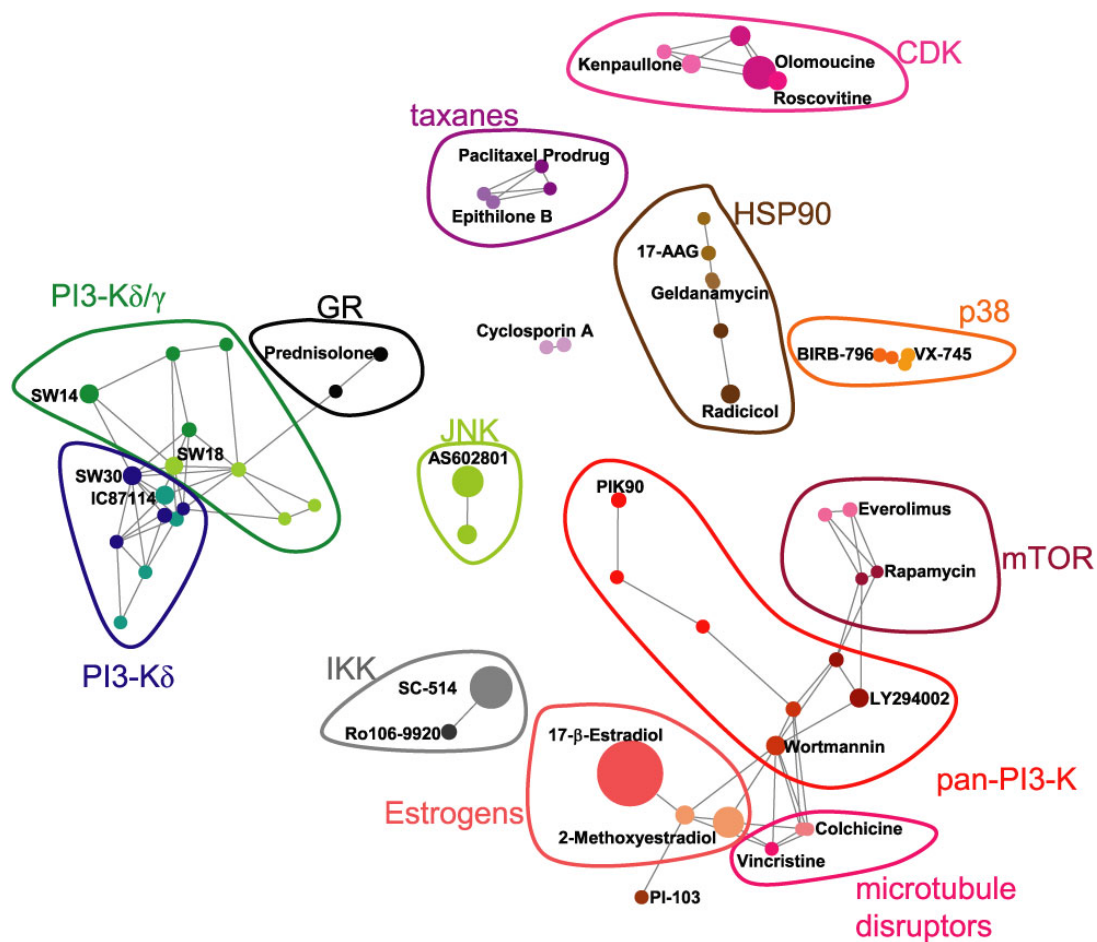


**Figure 3.5 - Function Similarity Map of PI3K inhibitors and other compounds.**

A Function Similarity Map of compounds from the SW series with other anti-inflammatories, PI3K inhibitors, and kinase inhibitors. This map is generated by subjecting the pairwise correlation data of BioMAP profiles to multidimensional scaling. Significant correlations are shown by gray lines. The distance between the compounds is inversely related to the similarity of their profiles. Compounds are color-coded, grouped by target class, and the area of the circle is proportional to the dose.

Figure 3.6

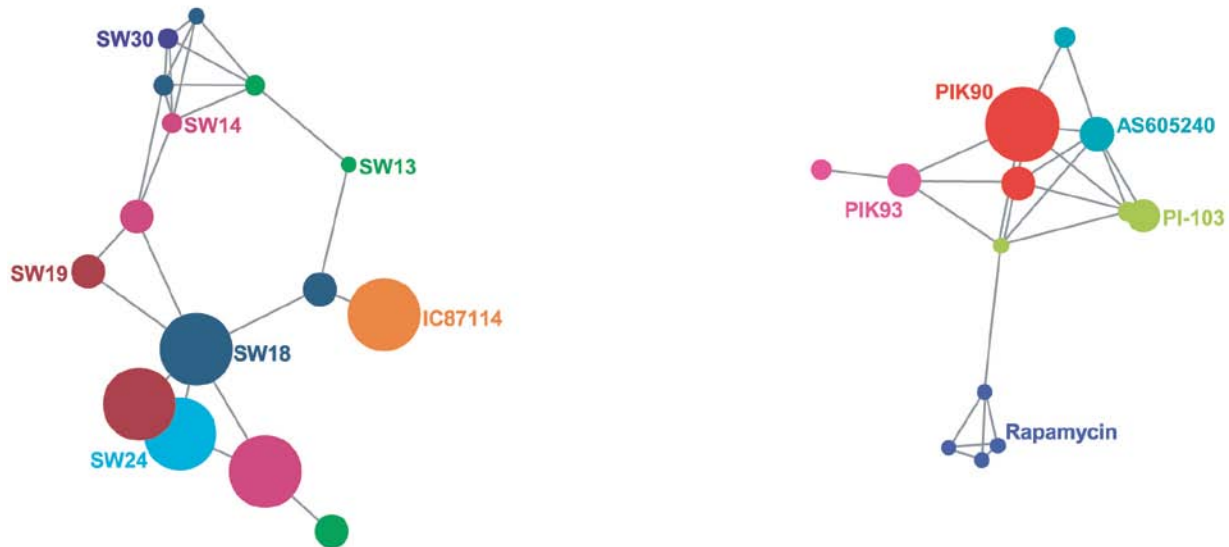


**Figure 3.6 - Functional Similarity Map of PI3K pathway inhibitors.**

A Functional Similarity Map of compounds in this work alongside other PI3K inhibitors. This map is generated by subjecting the pairwise correlation data of BioMAP profiles to multidimensional scaling. Significant correlations determined as described in Materials and Methods are shown by gray lines (FDR = 2%). The distance between the compounds is inversely related to the similarity of their profiles. Each compound is a different color. Compounds were tested at multiple concentrations with the area of the circle proportional to the dose

Interestingly, additional inhibition of PI3K $\alpha$  and PI3K $\beta$  (PIK90) did not further suppress inflammatory markers (Fig. 3.3B; LPS, SAg). In fact, when comparing the effects on E-selectin expression (SAg), selective inhibition of PI3K $\delta$  alone was more effective than pan-PI3K inhibition, but inhibition of PI3K $\delta/\gamma$  was the most effective (Fig. 3.3B; SAg). The most effective isoform combination at inhibition of LPS-induced TNF $\alpha$  production was also PI3K $\delta/\gamma$  (Fig. 3.3B; LPS). Additional PI3K $\alpha/\beta$  inhibition (PIK90), in addition to displaying undesirable anti-proliferative properties, did not significantly decrease TNF $\alpha$  expression and was identical to selective PI3K $\delta$  inhibition (Fig. 3.3B; LPS). These results together suggest a possible role for PI3K $\gamma$  in TNF $\alpha$  production.

Multiple routes through which PI3K $\gamma$  could regulate TNF $\alpha$  production exist. PI3K $\gamma$  interacts with phosphodiesterase 3B (PDE3B), regulating cyclic AMP (cAMP) levels and activation of protein kinase A (PKA), leading to increased heart contractility<sup>21</sup> and was also linked to PDE4<sup>106</sup>. PDE4 is the main cAMP hydrolyzing enzyme in immune cells, and has been pursued as a target for generating novel anti-inflammatories<sup>107</sup> that suppress LPS-induced TNF $\alpha$  production in monocytes<sup>108</sup>. Since PI3K $\gamma$  is required for PDE4 activity<sup>106</sup>, PI3K $\gamma$  inhibition may lead to diminished PDE4 activity and explain the TNF $\alpha$  suppression. However, the first link between PDEs and PI3K $\gamma$  involved a scaffolding, non-catalytic effect<sup>21</sup> and the PDE4-PI3K $\gamma$  link was discovered in a PI3K $\gamma$  knockout mouse<sup>106</sup>, which has no functional PI3K $\gamma$  so there is currently little evidence to suggest that PI3K $\gamma$  catalytic activity is regulating TNF $\alpha$  levels through PDE4.

TNF $\alpha$  is involved in several autocrine signaling loops <sup>109</sup> and it is possible that PI3K $\gamma$  is involved in amplifying such signals. TNF $\alpha$  activates PI3K $\gamma$  in endothelial cells leading to oxidant generation and NF- $\kappa$ B activation <sup>110</sup>. NF- $\kappa$ B also regulates production of TNF $\alpha$  <sup>111</sup> so TNF $\alpha$  may activate its own production by activating NF- $\kappa$ B through PI3K $\gamma$ . TNF $\alpha$  can upregulate its own mRNA synthesis in keratinocytes <sup>109</sup>, and if this happens in PBMCs, it provides an attractive model for PI3K $\gamma$  involvement in TNF $\alpha$  production and may explain why PI3K $\gamma$  inhibition lowers TNF $\alpha$  levels.

In broad terms, PI3K signaling can be divided into two pathways, a survival pathway ( $\alpha/\beta$ ) and inflammatory PI3K ( $\delta/\gamma$ ) pathway, yet inhibitors that target both units can lead to functional antagonism. For example, inhibition of PI3K $\delta/\gamma$  by SW14 resulted in suppression of E-selectin and TNF $\alpha$  but additional inhibition of PI3K $\alpha/\beta$  using PIK90 actually resulted in a smaller degree of suppression (Fig. 3.3B). This result highlighted the fact that targeted chemical inhibition can access information not available from genetic inactivation of one or more PI3K isoforms in knockout mice, which are difficult to obtain and can often suffer significant defects during development. Furthermore, results obtained using targeted inhibitors can be different from those obtained in animals with sustained genetic inactivation. PI3K $\delta$ /PI3K $\gamma$  knockout mice exhibited a more severe immune phenotype than mice lacking either isoform alone,<sup>25-26</sup> but the severity of that phenotype is likely due to sustained absence of both PI3K $\delta$  and PI3K $\gamma$  and may not be duplicated with pharmacological treatment.

Many clinical anti-inflammatory agents function through different targets yet all have the property of inhibiting immune cell function while leaving non-immune cells relatively unaffected. We asked if the PI3K $\delta/\gamma$  inhibitors exhibited this property and



which current anti-inflammatory agents they might resemble. The most closely related profile was that of the glucocorticoid receptor (GR) agonist, prednisolone. It is interesting that a particular multi-cellular profile can be achieved through two distinct mechanisms (kinase inhibition vs. nuclear hormone receptor activation). Although prednisolone is an effective anti-inflammatory agent, there have been efforts to identify “dissociating GR agonists” that separate anti-inflammatory from other GR effects (bone loss, cardiovascular disease) that limit their long term use <sup>112</sup>. The discovery that PI3K $\delta/\gamma$  inhibition can functionally mimic several anti-inflammatory features of prednisolone opens a new way to improve upon a proven class of anti-inflammatories (GR agonists) while targeting completely different enzymes, and could only have been realized through analysis of this compound series on primary human cells.

Despite the related responses of prednisolone and PI3K $\delta/\gamma$  inhibitors, the similarities may be limited to the cell types we analyzed. Cell types which have documented GR agonist responses (macrophages, coronary artery cells) were not included in our assays. The exceptionally broad cellular effects of GR agonists would likely be distinguished from PI3K $\delta/\gamma$  inhibitors if more cell types were analyzed. Despite these caveats, the use of primary human cells provides a powerful early assessment of differential inhibition of important signaling nodes (PI3Ks, nuclear receptors, JNKs, calcineurin, IKK).

With the new availability of small molecules capable of inhibiting the inflammatory PI3Ks ( $\delta/\gamma$ ) without inhibition of the ubiquitous growth-linked PI3Ks we are poised to begin to resolve the opposing effects of pan-PI3K inhibition and selective

inflammatory PI3K inhibition and to begin further validation of PI3K $\delta/\gamma$  as a target for the treatment of inflammatory disorders.

*Investigating the use of PI3K $\delta/\gamma$  dual inhibitors as a potential sepsis treatment*

Another of the inflammatory disorders we attempted to investigate was sepsis, a systemic unchecked inflammatory response to infection. In sepsis, the immune response becomes hyperactive and many inflammatory cells (mast cells<sup>113-115</sup>, macrophages<sup>116</sup>, and neutrophils<sup>113, 115, 117</sup>) contribute to the generation of a “cytokine storm” via release of excessive amounts of inflammatory mediators<sup>118</sup>, that often result in significant hemodynamic compromise and can cause multisystem organ failure and death if not treated promptly<sup>119</sup>. While it is clear that neutrophils and macrophages play an important role in this process, the role of mast cells in this immune response to infection is disputed. Originally thought of as solely contributing to allergic and anaphylactic response, it is now thought that mast cells also recognize infection and recruit other immune cells to the site of infection<sup>120-122</sup>. Based on this hypothesis, it was believed that mast cells would be protective in sepsis by engaging the innate immune response. However, in 2004, Wolters and coworkers showed that a particular mast cell product, Dipeptidyl peptidase I (DPPI), was harmful to the host in a bacterial peritonitis model of sepsis<sup>114</sup>. Interestingly, knocking out DPPI resulted in increased survival, despite increased bacterial loads confirming that the mortality was not directly the result of bacteria in the system, but rather the unchecked immune response. The detrimental effect of DPPI was found to be mediated through IL-6, a cytokine secreted by several immune cells<sup>114</sup>.

Since mast cell degranulation is dependent on both the activity of PI3K $\delta$  and PI3K $\gamma$ <sup>48-49</sup>, interfering with mast cell degranulation with our compounds is predicted to modify the complicated mediator balance in sepsis. We hypothesized that mast cell degranulation was detrimental to survival in mouse sepsis models, and that prevention of degranulation could reduce the severity of the “cytokine storm” during sepsis. When mast cells degranulate, they release several pro-inflammatory cytokines which serve to recruit other cytokine-secreting cells<sup>123</sup>. This degranulation process, which we believed to be the start of the cytokine storm that characterizes sepsis, has been shown to be dependent on both the activity of PI3K $\delta$  and PI3K $\gamma$ <sup>48-49</sup>. Blocking either isoform limits (but does not completely inhibit) the extent of mast cell degranulation<sup>48-49</sup>. We wanted to determine what level of PI3K $\gamma$  inhibition (in addition to PI3K $\delta$  inhibition) was necessary for the complete abrogation of mast cell degranulation and then by preventing mast cells from degranulating completely with various small molecule inhibitors we planned to ask if this approach increased survival in a mouse model of sepsis.

In our initial experiments with mouse mast cells, the mast cells were sensitized overnight with DNP-IgE, and then stimulated with the same ligand in the presence of our inhibitors. We included AS605420 and IC87114 as controls, as they had been previously shown to inhibit degranulation in a similar assay<sup>50</sup>. The mouse mast cells we used were extremely sensitive and despite several series of careful attempts, kept degranulating before sensitization and stimulation, rendering our efforts to replicate the published results futile.

Nevertheless, we were confident in the biochemical profile of our compounds. We next attempted to test the effectiveness of our best PI3K $\delta/\gamma$  dual inhibitor, SW14, in a

*Klebsiella pneumonia* infection mouse model of sepsis. After inoculating the mice, we treated them once a day with 15mg/kg of SW14 (in PBS with 1%DMSO) or a 1% DMSO in PBS control delivered intraperitoneally. The results were less than encouraging, with all but one of the mice dying by the third day. Interestingly, the sole surviving mouse did receive SW14, but we could not draw conclusions from just one surviving mouse. We tried several different vehicles to solubilize the SW series, and though some were more effective than others, all vehicles tended to adversely affect survival in mouse sepsis models because of the severity of the sepsis induced. The SW series was not soluble in the mildest vehicle (PBS) and even with DMSO only formed a sticky suspension, and we believe even the small percentage of DMSO had a detrimental effect on survival that may have offset any survival benefit conferred by SW14. In addition, we know that the fluorophenol present on SW14 can be a metabolic liability which would most likely result in increased clearance of SW14.

After considering the failure and the experimental complexities of the mast cell experiments, we decided that using the SW series in mouse models of sepsis was not a promising step forward. Concurrently, the biochemical profile of the SW series was generating several collaborations, and the series has ultimately proven to be useful in determining specific roles of PI3K isoforms in many systems.

#### *Using PI3K $\delta$ $\gamma$ inhibitors to elucidate fine points of PI3K signaling*

We collaborated with David Pearce's lab in order to determine which PI3K isoform was responsible for controlling epithelial Na<sup>+</sup> transport. This transport shares some similarities with insulin dependent glucose metabolism, and both were inhibited by

nonspecific PI3K inhibitors LY294002 and wortmannin<sup>124-126</sup>. We had previously used a panel of selective PI3K inhibitors to determine the role of PI3K $\alpha$  in insulin signaling<sup>16</sup>, and we used a similar approach to dissect which of the PI3K isoforms inhibited by LY294002 and wortmannin was actually responsible for controlling sodium transport via the epithelial Na<sup>+</sup> channel. Specifically, a multitargeted but class I selective PI3K inhibitor, PIK90, was used to determine if inhibition of class I PI3Ks had an effect. Once that was determined, SW14 and SW30 were used as selective PI3K $\delta$  and PI3K $\delta/\gamma$  dual inhibitors to determine if PI3K $\delta$  or PI3K $\gamma$  played a role and TGX 221 was used as a selective PI3K $\beta$  inhibitor. This method provided complete coverage of the class I PI3Ks, and clearly demonstrated a role for only PI3K $\alpha$ , and no other isoforms in epithelial sodium transport<sup>126</sup>. SW14 and SW30 were also used by Hamm in her investigation of which PI3K isoforms were involved in protease activated receptor (PAR) 1 and PAR4 mediated platelet aggregation<sup>127</sup>. Together their use indicated PAR4 and PAR1 to some extent required PI3K $\gamma$  but not PI3K $\delta$  activity<sup>127</sup>.

We collaborated with Gerry Krystal who studies hematopoietic-restricted SH2-containing inositol polyphosphate-5-phosphatase (SHIP). He noticed that SHIP was upregulated in bone marrow macrophages and mast cells after stimulation with LPS and cytosine-phosphate-guanosine (CpG) DNA motifs. Both LPS and CpG are recognized by TLRs as pathogen associated molecular patterns (PAMPs) that serve as markers of bacterial infection (and sometimes viral infection in the case of CpG). The LPS and CpG mediated increase in SHIP activity led to tolerance of LPS, preventing sensitization to LPS, and CpG and decreasing subsequent IFN- $\beta$  production, and this action was presumed to be due to SHIPs direct inhibition of the PI3K pathway. However it was not

known which PI3K isoforms contributed to the LPS and CpG responses, and Krystal and colleagues were unable to use any genetic methods because of the complexities previously discussed in chapter 1. PI3K $\delta$  and PI3K $\gamma$  were expected to play a role because they share the same limited expression profile as SHIP, and in order to determine their level of involvement in comparison to the other Class I PI3Ks we used a panel of selective PI3K inhibitors including SW18 and SW30.

The results implicated PI3K $\delta$  and PI3K $\gamma$  in cellular responses to CpG and LPS, specifically in IL-6, IFN $\beta$  and TNF $\alpha$  production<sup>128</sup>. The latter result was also replicated in our BioMAP results<sup>77</sup> (Figs 3.3 & 3.4) and confirmed that PI3K $\delta$ /PI3K $\gamma$  dual inhibition significantly decreased LPS induced TNF $\alpha$  production. The results also suggested that it was SHIPs negative regulation of PI3Ks, including PI3K $\delta$  and PI3K $\gamma$  that led to decreased IFN $\beta$  production which was truly responsible for blocking sensitization to LPS and CpG.

The SW series was also used by Kevin Shannon's lab to rule out PI3K $\delta$ 's contribution to ERK phosphorylation. Recently, the Shannon lab discovered a previously unknown link between PI3K and ERK. Originally, PI3K was thought to act only downstream of Ras, a small GTPase involved in many signaling cascades, in a pathway parallel to ERK. However the Shannon lab established a link between PI3K and Ras, through the action of phospholipase C $\gamma$ . They discovered that under GM-CSF stimulation, multi-targeted PI3K inhibition influenced Ras activity and subsequently inhibited ERK phosphorylation. Thus, the canonical downstream effector of Ras, PI3K, under certain conditions also acted upstream of Ras, influencing ERK activity. The Shannon lab needed to isolate which isoform of PI3K was acting upstream of Ras, and

they used a large panel of PI3K inhibitors, including SW13, SW14, SW18 and SW30 to determine if they could establish a link between PI3K $\delta$  or PI3K $\gamma$  and ERK phosphorylation. Ultimately, they were able to rule out the involvement of both PI3K $\delta$  and PI3K $\gamma$  in the regulation of Ras, and the evidence now only supports a role for PI3K $\alpha$  in that process.

## Chapter 4 –Design Rationale, Synthesis, Biochemical, and Cellular Characterization of a new series of PI3K inhibitors.

### *Design Rationale and synthesis of DL series*

Having explored the limits of the tolyl-quinazolinone scaffold, and appended both aryl and alkynyl groups to the scaffold, we realized that there was an area of chemical space that we had not yet probed. Prompted by the success of SW series 2 (Fig 2.4) and its emergent properties, we wanted to determine the effect of replacing the tolyl-quinazolinone selectivity element with a smaller group. Pyrazolopyrimidines with isopropyl, cyclobutyl, and other smaller R1 substituent groups have previously been shown to inhibit lipid kinases, but all had an aryl group in the R2 position<sup>64</sup> (Fig 4.1). We sought to investigate the properties of pyrazolopyrimidines with small R1 substituents and alkynyl linked affinity elements. Previous work in the Shokat laboratory suggested that protein kinases favored smaller R2 groups, while lipid kinases could tolerate larger R2 groups, and we believed that the extra length of the alkynyl linkage would preclude protein kinase binding<sup>64</sup>.

Extensive work exploring the SAR with aryl pyrazolopyrimidines had already been done, yet we noticed significant differences between the SAR of our tolyl quinazolinone aryl pyrazolopyrimidines (SW series 1), and that of our tolyl quinazolinone alkynyl pyrimidines (SW series 2), and we believed that the different properties engendered by the alkynyl linkage would be sustained despite the replacement of the tolyl quinazolinone with a smaller substituent. It had already been determined that small changes in the pyrazolopyrimidine structure led to very different activities on different targets<sup>64</sup>, so we planned to take advantage of this observation and expected our



synthetic efforts to yield molecules with activities highly divergent from the previous sets of pyrazolopyrimidines synthesized in the Shokat laboratory.

We explored isopropyl and cyclopentyl groups in the R1 position, and sought to achieve diversity through the R2 element substitutions. We joined BA19 to isopropyl iodide or iodocyclopentane in the presence of  $K_2CO_3$  and DMF to yield the iodinated pyrazolopyrimidines BA12 and BA80 respectively (Scheme 4.1). We then subjected both BA12 and BA80 to the palladium catalyzed Sonogashira coupling reaction with propargyl alcohol, yielding DL01 and DL03, which only differed in the R1 position (Table 4.1). DL01 was tested against all four class I PI3Ks, and only had significant activity against PI3K $\delta$  with an  $IC_{50}$  of 67nM. Surprisingly, the next most inhibited PI3K was not PI3K $\beta$  ( $IC_{50} = 15\mu M$ ), as would have been expected from previous data<sup>16</sup>, or PI3K $\gamma$  ( $IC_{50} = 1.9\mu M$ ), which would have been expected with a tolyl quinazolinone in the R1 position<sup>77</sup>, but rather PI3K $\alpha$ , with an  $IC_{50}$  of 933nM. DL03 displayed  $IC_{50}$ s larger than 6 $\mu M$  against all PI3Ks, suggesting that the bulkier cyclopentyl in the R1 position negatively affected binding.

Figure 4.1

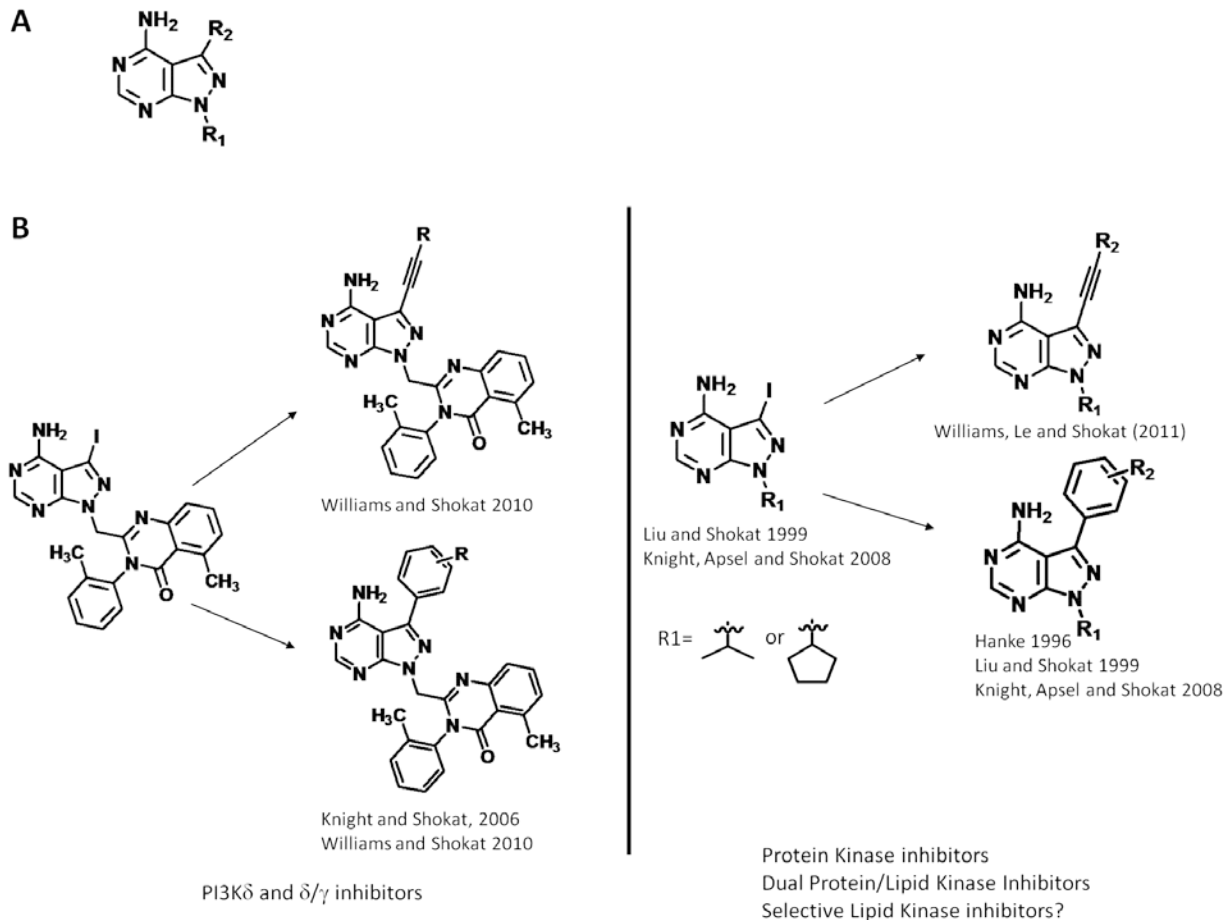


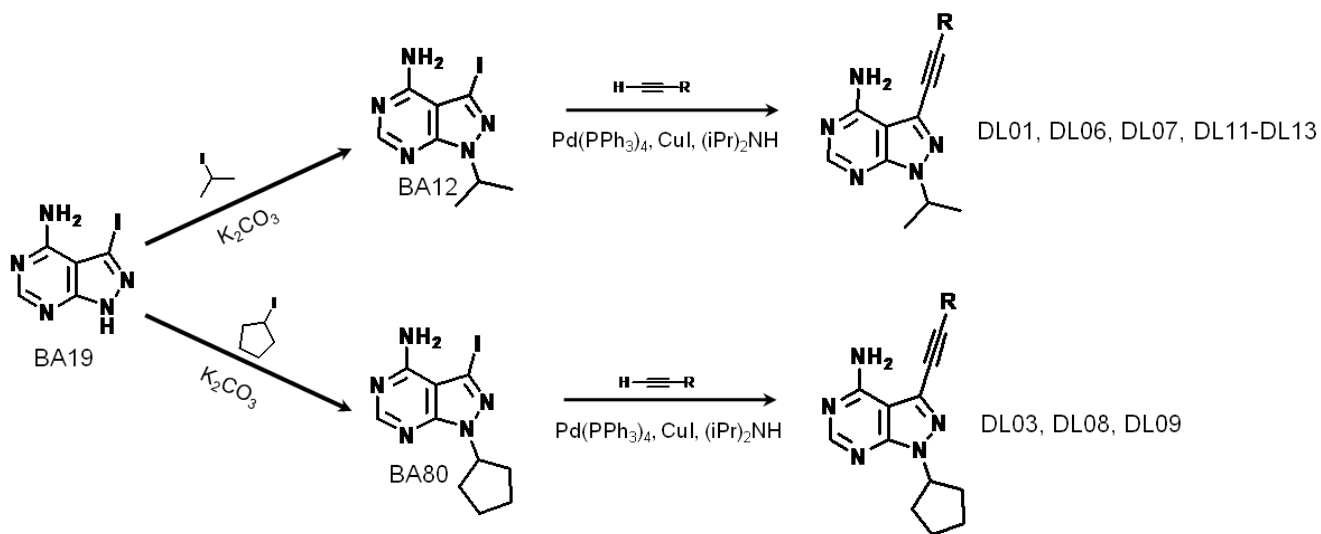
**Figure 4.1 – Pyrazolopyrimidines as multifaceted kinase inhibitors.**

A. The pyrazolopyrimidine scaffold can be modified to yield both protein and lipid kinase inhibitors depending on the substituents in the R1 and R2 positions.

B. Left panel – With a tolyl quinazolinone R1 substituent, PI3K $\delta$  and PI3K $\delta/\gamma$  inhibitors can be constructed from iodinated pyrazolopyrimidines with Palladium-catalyzed reactions<sup>16, 77</sup>.

Right Panel – Pyrazolopyrimidines with small alkyl R1 groups and alkynyl R2 substituents have not been published yet, but were the next logical synthetic steps following the success of the alkylnyl substituted tolyl quinazolinone pyrazolopyrimidines.

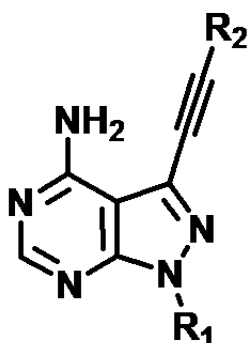
## Synthetic Scheme 4.1



### Scheme 4.1 - Synthesis of alkynyl substituted isopropyl and cyclopentyl pyrazolopyrimidines

All Reactions were conducted under argon at room temperature. Alkylation of BA19 proceeded in DMF under reflux conditions, while coupling reactions were at room temperature.

Table 4.1



Name	R <sub>1</sub>	R <sub>2</sub>	IC <sub>50</sub> μM (10 μM ATP)			
			PI3K $\alpha$	PI3K $\beta$	PI3K $\gamma$	PI3K $\delta$
DL01			0.933	15	1.9	0.067
DL03			>6	>6	>6	>6
DL06			0.053	0.664	0.113	0.040
DL07			0.034	0.316	0.069	0.021
DL08			>6	>6	2.3	1.2
DL09			0.045	0.568	0.194	0.030
DL11			>6	>6	>6	>6
DL12			>6	>6	>6	>6
DL13			>6	>6	>6	>6

**Table 4.1 - Structures and Biochemical IC<sub>50</sub>s for DL Series against Class I PI3Ks.**

Potent (IC<sub>50</sub><50nM) compounds are shaded in red while moderately potent compounds (IC<sub>50</sub> 50-100nM) are shaded in orange. DL03 and DL08, shaded in blue, differ from their more potent counterparts DL01 and DL06 only by the bulkier R<sub>1</sub> substituent which caused them to lose activity.

In order to more completely cover the chemical space, we next attempted to couple to a slightly larger group, but maintained the isopropyl in the R1 position to increase our chances of developing more potent molecules. We subjected BA12 to a Sonogashira coupling with 3-ethynylpyridine to yield DL06, and with 3-Hydroxyphenylacetylene to yield DL07. Our previous SAR suggested that these groups might be too large for the PI3K affinity pocket<sup>77</sup>, but it was important to develop new SAR with new smaller R1 substituents since the pyrazolopyrimidine's scaffold had been quite responsive to small changes in structure in the past, yielding very different activities with minimal structural changes<sup>64</sup>. Both of the bulkier substituents were tolerated well and both DL06 and DL07 were more potent than DL01 against the class I PI3Ks (Table 4.1). As with DL01, both DL06 and DL07 displayed the highest potency on PI3K $\delta$  followed by PI3K $\alpha$ , PI3K $\gamma$  and lastly PI3K $\beta$ . DL07's phenol provided the capability to simultaneously donate and accept hydrogen bonds, and was most likely better positioned than DL01's hydroxyl group as evidenced by the higher potency of DL07 overall. Replacement of the phenol moiety with a pyridinyl moiety (DL06) afforded a less potent compound, with IC<sub>50</sub>s generally twice that of DL07 (Table 4.1).

Encouraged by the increased potency of the bulkier R2 substituents, we next wanted to confirm whether the larger cyclopentyl group would negatively affect potency under the context of the same R2 groups. We subjected BA80 to a Sonogashira coupling with 3-ethynylpyridine to yield DL08, and with 3-Hydroxyphenylacetylene to yield DL09. The resultant IC<sub>50</sub>s confirmed our previous hypothesis that the cyclopentyl group was probably too large and did not provide optimal inhibition of the class I PI3Ks. DL08 was significantly less potent than DL06 against the class I PI3K isoforms with all IC<sub>50</sub>s

over 1 $\mu$ M, and the potency pattern was also altered, with PI3K $\delta$  and PI3K $\gamma$  being the most inhibited. Although DL09 retained significant potency against PI3K $\delta$  (30nM) and PI3K $\alpha$  (45nM), it was still at least 2-fold less potent than DL07. These data suggested that the alkynyl linked phenol served to drastically increase potency to a level unmatched by the other substituents we had tried on this particular scaffold, overcoming even the shortcomings of the cyclopentyl R1 group and reminiscent of the fluorophenol substituent on SW13.

With the next set of molecules we synthesized, we attempted to determine whether size or proper positioning of hydrogen bonding groups was more important in the R2 substituents for PI3K binding. We had already established that the cyclopentyl group would not provide the potency we needed so we kept the isopropyl as the R1 substituent. We subjected BA12 to a Sonogashira coupling with 2-ethynylaniline to yield DL11, with cyclopentylacetylene to yield DL12, and with 1-ethynylcyclopentanol to yield DL13 (Table 4.1). All three resultant molecules had little activity against the class I PI3Ks with IC<sub>50</sub>s of greater than 6 $\mu$ M. This suggested that mere bulk in the R2 substituent was not sufficient for PI3K activity, but as has been shown in the past the PI3K affinity pocket preferred strategically placed hydroxyl groups, or groups that could provide geometrically appropriate hydrogen bonds to key residues within the pocket<sup>16, 74, 77</sup>.

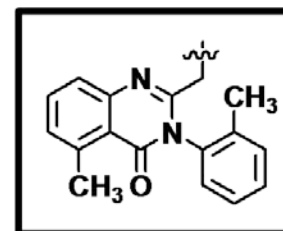
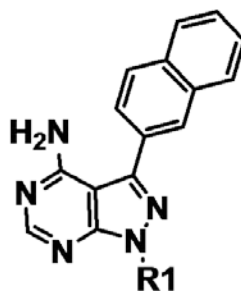
The DL series, similarly to the SW series, emphasized the importance of designing properly placed hydrogen bonds when constructing PI3K inhibitors. Compounds containing a cyclopentyl R1 group were much less potent PI3K inhibitors than the corresponding compound with an isopropyl, suggesting that the larger R1 group

precluded binding. This was consistent with other data collected in the Shokat laboratory with related compounds, showing that when the R2 group is held constant, increasing the molecular weight or bulk of the R1 substituent generally results in less potent compounds (Figure 4.2). Only the methionine switch inducing tolyl quinazolinone R1 substituent (Figure 4.2 inset) was able to reverse the trend and allow for potent PI3K $\delta$  and PI3K $\gamma$  inhibition.

#### *Testing the DL series outside the PI3K family*

Because PI3K inhibitors with phenolic groups and certain pyrazolopyrimidines with phenolic groups have been shown to inhibit the mammalian target of rapamycin (mTOR)<sup>16, 64</sup>, we tested DL01, DL06, DL07, and DL09 against mTOR along with established mTOR inhibitors PI-103<sup>16</sup> and PP242<sup>64</sup>. Neither DL01 nor DL06 were potent mTOR inhibitors and had IC<sub>50</sub>s of over 1 $\mu$ M. On the other hand, both DL07 and DL09 were potent mTOR inhibitors with DL07 being slightly more potent than PI-103 on mTOR and the bulkier DL09, slightly less potent as was to be expected from the SAR of the DL series (Table 4.2). Encouraged by the ability of DL07 to inhibit the serine/threonine kinase mTOR we tested DL07 (and DL06) against the protein kinase Src and the intractable Class III PI3K vps34. Both molecules showed no activity against either enzyme (Table 4.2).

Figure 4.2



	KS208	ZK159	ZK156	ZK165	ZK161	ZK162	KS63	ZK158	ZK147	ZK155
R <sub>1</sub>										
γ	570nM	2.9μM	4.5μM	4μM	16μM	5.1μM	100μM	6.8μM	17μM	6.3μM
δ	800nM	3.6μM	1.2μM	2μM	12μM	3μM	100μM	6.7μM	28μM	21μM

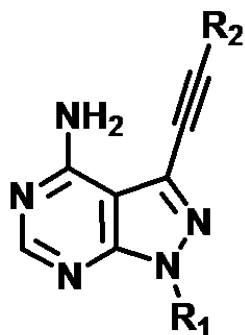
**Figure 4.2 – Size of R<sub>1</sub> substituent on pyrazolopyrimidines correlates with PI3K IC<sub>50</sub>s.**

A collection of data from compounds synthesized in the Shokat lab shows that as the R<sub>1</sub> substituent increases in bulk, while R<sub>2</sub> is held constant, the IC<sub>50</sub> against PI3Kδ and PI3Kγ increases.

Inset: The exception to this general trend is the tolyl quinazolinone substituent which induces the methionine switch and binds with high affinity to PI3Kδ and with lesser affinity to PI3Kγ.



Table 4.2



Name	R <sub>1</sub>	R <sub>2</sub>	IC <sub>50</sub> μM (10μM ATP)				
			mTOR	vps34	Src	RET	RET*
DL01			1.4	N.D	N.D	N.D	N.D
DL03			N.D	N.D	N.D	N.D	N.D
DL06			1.7	>6	>6	0.0063	2
DL07			0.006	>6	>6	0.0056	23
DL08			N.D	N.D	N.D	N.D	N.D
DL09			0.014	N.D	N.D	0.009	N.D
DL11			N.D	N.D	N.D	N.D	N.D
DL12			N.D	N.D	N.D	N.D	N.D
DL13			N.D	N.D	N.D	N.D	N.D

Table 4.2 - Structures and Biochemical IC<sub>50</sub>s for DL Series against other kinases.

N.D. = not determined

RET\* = RETV804L, a known mutation that renders RET insensitive to most ATP-competitive kinase inhibitors.

### *Insights from the crystal structure of DL06 and DL07 with PI3K $\delta$*

As a result of the unique PI3K inhibitory profile of the DL series, we sent the two most potent members of the series DL06 and DL07 to our collaborators at Cambridge who solved the crystal structure of both DL06 and DL07 with PI3K $\delta$ <sup>74</sup>. The crystal structures for both DL06 and DL07 were remarkably similar (Figure 4). Methionine 752, which is the PI3K $\delta$ 's equivalent to PI3K $\gamma$ 's methionine 804 was in the "up" position as we expected with a molecule too small to engage the methionine switch. The standard hinge hydrogen bonds between the pyrimidine moiety of DL06 and DL07 and the backbone carbonyl and amino groups of glutamate 826 and valine 828 were present and anchored both compounds in the correct orientation (Figure 4.3A,B). The pyridinyl moiety of DL06 and the phenol moiety of DL07 were both projected into the affinity pocket of PI3K $\delta$ , and in the case of DL07, the phenolic hydroxyl group made hydrogen bonds with lysine 779, and aspartate 911, picking up some of the key interactions we previously identified as necessary for gaining potency with PI3K $\delta$  (Figure 4.3 A,B). DL06's pyridinyl moiety also projected into PI3K $\delta$ 's affinity pocket within hydrogen bonding distance of lysine 779 and aspartate 911 (Figure 4.3B). This was unexpected because the aromatic pyridine is expected to have an sp<sup>2</sup> hybridized nitrogen whose lone pairs can hydrogen bond on edge, in the same plane as the pyridine ring, not above and below it. It may be only coincidence that DL06's pyridinyl nitrogen is within hydrogen bonding distance of both lysine 779 and aspartate 911; however when the structures of DL06 and DL07 with PI3K $\delta$  are superimposed, there is what appears to be a concerted movement of lysine 779, aspartate 911 and isoleucine 825 that tracks with the pyridinyl

nitrogen (Figure 4.3C). It seems implausible that the pyridine would be able to retain its aromaticity while engaging in hydrogen bonds with that particular geometry, so it is still possible that the proximity to some of the key residues in PI3K $\delta$ 's affinity pocket is not significant.

Figure 4.3

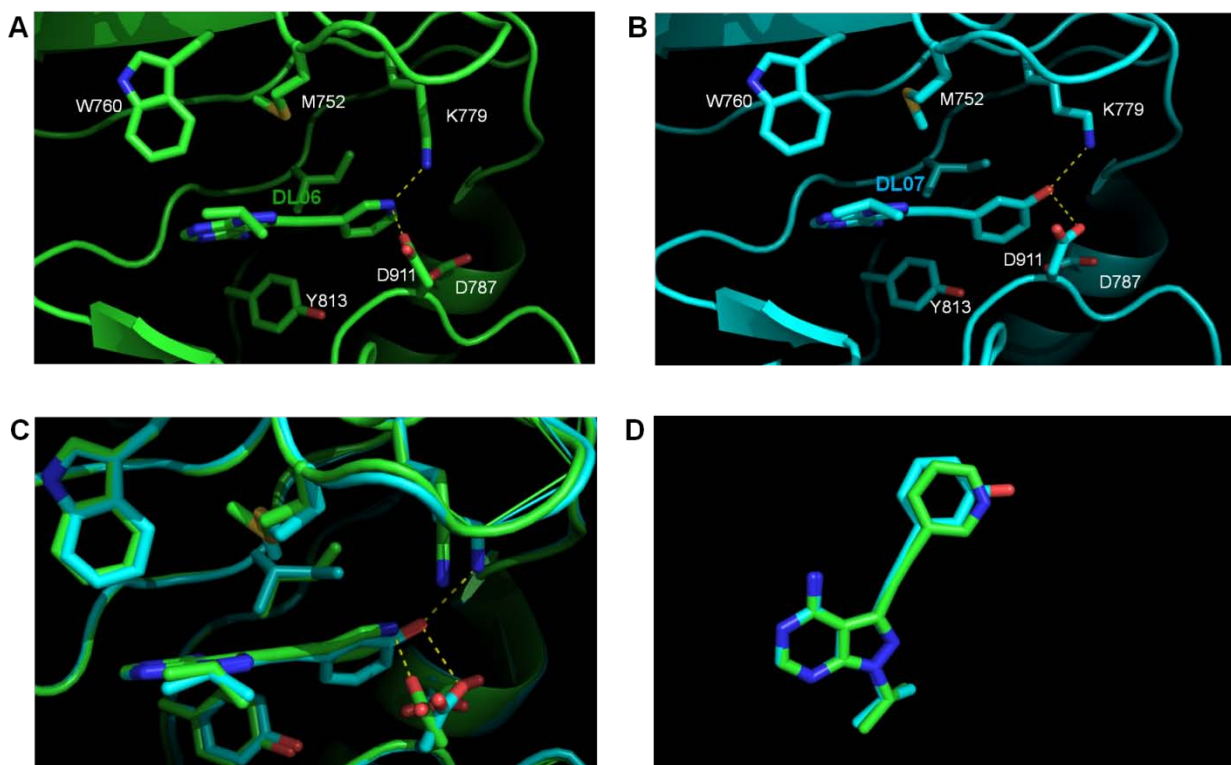


**Figure 4.3 – Crystal Structure of DL06 and DL07 with PI3K $\delta$ <sup>74</sup>.**

- A. Crystal structure of DL06 in PI3K $\delta$ . Met752 (Met804 in PI3K $\gamma$ ) is in the “up” position, and DL06’s pyridinyl affinity element appears to make interactions in the PI3K “affinity” pocket with Lys779 and Asp 911.
- B. Crystal structure of DL07 in PI3K $\delta$ . Met752 (Met804 in PI3K $\gamma$ ) is in the “up” position, and DL07’s phenol affinity element makes interactions in the PI3K “affinity” pocket with Lys779 and Asp 911.
- C. Binding mode of DL06 (green) and DL07 (cyan) is identical, and both molecules are highly superimposable. Despite the  $sp^2$  hybridization of the pyridinyl nitrogen of DL06, Lys779 and Asp911 appear to track with it, moving to maintain what appears to be some sort of electrostatic interaction. The phenolic affinity element of DL07 is slightly twisted out of plane with respect to DL06’s pyridinyl affinity element.
- D. Overlay of PI3K $\delta$ -bound DL06 (green) and DL07 (cyan), the pyrazolopyrimidine cores are exactly superimposable, and only small variations exist with the R1 isopropyl subunit.

### *Application of DL07 toward an AML disease model*

DL07's inhibition of mTOR made it quite similar to PI-103 in terms of its PI3K inhibitory profile. PI-103 has been shown to be an effective anti-leukemic agent in acute myeloid leukemia, presumably because of its dual effect on PI3K and mTOR. Remarkably, although the vast majority of AML cells expressed PI3K $\delta$ , and in many cases it was the only PI3K expressed, PI3K $\delta$  inhibition was ineffective at killing AML cells<sup>129-131</sup>. We hypothesized that similarly to PI-103; the additional PI3K $\alpha$  and mTOR activity of DL07 would be enough to kill AML cells. DL06, which had PI3K $\alpha$  activity but no mTOR activity, would allow us to assess the contribution of mTOR inhibition to the effectiveness of PI-103 and DL07.

To evaluate this, we first wanted to determine the effect of DL06, DL07 and a large panel of PI3K inhibitors, including PI-103 and selected members of the SW series on the biochemical signaling in mouse bone marrow macrophages (BMM $\Phi$ ). We used wild-type mice and mice with a RAS-mutation that mimics most of the AML phenotype<sup>132</sup>. Mice were sacrificed, and the long leg bones were extracted. The tips of the bones were cut off and then the bone marrow was flushed out of the bones using 10% fetal bovine serum supplemented IMDM media. The resultant cells were cultured in the presence of macrophage medium (IMDM, 20% bovine growth serum, 1% pen/strep, and 50ng/mL of M-CSF) at 37°C and 5%CO<sub>2</sub>. After 48 hours, 4mL macrophage medium supplemented with 12% FBS, and 10 $\mu$ L of M-CSF was added. Within four days, only macrophages remained. We treated stimulated the macrophages with GM-CSF in the presence of DL06, DL07, DL09, SW13, SW14, SW30, PI-103, PIK90, AS605240, and other compounds. We then fixed the cells and then performed a Western blot to analyze

the effects of our compounds on PI3K and ERK signaling. PI-103 was able to block the formation of both pAkt, and pERK, and we expected to see the same thing with DL07. All the compounds with PI3K activity blocked the formation of pAkt, but surprisingly, DL07 also increased the phosphorylation of ERK (Figure 4.4). No other molecule in the panel had the same effect on ERK, except the structurally related DL09 (Figure 4.4). Importantly DL06 did not affect ERK phosphorylation, so we hypothesized that it was the mTOR activity of DL07 and DL09 that was responsible for the observed effect. This explanation was not completely satisfying because PI-103, which also had mTOR activity, did not display the same effect on ERK, but at the time, the mTOR inhibition was the only significant difference we had confirmed between DL06 and DL07.

We also thought it was possible that DL07 despite being structurally similar to DL06 had one or two other targets that DL06 did not share. Since Raf inhibitors have been shown to increase pERK under certain conditions<sup>133-134</sup> we hypothesized that DL07, but not DL06 may have some Raf activity. In order to confirm this and identify any other previously overlooked targets, we subjected DL06, DL07 and DL01 to Invitrogen's kinase screening services. Both DL01 and DL06 were fairly selective, and only inhibited three and four protein kinases to greater than 80% inhibition at 10 $\mu$ M respectively (Appendix). DL07 on the other hand, in addition to inhibiting Raf, inhibited over 100 protein kinases to greater than 80% inhibition at 10 $\mu$ M (Figure 4.5). The extreme and unexpected promiscuity of DL07 prevented us from answering our original question of whether mTOR inhibition in DL07's profile would make it effective in combating AML. However, it did show that molecules with very close structures can display vastly different selectivities among the protein kinases.

Figure 4.4

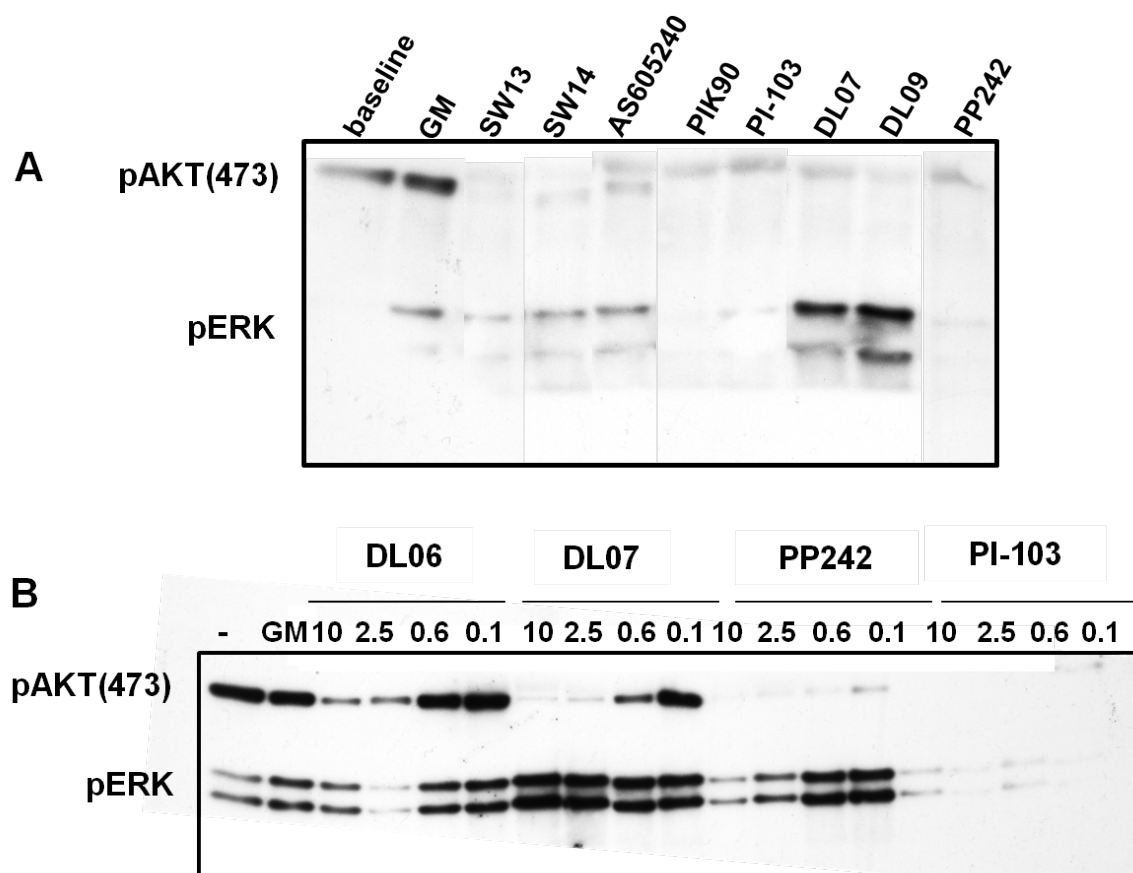


**Figure 4.4 – Effect of selected compounds on ERK phosphorylation in macrophages.**

A. Mouse bone marrow macrophages were cultured in macrophage medium (IMDM, 20% bovine growth serum, 1% pen/strep, and 50ng/mL of M-CSF) at 37°C and 5%CO<sub>2</sub>, stimulated with GM-CSF in the presence of various inhibitors of the PI3K pathway. Cells were fixed and a western blot performed to analyze pAKT and pERK levels. DL07 and DL09 paradoxically increased levels of pERK, whereas all other PI3K pathway inhibitors lowered pERK levels.

B. Western blots performed as in A, but with escalating doses of compounds with PI3K and/or mTOR activity. Only DL07 increased levels of pERK, but the structurally related DL06 did not.

Figure 4.5

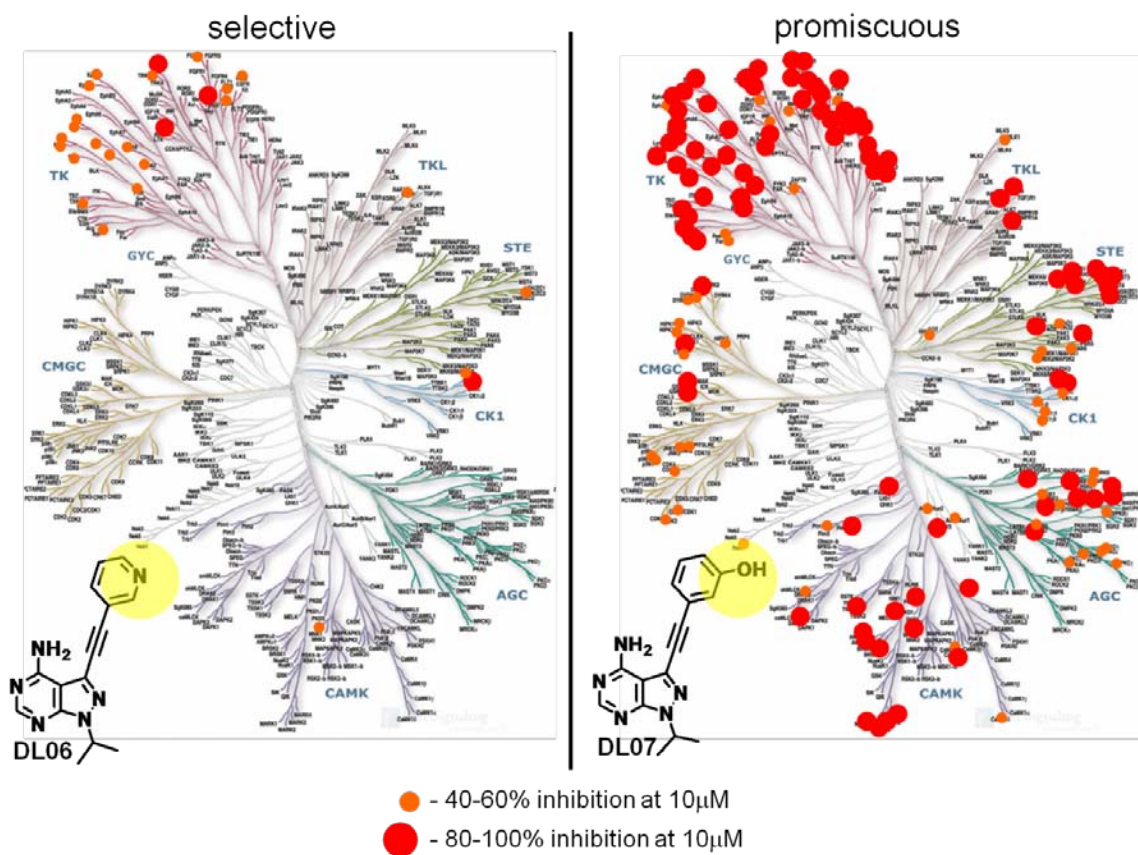


**Figure 4.5 – Kinome inhibition of DL06 and DL07**

DL06 (left) and DL07 (right) were tested against a panel of over 200 protein kinases at 10µM. Kinases inhibited from 40-60% were covered by an orange circle, and kinases inhibited greater than 80% were covered with a red circle. Despite the small structural variation between DL06 and DL07, DL07's inhibition of the kinome is significant while DL06 is quite selective.

For full kinase table and inhibition data see Appendix.



### *Investigating the unusual promiscuity of DL07*

DL01 and DL06 represented molecules that have PI3K activity, but were quite selective for the lipid kinases over the protein kinases, whereas the structurally similar DL07 also had PI3K activity, mTOR activity and inhibited several other protein kinases including Abl, Ret, Raf, EGFR, FLT3, and over 100 more (Figure 4.5). DL07's inhibitory activity covered the tyrosine kinase superfamily and certain branches of the CAMK, AGC and STE kinase superfamilies (Figure 4.5). As a result of its unique structure, DL07 is able to act as a dual lipid/protein kinase inhibitor with broad coverage of both families.

We believe that this can be explained in part by a phenomenon we observed in the SW series. Beforehand, we had discovered the importance of properly placed hydrogen bonding elements to the potency of the SW chemical series, and this situation is probably influenced by the hydrogen bonding capabilities of the phenol in DL07. DL06 cannot maintain the same hydrogen bonds as DL07, and since that is the only structural difference between the two compounds, this is likely to be the key in explaining the different selectivities. DL01 does have a hydroxyl group, and thus similar hydrogen bonding potential as DL07, but in this case our data suggested that the hydrogen bonds of DL01's hydroxyl group were not fully realized because they existed in the wrong geometry or orientation, or simply did not extend far enough within the affinity pocket to provide the optimal distance to the other hydrogen bonding residues of the protein kinases. This phenomenon was observed in reverse for the SW series. For the SW series, SW25 and SW30 correspond to DL07 and DL01. However it was SW30 that possessed the appropriate geometry and placed its hydrogen bonding element within the

proper distance of the correct residues and as a result, displayed much more potency against PI3K $\delta$  than SW25 (Table 2.2)

Replacement of the SW series' tolyl quinazolinone with an isopropyl afforded a new series of compounds with different SAR, and sometimes reversed SAR trends. Removal of the tolyl quinazolinone allowed the molecules of the DL series to sit in the binding pocket of PI3K and protein kinases differently. Since the kinase did not have to accommodate the bulky tolyl quinazolinone, which previously needed to be accommodated for successful binding, different orientations could be sampled. Formerly, the tolyl quinazolinone set the binding mode, and once it and the hinge hydrogen bonds were accommodated, there was not much freedom to vary the position of the affinity element, and sample the various orientations, searching for the most thermodynamically stable. Since the tolyl quinazolinone no longer needed to be accommodated with the DL series, those smaller inhibitors only needed to satisfy the hinge hydrogen bond requirements, and thus we observed a different SAR because the molecule was less constrained.

DL07 represents a multi-kinase inhibitor with a molecular weight of only 294, well under the 500 molecular weight cutoff established by Lipinski. It is remarkable that we were able to develop a molecule with nanomolar potency on many targets while keeping the molecular weight so low. This is especially significant in light of DL06, a molecule of similar molecular weight and structure that was quite selective for the PI3K family over any other protein kinases. Both molecules represent fairly simple, but powerful structures that have the potential for further modifications that might further


enhance selectivity or potency while still allowing the resultant molecules to remain a reasonable size and maintain their drug-likeness.


We were surprised by the large number of kinases inhibited by DL07, and we wanted to determine whether because of its inhibitory profile, DL07 would be able to halt proliferation of certain cancer cell lines. We tested DL07 in parallel with an mTOR inhibitor PP242 and a BRAF inhibitor PLX4720 in a KRAS mutated cell line, two KRAS/PI3K mutant cell lines and two BRAF mutated cell lines. Despite its broad kinase inhibition, DL07 was actually less effective at killing cells than PP242 and PLX4720, in most of the cell lines tested (Figure 4.6). It did show some modest proliferation inhibition in the cell lines with KRAS mutations, and especially in the SW1116 cell line, which had been mostly insensitive to previous compounds. DL07 however was generally ineffective in the cell lines in which proliferation was driven by BRAF. The overall lack of efficacy for DL07 suggested that inhibiting the right kinase or set of kinases was actually much more effective than inhibiting a large number of potentially irrelevant kinases. In other words, in this case the particular kinases inhibited are much more important than the quantity of the kinases inhibited. We noticed this same phenomenon with PIK90 in the BioMAP assays (Chapter 3). Selective PI3K $\delta$  and PI3K $\gamma$  dual inhibition was more effective at reducing inflammation than PIK90's inhibition of all four PI3K isoforms. In fact, the additional inhibition of PI3K $\alpha$  and PI3K $\beta$  with PIK90 on top of PI3K $\delta$  and PI3K $\gamma$  was actually much less effective<sup>77</sup>. In that case, and perhaps in this case as well, inhibiting kinases with opposing functions led to functional antagonism, such that increasing the number of kinases inhibited did not lead to a greater effect, but actually was less effective than the appropriate inhibition of the relevant


kinases. Additionally, some of the kinases inhibited by DL07 may not be relevant in cell survival for those particular cell lines, and thus their inhibition is not predicted to affect these processes. Still, it was important for us to verify the reported inhibition data of some of our compounds with our own radioactivity based kinase assays<sup>65</sup>. We chose to evaluate the inhibition of DL06 and DL07 on RET, a kinase inhibited by both DL06 and DL07, and a target of interest because of the central role it plays in the highly metastatic medullary thyroid carcinoma. Both DL06 and DL07 were potent inhibitors of RET and had IC<sub>50</sub>s of 6.3nM and 5.6nM respectively (Table 4.2). However, when we tested against RET V804L (a typical kinase inhibitor resistance mutation in which the valine gatekeeper residue is mutated to a larger leucine, precluding the binding of most kinase inhibitors) we noticed a significant drop in potency. Still, DL06 was affected much more by this mutation, displaying an IC<sub>50</sub> of 23μM, while DL07's IC<sub>50</sub> ranged from 1μM to 3μM (Table 4.2).


Figure 4.6

		Inhibition of cell proliferation EC <sub>50</sub> (μM)				
		Cells	PP242	PLX 4720	DL07	PP242+PLX 4720
KRAS Mut	SW1116	5.70	>20	6.24	14.00	
KRAS/PI3K	HCT 15	0.16	54.07	2.05	0.42	
	COLO 201	0.23	>20	3.76	0.75	
BRAF V600E	HT 29	0.23	0.11	26.64	0.12	
	COLO 205	0.24	0.09	28.22	0.30	

 < 0.10μM

 0.11μM – 1.0μM

 1.10μM – 10.0μM

 >10.0μM

**Figure 4.6 – DL07 does not potently inhibit cell proliferation.**

Cancer cell lines were cultured in the presence of various concentrations of inhibitors for 72-96 hours.

Inhibition of cell proliferation was assayed by Alamar Blue reduction.

### *Lessons from the DL series*

Several lessons can be extracted from the DL series and from their comparison with the SW series. Firstly, small changes in chemical structure can bear significant consequences for potency and selectivity, especially when the small changes alter the hydrogen bonding potential of the resultant molecule. The importance of making the appropriate hydrogen bonds was highlighted by the substantial selectivity differences between DL06 and DL07. The fact that we were able to develop such a large selectivity range with a few variations in structure indicated that the potential for pyrazolopyrimidines as lipid and/or protein kinase inhibitors (both selective and promiscuous) has yet to be exhausted, and as a scaffold pyrazolopyrimidines still can and should continue to be mined as they are a privileged scaffold that can straddle both lipid and protein kinase inhibitor chemical space. Additionally, we discovered that although it is possible to rationally design dual protein-lipid kinase inhibitors<sup>64</sup>, such compounds can also be uncovered serendipitously, and kinome-wide screening is essential to most kinase inhibitor development efforts in order to be fully informed on a compound's selectivity. Finally, we learned that while elimination of portions of a compound's structure may not drastically affect the binding mode, it may affect the binding order or affect which portions of the inhibitor the enzyme gives preference to. If a bulky group no longer needs to be accommodated, the rest of the molecule is free to relax into its preferred binding mode. That mode may be grossly similar, but minute changes may be allowed that were previously forbidden, and those small changes can lead to considerable SAR and IC<sub>50</sub> differences.

Data generated with the DL series has also opened interesting new avenues of investigation. The kinases inhibited by DL07 were mainly in the tyrosine kinase superfamily, but there was also strong representation in the CAMK group and the STE kinases. It would be informative to uncover what, if anything the kinases inhibited by DL07 share. Are there specific residues within the “affinity” pocket that are essential to binding and shared by all DL07-sensitive kinases? Is the overall “affinity” pocket more hydrophilic because of its hydrogen bonding potential, or is it more hydrophobic, which would suggest that it is the displacement of water from the pocket which renders the kinases sensitive to DL07. Alternatively, it is possible that the kinases that are insensitive to DL07 all share a particular feature. However since so many different factors can render a kinase insensitive to an inhibitor, it is generally more likely for shared qualities to sensitize a kinase to an inhibitor rather than desensitize it. In other words, there is likely to be a DL07 Anna Karenina principle at work; DL07-sensitive kinases are all alike, but DL07-insensitive kinases are all insensitive in their own peculiar way. It would also be informative to solve the crystal structure of DL07 and DL06 with a target that both inhibit well, and one that only DL07 inhibits well. These structures would most likely provide insight to what specific interactions are made (or possibly avoided) with DL07s phenol that cannot be utilized by DL06’s pyridinyl moiety.

In our efforts to further mine the pyrazolopyrimidine chemical space, we discovered a very selective PI3K inhibitor, and a closely related analog that was very promiscuous. The significant disparity in selectivity between the two molecules did not correspond to the modest structural variation, and the cause of this remains an active area of investigation.

## Chapter 5 –Summary, Future Work, and Clinical Implications

### *Further investigation with the SW series*

In chapters 2 and 3 our successful design a series of PI3K $\delta$  and PI3K $\delta/\gamma$  inhibitors to engage the methionine switch in PI3K $\gamma$  and PI3K $\delta$  was outlined. We evaluated the designed PI3K $\delta/\gamma$  inhibitors and determined that they possessed anti-inflammatory capabilities, and were not only a prototype for novel anti-inflammatory compounds that inhibit PI3K $\gamma$  and PI3K $\delta$ , but useful tools to study the inhibition of PI3K $\delta$  and PI3K $\gamma$  in a realistic time-frame with fairly drug-like small molecules. We are confident that our discoveries will have a significant impact on the PI3K drug discovery field, and are hopeful that molecules designed by Intellikine based on the basic principles outlined in this thesis will be successful in clinical trials and will be a noteworthy step on the path toward the approval of the first drugs specifically designed to target PI3K $\delta$  and PI3K $\gamma$ . We also successfully leveraged the lessons learned from the SW series to design a new series of PI3K inhibitors (DL series), a subset of which displayed vastly different levels of selectivity.

One of the most interesting phenomena noted with the SW series was the significant decrease of LPS-induced TNF $\alpha$  production by PI3K $\delta/\gamma$  inhibition, and the reversal of that decrease once PI3K $\alpha$  and PI3K $\beta$  inhibition was dosed in (Figure 3.3B). This suggested that PI3K $\alpha$  and PI3K $\beta$  inhibition antagonized the inhibition of PI3K $\delta$  and PI3K $\gamma$ , rendering it mostly impotent, and making pan-PI3K inhibition much less effective than selective PI3K $\delta/\gamma$  inhibition. We also noticed this multiple kinase antagonism phenomenon was recapitulated when we saw that DL07, despite its impressive



multikinase inhibition, was not that toxic to cells at all, but inhibitors with more limited kinase inhibition had increased efficacy (Figure 4.6). While we have speculated briefly on what may be responsible for decrease of TNF $\alpha$  levels when PI3K $\gamma$  activity was added to the compounds, we have not collected all the data to prove or disprove any of the theories outlined in Chapter 3. The first theory discussed hinged on the involvement of PDE4, a cAMP hydrolyzing enzyme present in immune cells. Inhibition of PDE4 does suppress TNF $\alpha$  levels, and thoughtful reviewers have queried whether our molecules have PDE4 activity. The direct inhibition of PDE4 is highly unlikely because it would be an off-target effect. The SW series has been shown to have no significant off-target activity within the kinase superfamily, the most likely place for off-target activities to appear. Logically then, the possibility is very slight that the SW series would possess activity further outside the kinases in the unrelated phosphodiesterases. When the structure of SW18 was entered into a program developed at UCSF<sup>135-136</sup> to predict any off-target activities, no off-target activities were predicted. Additionally, the dramatic drop in TNF $\alpha$  levels correlated very strongly with additional PI3K $\gamma$  activity, and it is highly unlikely that the same structural changes that increased PI3K $\gamma$  activity through parameters which we designed based on early observations, would also result in increased PDE4 activity. The different structures of the compounds that all possessed PI3K $\gamma$  activity and decreased TNF $\alpha$  production (The TNF $\alpha$  effect of SW14's fluorophenol affinity element was comparable to that of SW19's indole affinity element - Appendix), suggested that the drop in TNF $\alpha$  levels was tied into PI3K $\gamma$  activity and not a potential PDE4 off-target activity, which would more likely be present in only one molecule, not three or four. If PDE4 is involved with this phenomenon at all, it is more

likely is that it is an indirect effect somehow mediated by PI3K $\gamma$ . Future work could include biochemical testing of select members of the SW series against purified PDE4, in order to rule out direct inhibition of PDE4 by the SW series. Later experiments could test the activity of PDE4 in cells treated with PI3K $\gamma$  inhibitors to see if PDE4 activity is altered at all through inhibition of PI3K $\gamma$  or any of the PI3Ks. If successful, those experiments could be repeated in PI3K $\gamma$  knockout and kinase-dead cell lines to determine whether the SW series effect on PDE4 was independent of PI3K $\gamma$  catalytic activity, or mediated through a yet undiscovered off-target activity.

A more likely scenario through which PI3K $\gamma$  influences TNF $\alpha$  levels is through the action of NF $\kappa$ B. TNF $\alpha$  has already been shown to activate PI3K $\gamma$ , leading to NF $\kappa$ B activation<sup>110</sup>. NF $\kappa$ B activation in turn can increase the levels of TNF $\alpha$ <sup>111</sup>, so it is possible that TNF $\alpha$ 's activation of PI3K $\gamma$  would lead to further production of TNF $\alpha$  through NF $\kappa$ B. In order to test that, we would first need to verify that in PBMCs TNF $\alpha$  does activate PI3K $\gamma$ . This is possible to do by measuring the cytoplasmic and membrane associated levels of PI3K $\gamma$ , before and after treatment with TNF $\alpha$ . As PI3K $\gamma$  is activated it is translocated from the cytoplasm to the inner leaflet of the membrane, in close proximity to its substrate PIP<sub>2</sub>. Upon treatment with TNF $\alpha$ , if activated, we expect to see the fraction of membrane-associated PI3K $\gamma$  increase while the cytoplasm-associated fraction will decrease. This approach has already been successful with endothelial cells and it should be possible to modify the approach slightly to work with PBMCs<sup>110</sup>. The next step would then be to verify that PI3K $\gamma$  activity is necessary for NF $\kappa$ B activation. PBMCs can be stimulated with TNF $\alpha$  in the presence of various members of the SW

series with varying PI3K $\gamma$  activity, as well as SW23, the SW series' negative control. NF $\kappa$ B translocation to the nucleus, a readout of its activation, can be measured in each case, and the PI3K $\gamma$  dependence of NF $\kappa$ B's functional activation can be determined. If PI3K $\gamma$  does influence NF $\kappa$ B activation, then we would expect to see decreasing activity of NF $\kappa$ B (readout as decreasing NF $\kappa$ B nuclear fraction) that correlated with the PI3K $\gamma$  potency of the selected members of the SW series. These experiments can be repeated with PI3K $\gamma$  kinase-dead cells to ensure that the effect seen is due to inhibition of PI3K $\gamma$  catalytic activity, and not any as yet undiscovered off-target effects.

Although NF $\kappa$ B is a likely linker between PI3K $\gamma$  inhibition and decreasing TNF $\alpha$  levels, it is possible that neither NF $\kappa$ B nor PDE4 play a significant role in mediating the drop in TNF $\alpha$  production. TNF $\alpha$  levels are influenced by several factors, which can be investigated further if the more likely options are invalidated.

#### *Further investigation with the DL series*

The new series of inhibitors (DL series) represents a rich set of small molecule chemical tools that has yet to be fully explored. Of most import, the amazing selectivity difference present between DL06 and DL07 with such a small structural change. Although we have a list of the kinases inhibited by both DL06 and DL07, we have yet to understand how that information would affect cellular physiology. Members of the DL series (DL01, DL06 – DL09) are perfect candidates for BioMAP analysis. In that set of molecules there is a large span of selectivities, and with BioMAP analysis we would be able to determine how DL07's inhibition of so many kinases affects multiple cellular functions. It would also be worthwhile to compare the signatures of DL06 and DL07, to

quantify the difference that a small structural change can make, and eventually to compare the profiles of the DL series to see if they resemble any particular classes of compounds or whether they have carved out their own niche in drug-like chemical space. The BioMAP results may also shed light on the inability of DL07 to block proliferation of cancer cell lines, despite inhibiting over 100 kinases at 10 $\mu$ M.

Another interesting area of investigation around the DL series would be the exact structural features of DL07 that allow its promiscuity. To this end, solving the crystal structure with three different segments of protein kinases may prove valuable. The first segment would be the DL sensitive kinases (protein kinases inhibited by both DL06 and DL07, like RET or ROS1), the second segment would be the DL07-sensitive kinases those inhibited only by DL07 (e.g. ZIPK, ALK, EGFR, VEGFR, mTOR, JAK), and the last segment would be those insensitive to both inhibitors (ERK2, p38 $\gamma$ , p38 $\delta$ , MET, NEK). With the last group especially, there might be some challenges, but a less risky alternative approach would be to take a kinase that is slightly inhibited by DL07, and substitute that for the DL07-insensitive kinase. We could enter into collaborations with structural laboratories to solve the structures, or we could search through the list of kinases in each segment and determine which structures, if any, have already been solved, and then use similar conditions in our attempts to grow crystals.

Identifying some of the common structural features present in the second group of kinases would help us begin to answer one of the most intriguing questions raised by the initial observations around the DL series, namely what makes a kinase DL07-sensitive or DL07 insensitive. Toward the end of answering that question, we could also undertake bioinformatic studies of the three groups of kinases to supplement the crystallographic

data. We could align the kinases and look for elements that are shared within particular groupings of kinases, and from there generate testable hypothesis about the key features necessary for DL07 sensitivity or insensitivity and eventually convert between the two kinds of kinases with appropriately designed mutations.

Insights from the crystal structure, in addition to steering the bioinformatic analysis, may also be useful in guiding the synthesis of additional members of the DL series. None of the molecules in the DL series was able to duplicate the potency and promiscuity of DL07, with the possible exception of DL09, which shared the same affinity/R2 element (Table 4.1). Work with the SW series suggests that synthesis of a fluorophenol analog of DL07 might be more potent against the PI3Ks, but it is not known how the presence of the fluorophenol will affect potency against the other protein kinases. We also could move DL07's hydroxyl group around the aryl ring, identifying the optimal position for its hydrogen bonding capabilities. Additionally, we have already hypothesized that the dual hydrogen bond acceptor/donor role of the phenol is quite important, but have yet to exhaustively test that hypothesis. We could attempt to cap the hydroxyl with a methyl group, or substitute it with various indoles as we did with the SW series. Alternatively we could attempt to remove all hydrogen bonding capability from DL07, replacing the phenol with a phenyl ring, or a bulkier naphthyl group that would also report on the bounds of the 'affinity' pocket within protein kinases. Various heterocyclic rings may also be utilized with the aim of recapturing some hydrogen bonding interactions.

Despite its many interesting attributes, the DL series does not immediately lend itself well to further development by biotech or pharmaceutical companies. The extreme

promiscuity of DL07 (and probably DL09) is a liability, and apart from that, the profile of the rest of the series has already been mostly achieved by other scaffolds. Although DL06's inhibition of RET is interesting, there have been other pyrazolopyrimidines reported with RET activity<sup>64</sup>. The combination of PI3K and RET may be attractive in certain particular cases, but overall, the SW series is much more attractive, and goes further to address some of the unmet and undermet needs in the biotech and pharmaceutical space.

#### *Using PI3K $\delta$ and PI3K $\delta/\gamma$ inhibitors in the clinic*

Inhibitors targeting PI3K, especially PI3K $\delta$  or PI3K $\delta/\gamma$  are only just beginning to be developed by drug companies. Although most if not all major pharmaceutical companies have some sort of PI3K program and there are many early clinical trials being conducted, specific inhibitors geared toward inflammation only make up a minority of the programs. For reasons outlined in chapter 2, achieving isoform selectivity within the PI3K family or any kinase family can be a daunting task. Multi-targeted, or family-directed inhibitors are simply easier and faster to develop, and the indications such as oncology, in which the off-target effects are tolerated and sometimes even welcomed, dominate the PI3K pharmaceutical space. Still, there have been a few compounds reported as isoform-selective, with the potential to be used in diseases other than cancer. Chronic diseases, like inflammation and autoimmune disorders, necessarily require compounds with little to no toxicity, and negligible off-target effects, which is difficult to achieve with multi-targeted PI3K inhibitors; only selective inhibitors of PI3K $\delta$  and/or PI3K $\gamma$  will be tolerated for prolonged periods of time.

Of all the PI3K inhibitors to date that have been in or are about to enter clinical trials, there have only been four that have demonstrated some selectivity for PI3K $\delta$  and/or PI3K $\gamma$  over the other isoforms. The first, TG100-115, developed by TargeGen, which was recently acquired in July 2010 by Sanofi-Aventis, was directed toward both PI3K $\gamma$  and PI3K $\delta$ . It initially attracted attention because of claims of its PI3K $\gamma/\delta$  selectivity and effectiveness at preventing myocardial infarction injury. Close scrutiny of the biochemical data shows that TG100-115 was only of middling potency and not as selective for PI3K $\gamma$  and PI3K $\delta$  as originally claimed. Its IC<sub>50</sub>s against the Class I PI3Ks are as follows PI3K $\alpha$  – 5.6 $\mu$ M, PI3K $\beta$  – 858nM, PI3K $\delta$  – 235nM, PI3K $\gamma$  – 83nM<sup>76</sup>. With only 4-fold selectivity between one of the desired isoforms (PI3K $\delta$ ), and an undesired isoform (PI3K $\beta$ ), and only 10-fold selectivity between PI3K $\delta$  and PI3K $\alpha$ , doses would have to be very tightly controlled in order to avoid inhibition of PI3K $\alpha$  and PI3K $\beta$  while maintaining activity against PI3K $\delta$  and PI3K $\gamma$ .

This matter of selectivity is complicated further because the IC<sub>50</sub>s reported were determined at an ATP concentration of only 3 $\mu$ M<sup>76</sup> (while we routinely test our compounds at concentrations of at least 10 $\mu$ M ATP<sup>16, 64, 77</sup>). Since, like most kinase inhibitors, TG100-115 is ATP-competitive, the ATP concentration strongly affects the observed IC<sub>50</sub>. With higher ATP concentrations, IC<sub>50</sub>s increase and the compound appears to be less potent because it is competing with ATP for access to the kinase's binding site<sup>63</sup>. Cellular concentrations of ATP range from 1mM to 5mM, and for TG100-115 to compete with these high concentrations of ATP, the dose would need to be very high<sup>63</sup>, and at such high doses and with low and barely adequate selectivity windows, it cannot be guaranteed that TG100-115 would not inhibit PI3K $\alpha$  and PI3K $\beta$  in the human

body. However, despite the modest selectivity for PI3K $\gamma$  and PI3K $\delta$ , TG100-115 was still entered into phase I clinical trials in 2005. While being the first to enter the clinic it was far from the best, especially in terms of potency and selectivity, which may be why it was never enrolled in phase II trials, and has currently been removed from TargeGen's pipeline. Still, despite its shortcomings, TG100-115 played a very important role, proving that dual inhibition of PI3K $\delta$  and PI3K $\gamma$  was at least possible, and despite its lack of complete selectivity could still be anti-inflammatory.

*Calistoga's PI3K $\delta$  selective compounds for hematologic malignancies and inflammation*

The next two isoform-selective compounds in clinical trials were developed by Calistoga, and are CAL101 and CAL263, designed for use in blood cancers and inflammation respectively. Both compounds have successfully completed phase I trials and will undergo phase II trials soon. Although most PI3K inhibitors for oncology are multi-targeted, PI3K $\delta$ -selective inhibitors are being developed for certain types of hematological malignancies. As a result of its restricted expression pattern, PI3K $\delta$  is often the only PI3K capable of transducing signals from receptor tyrosine kinases in blood cancer cells. The underlying premise behind the use of CAL101 in cancers comes from the observations about PI3K $\delta$ 's involvement with B cells. Early results with PI3K $\delta$  knockout mice and PI3K $\delta$  kinase-dead knock-in mice suggested that PI3K $\delta$  was intimately involved with B cell receptor induced proliferation<sup>44, 56, 137</sup>. These results were confirmed with IC87114, a PI3K $\delta$  selective inhibitor and likely precursor to CAL101<sup>138</sup>. Additionally, those experiments showed that B cells were very sensitive to PI3K $\delta$  inhibition, much more sensitive than the other immune cells tested. These data



supported the use of PI3K $\delta$  inhibitors in B cell malignancies. Also, by focusing on malignancies with a strong B cell component they may avoid the AML paradox noted in chapter four. Moreover, in AML and other myeloid leukemias, the cells that undergo unrestricted proliferation are the myeloid cells, which are precursors to macrophages, neutrophils, and most of the other major players in innate immunity. In contrast, lymphocytic leukemias arise from uncontrolled proliferation of lymphoid cells (B, T and natural killer cells) or lymphoid precursor cells, the majority of which are involved in adaptive immunity, and whose functions are quite sensitive to PI3K $\delta$  inhibition.

Another interesting note is that CAL101 is reported to cause apoptosis<sup>139</sup>. This is the first report of a selective PI3K $\delta$  inhibitor causing apoptosis; in fact, it has been shown that non-cancerous B cells can develop without functioning PI3K $\delta$ <sup>44, 56, 137</sup>, though their numbers and proliferation is reduced. This is the most perplexing part of the data with CAL-101, though it is possible that through the mutations accrued to become cancerous, the malignant B cells lost a portion of their resilience, forcing them to depend solely on PI3K $\delta$ . The diseases for which CAL-101 is being considered a valid therapy are non-Hodgkin's lymphoma, mantle cell lymphoma, and chronic lymphocytic leukemia, all cancers derived from B cells.

CAL101 is a potent PI3K $\delta$  inhibitor similar in structure to PIK39<sup>140</sup> and its IC<sub>50</sub>s against the Class I PI3Ks are as follows PI3K $\alpha$  – 820nM, PI3K $\beta$  – 565nM, PI3K $\delta$  – 2.5nM, PI3K $\gamma$  – 89nM<sup>140</sup>. Its selectivity profile is better than that of TG100-115: CAL-101's selectivity over PI3K $\gamma$  is approximately 40-fold, while it displays approximately 300-fold selectivity over PI3K $\alpha$ . In the clinic treatment with CAL-101 resulted in 57% response in patients with non-Hodgkin's lymphoma, 67% response in patients with

mantle cell lymphoma, and 30% response in patients with chronic lymphocytic lymphoma (CLL), importantly of all the CLL patients treated 94% showed a reduction of greater than 50% in lymph node disease.

Calistoga's second compound in clinical trials, CAL-263 is a PI3K $\delta$  inhibitor being evaluated for treatment of asthma, inflammation and possibly rheumatoid arthritis. There is little data on CAL-263, but chances are its structure and selectivity profile will be quite similar to PIK39, IC87114, and CAL-101. CAL-263 has been shown to be tolerated well, with good safety and pharmacodynamic data with a once daily oral dosing regimen.

#### *Intellikine's approach to inflammation and hematologic malignancies*

While Calistoga has chosen to pursue compounds that only inhibit PI3K $\delta$ , Intellikine is pursuing a dual inhibitor approach to combat inflammation and hematologic malignancies. We licensed our patent on PI3K $\delta$  and PI3K $\gamma$  dual inhibitors to Intellikine and they are hoping to reap the benefits of additional PI3K $\gamma$  inhibition to treat inflammatory diseases. Intellikine's most advanced PI3K inhibitor based on our patent, INK1197, will begin clinical trials in inflammatory diseases before the end of 2011. The major advantage INK1197 possesses over CAL-263, and CAL-101 is the incorporation of PI3K $\gamma$  activity. PI3K $\delta$  is not the only PI3K involved in inflammation<sup>38, 46, 60, 75</sup>, and our data has shown that the combination of PI3K $\delta$  and PI3K $\gamma$  is the more effective than simply PI3K $\delta$  inhibition alone<sup>77</sup>. PI3K $\delta$  inhibition might be effective, but the addition of PI3K $\gamma$  inhibition without inhibiting PI3K $\alpha$  and PI3K $\beta$  is much more so<sup>77</sup>. A compound with this profile has the ability to block inflammatory signals from both GPCRs and

RTKs, and is predicted to combine the benefits of a PI3K $\gamma$  inhibitor and a PI3K $\delta$  blockade<sup>38, 77</sup>. This would be especially relevant in a complicated disease like rheumatoid arthritis, in which many different cell types contribute to the different stages of pathology. However, additional PI3K $\gamma$  activity might not increase efficacy in B cell dominated cancers, since PI3K $\delta$ 's role is so prominent, but because of PI3K $\gamma$ 's more prominent role in T cells<sup>44</sup>, inhibitors with additional PI3K $\gamma$  activity may be useful in treating hematologic cancers with B and T cell components.

Undoubtedly, there are several other small pharmaceutical and biotech companies with PI3K $\delta$  programs that are moving toward preclinical development. Each program logically attempts to leverage the individual strengths of the company, while trying to attract attention from the larger companies to eventually make lucrative deals. Of note are Exelexis' XL499 and Karus Therapeutics' KAR1141 for inflammation and KAR1139 a PI3K $\delta/\beta$  dual inhibitor that may enter preclinical development for cancer. Currently there are no data on any of these compounds, but Exelexis has a strong history with kinase inhibitors and has two PI3K inhibitors in clinical trials. The question with XL499 is whether it will truly be a selective inhibitor. Thus far, Exelexis's PI3K compounds have been designed as multi-targeted inhibitors, and they have not demonstrated an ability to develop isoform-selective compounds yet. Karus is concurrently developing HDAC and PI3K inhibitors for both inflammation and cancer. The combination of PI3K $\delta$  and PI3K $\beta$  was previously pursued by Thrombogenix<sup>78</sup> which later changed its name to Kinacia and then merged with Cerylid Biosciences. The TGX compound series primarily inhibited PI3K $\beta$  with residual PI3K $\delta$  activity, but is no longer being pursued as a therapeutic. Eventually several isoform-selective PI3K inhibitors will proceed through

clinical trials, and we are confident that at least one will be approved as a drug for either inflammatory disorders or for cancer.

*Using PI3K $\delta$ , PI3K $\delta/\gamma$ , and PI3K $\gamma$  inhibitors to treat cancer*

The effective use of PI3K $\delta$  or PI3K $\delta/\gamma$  inhibitors in cancer is not a trivial matter. The first attempts to validate PI3K $\delta$  as a cancer target, by attempting to use IC87114 to inhibit AML cell proliferation were not very successful<sup>129</sup>, and the use of multi-targeted PI-103 was more effective<sup>141</sup>; however Calistoga seems to have achieved some level of success with CAL-101. At the very least, this suggests that the proper targeting is required for efficacy in cancer. CAL-101 demonstrated that PI3K $\delta$  inhibition can be successful in treating the subset of cancers with a significant B cell component. Still Calistoga's results are somewhat puzzling and have not been replicated with any other PI3K $\delta$  inhibitors to our knowledge. While their data should be acknowledged as valuable, their explanation is less than satisfying and does not fully address the underlying complexities.

The efforts of Karus and Thrombogenix to use the natural ability of some classes of PI3K inhibitors that cross-inhibit PI3K $\delta$  and PI3K $\beta$ <sup>16</sup> to design dual PI3K $\delta/\beta$  inhibitors may prove promising with certain types of cancers. PI3K $\beta$  has been associated with the growth and survival of cancer cells that are deficient in PTEN, a negative regulator of PI3K activity<sup>142</sup>. It then follows that if there is a blood cancer deficient in PTEN, then dual inhibition of PI3K $\delta$  and PI3K $\beta$  would be beneficial. Although not many blood cancers exhibit PTEN loss as a hallmark, PTEN loss is seen in the formation of leukemic stem cells<sup>143</sup>, and in some lymphoid malignancies<sup>144</sup> suggesting that dual

PI3K $\delta$ /PI3K $\beta$  inhibitors could be useful in chronic myeloid leukemia (CML), B cell acute lymphoid leukemia (B-ALL)<sup>143</sup>, and B cell lymphomas<sup>145</sup>.

The combination of PI3K $\delta$  and PI3K $\gamma$  will probably be most effective as an anti-inflammatory because the strong role of PI3K $\gamma$  in inflammation; however there is a place for inhibitors with PI3K $\gamma$  activity in cancer treatment. The utility of PI3K $\gamma$  inhibitors in cancer can be divided into direct effects (on malignant cells) and indirect effects. If a cancer has a cellular component that is particularly affected by PI3K $\gamma$  (e.g. T cells), then that is probably a good indication for including additional PI3K $\gamma$  activity in the therapeutic molecule. In such a case, the benefit of a PI3K $\gamma$  inhibitor would be direct, and based on an effect within the actual malignancy. For example, because PI3K $\gamma$  plays a direct role in thymocyte development and T cell activation, and the overexpression of the p101 activating subunit of PI3K $\gamma$  contributes to T cell survival and may play a role in development of T cell lymphoma<sup>146</sup>, and could possibly play a role in the development of thymomas the inhibition of PI3K $\gamma$  could be beneficial in treating those disorders.

PI3K $\gamma$  inhibition can indirectly affect cancer through its effect on the tumor environment through certain immune cells, especially monocytes and macrophages. PI3K $\gamma$  is required for chemotaxis and migration of monocytes and macrophages toward chemotactic signals<sup>18, 81</sup>. It has long been known that macrophages invade tumors and can comprise up to 80% of tumor volume, and usually average about 20-30% of tumor cells (tumor associated macrophages – TAMs)<sup>147</sup>. The interactions between tumor cells, their microenvironment and the immune system is quite complicated and a detailed explanation, while interesting, is beyond the scope of this work, but it is clear that tumors often secrete chemokines and cytokines to recruit various immune cells and co-opt the

immune system in order to foster angiogenesis, tissue remodeling, and metastasis<sup>148-152</sup>. The natural wound-healing capabilities of macrophages and other cells are corrupted by the tumor and used to create a microenvironment that is beneficial to the tumor<sup>148-152</sup>. Much of the initial signaling to recruit the immune cells and begin these processes, including angiogenesis and metastasis is controlled by GPCR interactions with their respective ligands<sup>153</sup> including stromal cell-derived factor 1 (SDF-1/CXCL12)<sup>153</sup>, IL-8 (CXCL8)<sup>153</sup>, and MCP-1<sup>148</sup>. Loss of PI3K $\gamma$  activity, either through inhibition or genetic inactivation significantly reduces the responses of macrophages and monocytes to these signals and those of other GPCR ligands<sup>18, 77, 81</sup>. M-CSF, has also been shown to be important in macrophage recruitment by tumors<sup>148, 150-151, 154</sup>, and we have confirmed that a PI3K $\delta/\gamma$  inhibitor (SW14) blocks the response of monocyte (macrophage precursors) to both M-CSF and MCP-1<sup>77</sup> (Figure 3.1). There is therefore strong biochemical evidence to suggest that PI3K $\gamma$  inhibition can block macrophage accumulation in cancer. This is likely to decrease the invasive properties, angiogenesis, and diminish the lethality of certain cancers. In addition to the angiogenesis and metastasis promoting capabilities of TAMs, the wound-healing capabilities of TAMs are also influenced by TNF $\alpha$ <sup>149, 152</sup>, a major macrophage product we have already shown is decreased by PI3K $\delta/\gamma$  inhibitors<sup>77, 128</sup> (Figures 3.3 and 3.4). In fact, Meng and coworkers recently suggested that the blockade of TNF $\alpha$  in order to sensitize tumors to radiation therapy was clinically relevant<sup>149</sup>. PI3K $\delta/\gamma$  inhibitors would block the GPCR signaling between tumors and macrophages, and limit TNF $\alpha$  production which could cripple the TAMs, and further sensitize the cancer to other therapeutics.

Despite the promising biochemistry and immunological background for PI3K $\gamma$  inhibition in certain cancers, it is important to remember that these ideas, are just being proposed and are still in their infancy, and have not yet been tested in the clinic. Furthermore, the types of cancers that metastasize and are subject to macrophage invasion necessarily are those that form solid tumors. Leukemias and lymphomas, the very malignancies most susceptible to PI3K $\delta$  and PI3K $\gamma$  inhibition arise in the blood and lymphatic systems, and by nature do not truly metastasize in the same way that solid tumors do. Thus in order to affect the TAMs and tumor microenvironment it might be more effect to include PI3K $\gamma$  activity in a multi-targeted molecule that already inhibits PI3K $\alpha$  and mTOR at the very least, instead of merely incorporating it into a molecule selective for PI3K $\delta$ .

#### *Drawbacks to the use of PI3K $\delta$ and PI3K $\delta/\gamma$ inhibitors*

No drug is perfect, and despite the promise of isoform selective PI3K $\delta$  and PI3K $\delta/\gamma$  inhibitors, there are still some drawbacks and some pitfalls that should be avoided. Two immediately come to mind. First is the risk of increased infection because of the potential for immune system suppression of these compounds. Second, and related is the alteration of the immune system balance these compounds may cause. Regarding the first point, it is important to note that knockout mice that have lived their entire lives without PI3K $\delta$ , PI3K $\gamma$  or both were not described as especially sickly or more subject to infection than their wild-type mates. Additionally, none of the genetically altered mice lacked any type of immune cells. The effects of knocking out the immune-associated PI3Ks seemed to be largely limited to the responsiveness of the immune cells to certain

stimuli, and in some cases inhibition of certain cellular processes (fully outlined in Chapter 2).

Still, blocking PI3K $\gamma$  and PI3K $\delta$  could prevent the immune system from responding appropriately to infection, recruiting enough of the proper immune cells and mounting a suitable immune response to clear the infection. Consequently, researchers wondered how such mice would respond when challenged with infections. Hirsch and colleagues demonstrated that the ability of macrophages to clear bacteria in the peritoneum was hindered in mice lacking PI3K $\gamma$ , but because the bacterial doses used were sublethal, it did not translate into increased mortality<sup>18</sup>. Later Maus and colleagues assessed the contribution of PI3K $\gamma$  to combating a pneumococcal infection and showed that lack of PI3K $\gamma$  activity (either through inhibition or genetic activation) led to reduced clearance of *Streptococcus pneumoniae*, and negatively affected survival in *S. pneumoniae* lung infection<sup>155</sup>. These data taken together would suggest that an inhibitor with PI3K $\gamma$  activity has the potential to negatively alter the immune system, but PI3K $\gamma$  activity was recently implicated in the pathogenesis of sepsis<sup>156</sup>. Both PI3K $\gamma$  knockout mice, and those treated with AS605240 (a PI3K $\gamma$ -directed inhibitor) showed increased survival in a severe CLP model of sepsis<sup>156</sup>. This result was somewhat counterintuitive given the fear that inhibition of PI3K $\gamma$  would lead to a less responsive immune system. It appears that despite the fears in the field, PI3K $\gamma$  actually protected the mice from septic organ damage. Miller and coworkers suggest that the lack of PI3K $\gamma$  activity is beneficial during severe sepsis partially because it prevents the overstimulation of the immune system, which hampers neutrophils recruitment and bacterial clearance.



With two conflicting ideas and data sets on the effect of PI3K $\gamma$  on infection, the issue remains unresolved. The true resolution will not come in mice, but will be answered with humans in the clinic. Only then will we be able to understand fully how inhibition of PI3K $\delta$  and/or PI3K $\gamma$  truly affects human susceptibility to and clearance of infections. Calistoga reported that for CAL-101, there was a modest prevalence of infections with 18% of patients displaying pneumonia, 4% displaying general infection, 2% of patients showing bacteremia and 2% with brain abscesses. If each event was unique and limited to one patient, then we can conclude that within the cohort, 26% of members had some sort of infection, yet these side effects were not serious enough to stop treatment, or halt the progression of CAL-101.

PI3K $\delta$  inhibition (both pharmacologically and genetically) has been shown to enhance IgE production in mice<sup>157-158</sup>. This is paradoxical because inhibition of PI3K $\delta$  reduces mast cell degranulation and activation upon binding of IgE<sup>49-50</sup>, and thus PI3K $\delta$  is currently being pursued as a therapeutic target for allergies. This data suggests that PI3K $\delta$  inhibitors might lose their efficacy over time as they are forced to compete with ever-increasing levels of IgE. Of even more concern, is the body's reaction to being taken off the PI3K $\delta$  inhibitor; if blockade of PI3K $\delta$  activity enhances IgE production while diminishing the body's response to IgE, removal of the PI3K $\delta$  inhibition would allow previously impaired mast cells to respond to the much larger concentrations of circulating IgE, possibly leading to severe allergic reactions or even anaphylaxis. These are only speculations, however and must be finally confirmed in the clinic. Calistoga has not yet reported on the IgE levels in the patients treated with the PI3K $\delta$  inhibitor CAL-101, but it would be interesting to see if those that received CAL-101 become more

susceptible to allergic reactions once the treatment was stopped, or at least displayed higher levels of IgE during treatment.

Another drawback of PI3K $\delta$  and PI3K $\delta/\gamma$  inhibitors is the question of their efficacy. While there is strong evidence that PI3K $\delta$  and PI3K $\delta/\gamma$  inhibitors will be effective at combating inflammation, there is not as strong a foundation of evidence with cancer yet. The ultimate question is whether lack of PI3K activity (especially PI3K $\delta$ ) can cause cellapoptosis. While it is possible that PI3K $\delta$  and PI3K $\delta/\gamma$  inhibitors will be used in combination with other therapies, it does not remove the burden of efficacy. Calistoga's CAL-101 appears to have achieved some efficacy (and it seems that the cancer needs to be selected to give the best chances of success), but efficacy is something that must be clearly demonstrated for every indication, and may be more difficult to show in cancer. Still, it is troubling that Intellikine and others have tried to repeat Calistoga's results and have not seen PI3K $\delta$  inhibition causing apoptosis. In our own experiments in the Shokat lab, we have had difficulty inducing apoptosis with multi-targeted PI3K inhibitors in cancer cell lines, and we have not been able to kill any cells with our most potent PI3K $\delta$  inhibitor, so the question of whether PI3K inhibition can cause apoptosis still remains to be answered satisfactorily.

### *Conclusion*

Much of our efforts and thinking have tracked with the clinical trials of isoform selective PI3K inhibitors, and have been focused on inflammatory diseases and cancer. Still PI3K $\delta/\gamma$  inhibitors can be useful beyond general inflammation and cancer applications. Rheumatoid arthritis is a very complex disease, and before the advent of

PI3K $\delta/\gamma$  dual inhibitors it was hard to imagine a single agent that could have effects in all the cell types and signaling pathways that are dysregulated in rheumatoid arthritis. Additionally, PI3K $\delta/\gamma$  inhibitors would probably be effective in treating asthma, ischemia reperfusion injury (including that of myocardial infarction), lupus, and possibly multiple sclerosis<sup>38</sup>.

There is a lot of promise in this field and amazing breakthroughs and discoveries will be made in the next 10-15 years. It is even possible, that we will see at least one isoform selective inhibitor marketed as a drug within that time as well. Nevertheless, the lessons learned during the clinical trials will be invaluable and change the way we look at designing selective inhibitors and their use in complex human diseases.

## References

1. Sauer, B., *Inducible gene targeting in mice using the Cre/lox system*. Methods, 1998. **14**(4): p. 381-92.
2. Nagy, A., *Cre recombinase: the universal reagent for genome tailoring*. Genesis, 2000. **26**(2): p. 99-109.
3. Knight, Z. and K. Shokat, *Chemical genetics: Where genetics and pharmacology meet*. Cell, 2007. **128**(3): p. 425-430.
4. Jaeschke, A., M. Karasarides, J.J. Ventura, A. Ehrhardt, C. Zhang, R.A. Flavell, et al., *JNK2 is a positive regulator of the cJun transcription factor*. Molecular Cell, 2006. **23**(6): p. 899-911.
5. Heck, S., X. Qian, and M. Velleca, *Genetically engineered mouse models for drug discovery: new chemical genetic approaches*. Curr Drug Discov Technol, 2004. **1**(1): p. 13-26.
6. Zambrowicz, B.P. and A.T. Sands, *Modeling drug action in the mouse with knockouts and RNA interference*. Drug Discovery Today: TARGETS, 2004. **3**(5): p. 198-207.
7. Cox, J.S., C.E. Shamu, and P. Walter, *Transcriptional induction of genes encoding endoplasmic reticulum resident proteins requires a transmembrane protein kinase*. Cell, 1993. **73**(6): p. 1197-206.
8. Patil, C. and P. Walter, *Intracellular signaling from the endoplasmic reticulum to the nucleus: the unfolded protein response in yeast and mammals*. Curr Opin Cell Biol, 2001. **13**(3): p. 349-55.
9. Mori, K., W. Ma, M.J. Gething, and J. Sambrook, *A transmembrane protein with a cdc2+/CDC28-related kinase activity is required for signaling from the ER to the nucleus*. Cell, 1993. **74**(4): p. 743-56.
10. Shamu, C.E. and P. Walter, *Oligomerization and phosphorylation of the Ire1p kinase during intracellular signaling from the endoplasmic reticulum to the nucleus*. EMBO J, 1996. **15**(12): p. 3028-39.
11. Papa, F.R., C. Zhang, K. Shokat, and P. Walter, *Bypassing a kinase activity with an ATP-competitive drug*. Science, 2003. **302**(5650): p. 1533-7.
12. Davis, R.J., *Signal transduction by the JNK group of MAP kinases*. Cell, 2000. **103**(2): p. 239-52.
13. Bi, L., I. Okabe, D. Bernard, A. Wynshaw-Boris, and R. Nussbaum, *Proliferative defect and embryonic lethality in mice homozygous for a deletion in the p110 alpha subunit of phosphoinositide 3-kinase*. J Biol Chem, 1999. **274**(16): p. 10963-10968.
14. Brachmann, S.M., K. Ueki, J.A. Engelman, R.C. Kahn, and L.C. Cantley, *Phosphoinositide 3-kinase catalytic subunit deletion and regulatory subunit deletion have opposite effects on insulin sensitivity in mice*. Mol Cell Biol, 2005. **25**(5): p. 1596-607.

15. Terauchi, Y., Y. Tsuji, S. Satoh, H. Minoura, K. Murakami, A. Okuno, et al., *Increased insulin sensitivity and hypoglycaemia in mice lacking the p85 alpha subunit of phosphoinositide 3-kinase*. *Nat Genet*, 1999. **21**(2): p. 230-5.
16. Knight, Z., B. Gonzalez, M. Feldman, E. Zunder, D. Goldenberg, O. Williams, et al., *A pharmacological map of the PI3-K family defines a role for p110 alpha in insulin signaling*. *Cell*, 2006. **125**(4): p. 733-747.
17. Sasaki, T., J. Irie-Sasaki, R. Jones, A. Oliveira-dos-Santos, W. Stanford, B. Bolon, et al., *Function of PI3K gamma in thymocyte development, T cell activation, and neutrophil migration*. *Science*, 2000. **287**(5455): p. 1040-1046.
18. Hirsch, E., V. Katanaev, C. Garlanda, O. Azzolino, L. Pirola, L. Silengo, et al., *Central role for G protein-coupled phosphoinositide 3-kinase gamma in inflammation*. *Science*, 2000. **287**(5455): p. 1049-1053.
19. Crackower, M., G. Oudit, I. Kozieradzki, R. Sarao, H. Sun, T. Sasaki, et al., *Regulation of myocardial contractility and cell size by distinct PI3K-PTEN signaling pathways*. *Cell*, 2002. **110**(6): p. 737-749.
20. Nienaber, J.J., H. Tachibana, S.V. Naga Prasad, G. Esposito, D. Wu, L. Mao, et al., *Inhibition of receptor-localized PI3K preserves cardiac beta-adrenergic receptor function and ameliorates pressure overload heart failure*. *J Clin Invest*, 2003. **112**(7): p. 1067-79.
21. Patrucco, E., A. Notte, L. Barberis, G. Selvetella, A. Maffei, M. Brancaccio, et al., *PI3K gamma modulates the cardiac response to chronic pressure overload by distinct kinase-dependent and -independent effects*. *Cell*, 2004. **118**(3): p. 375-387.
22. Clayton, E., G. Bardi, S. Bell, D. Chantry, C. Downes, A. Gray, et al., *A crucial role for the p110 delta subunit of phosphatidylinositol 3-kinase in B cell development and activation*. *J Exp Med*, 2002. **196**(6): p. 753-763.
23. Jou, S., N. Carpino, Y. Takahashi, R. Piekorz, J. Chao, N. Carpino, et al., *Essential, nonredundant role for the phosphoinositide 3-kinase p110 delta in signaling by the B-cell receptor complex*. *Mol Cell Biol*, 2002. **22**(24): p. 8580-8591.
24. Puri, K., T. Doggett, J. Douangpanya, Y. Hou, W. Tino, T. Wilson, et al., *Mechanisms and implications of phosphoinositide 3-kinase delta in promoting neutrophil trafficking into inflamed tissue*. *Blood*, 2004. **103**(9): p. 3448-3456.
25. Webb, L., E. Vigorito, M. Wymann, E. Hirsch, and M. Turner, *Cutting edge: T cell development requires the combined activities of the p110 gamma and p110 delta catalytic isoforms of phosphatidylinositol 3-kinase*. *J Immunol*, 2005. **175**(5): p. 2783-2787.
26. Swat, W., V. Montgrain, T. Doggett, J. Douangpanya, K. Puri, W. Vermi, et al., *Essential role of PI3K delta and PI3K gamma in thymocyte survival*. *Blood*, 2006. **107**(6): p. 2415-2422.
27. Alaimo, P.J., Z.A. Knight, and K.M. Shokat, *Targeting the gatekeeper residue in phosphoinositide 3-kinases*. *Bioorg Med Chem*, 2005. **13**(8): p. 2825-36.
28. Hanks, S.K. and T. Hunter, *Protein kinases 6. The eukaryotic protein kinase superfamily: kinase (catalytic) domain structure and classification*. *FASEB J*, 1995. **9**(8): p. 576-96.

29. Manning, G., G.D. Plowman, T. Hunter, and S. Sudarsanam, *Evolution of protein kinase signaling from yeast to man*. Trends Biochem Sci, 2002. **27**(10): p. 514-20.
30. Manning, G., D.B. Whyte, R. Martinez, T. Hunter, and S. Sudarsanam, *The protein kinase complement of the human genome*. Science, 2002. **298**(5600): p. 1912-34.
31. Bishop, A.C., K. Shah, Y. Liu, L. Witucki, C. Kung, and K.M. Shokat, *Design of allele-specific inhibitors to probe protein kinase signaling*. Curr Biol, 1998. **8**(5): p. 257-66.
32. Bishop, A.C., J.A. Ubersax, D.T. Petsch, D.P. Matheos, N.S. Gray, J. Blethrow, et al., *A chemical switch for inhibitor-sensitive alleles of any protein kinase*. Nature, 2000. **407**(6802): p. 395-401.
33. Bishop, A.C., O. Buzko, and K.M. Shokat, *Magic bullets for protein kinases*. Trends Cell Biol, 2001. **11**(4): p. 167-72.
34. Levinson, N.M., O. Kuchment, K. Shen, M.A. Young, M. Koldobskiy, M. Karplus, et al., *A Src-like inactive conformation in the abl tyrosine kinase domain*. PLoS Biol, 2006. **4**(5): p. e144.
35. Schindler, T., W. Bornmann, P. Pellicena, W.T. Miller, B. Clarkson, and J. Kuriyan, *Structural mechanism for STI-571 inhibition of abelson tyrosine kinase*. Science, 2000. **289**(5486): p. 1938-42.
36. Seeliger, M.A., B. Nagar, F. Frank, X. Cao, M.N. Henderson, and J. Kuriyan, *c-Src binds to the cancer drug imatinib with an inactive Abl/c-Kit conformation and a distributed thermodynamic penalty*. Structure, 2007. **15**(3): p. 299-311.
37. Hirsch, E., E. Ciruolo, A. Ghigo, and C. Costa, *Taming the PI3K team to hold inflammation and cancer at bay*. Pharmacol Therapeut, 2008. **118**(2): p. 192-205.
38. Rommel, C., M. Camps, and H. Ji, *PI3K delta and PI3K gamma: partners in crime in inflammation in rheumatoid arthritis and beyond?* Nat Rev Immunol, 2007. **7**(3): p. 191-201.
39. Cantley, L., *The phosphoinositide 3-kinase pathway*. Science, 2002. **296**(5573): p. 1655-1657.
40. Deane, J. and D. Fruman, *Phosphoinositide 3-kinase: Diverse roles in immune cell activation*. Annu Rev Immunol, 2004. **22**: p. 563-598.
41. Katso, R., K. Okkenhaug, K. Ahmadi, S. White, J. Timms, and M. Waterfield, *Cellular function of phosphoinositide 3-kinases: Implications for development, immunity, homeostasis, and cancer*. Annu Rev Cell Dev Biol, 2001. **17**: p. 615-675.
42. Puri, K., T. Doggett, C. Huang, J. Douangpanya, J. Hayflick, M. Turner, et al., *The role of endothelial PI3K-gamma activity in neutrophil trafficking*. Blood, 2005. **106**(1): p. 150-157.
43. Vanhaesebroeck, B., K. Ali, A. Bilancio, B. Geering, and L. Foukas, *Signalling by PI3K isoforms: insights from gene-targeted mice*. Trends Biochem Sci, 2005. **30**(4): p. 194-204.
44. Okkenhaug, K. and B. Vanhaesebroeck, *PI3K-signalling in B- and T-cells: insights from gene-targeted mice*. Biochem Soc Trans, 2003. **31**: p. 270-274.
45. Marone, R., V. Cmijanovic, B. Giese, and M. Wymann, *Targeting phosphoinositide 3-kinase - Moving towards therapy*. Biochim Biophys Acta Protein Proteomics, 2008. **1784**(1): p. 159-185.

46. Ruckle, T., M. Schwarz, and C. Rommel, *PI3K gamma inhibition: towards an 'aspirin of the 21st century'?* Nat Rev Drug Discov, 2006. **5**(11): p. 903-918.
47. Konrad, S., S. Ali, K. Wiege, S. Syed, L. Engling, R. Piekorz, et al., *Phosphoinositide 3-Kinases gamma and delta, Linkers of Coordinate C5a Receptor-Fc gamma Receptor Activation and Immune Complex-induced Inflammation.* J Biol Chem, 2008. **283**(48): p. 33296-33303.
48. Laffargue, M., R. Calvez, P. Finan, A. Trifilieff, M. Barbier, F. Altruda, et al., *Phosphoinositide 3-kinase gamma is an essential amplifier of mast cell function.* Immunity, 2002. **16**(3): p. 441-451.
49. Ali, K., A. Bilancio, M. Thomas, W. Pearce, A. Gilfillan, C. Tkaczyk, et al., *Essential role for the p110 delta phosphoinositide 3-kinase in the allergic response.* Nature, 2004. **431**(7011): p. 1007-1011.
50. Ali, K., M. Camps, W. Pearce, H. Ji, T. Ruckle, N. Kuehn, et al., *Isoform-specific functions of phosphoinositide 3-kinases: p110 delta but not p110 gamma promotes optimal allergic responses in vivo.* J Immunol, 2008. **180**(4): p. 2538-2544.
51. Reif, K., K. Okkenhaug, T. Sasaki, J. Penninger, B. Vanhaesebroeck, and J. Cyster, *Cutting edge: Differential roles for phosphoinositide 3-kinases, p110 gamma and p110 delta, in lymphocyte chemotaxis and homing.* J Immunol, 2004. **173**(4): p. 2236-2240.
52. Condliffe, A., K. Davidson, K. Anderson, C. Ellson, T. Crabbe, K. Okkenhaug, et al., *Sequential activation of class IB and class IA PI3K is important for the primed respiratory burst of human but not murine neutrophils.* Blood, 2005. **106**(4): p. 1432-1440.
53. Knight, Z., G. Chiang, P. Alaimo, D. Kenski, C. Ho, K. Coan, et al., *Isoform-specific phosphoinositide 3-kinase inhibitors from an arylmorpholine scaffold.* Bioorg Med Chem, 2004. **12**(17): p. 4749-4759.
54. Berndt, A., S. Miller, O. Williams, D.D. Le, B.T. Houseman, J.I. Pacold, et al., *The p110delta structure: mechanisms for selectivity and potency of new PI(3)K inhibitors.* Nat Chem Biol, 2010. **6**(3): p. 244.
55. Ito, K., G. Caramori, and I. Adcock, *Therapeutic potential of phosphatidylinositol 3-kinase inhibitors in inflammatory respiratory disease.* J Pharmacol Exp Therapeut, 2007. **321**(1): p. 1-8.
56. Okkenhaug, K., A. Bilancio, G. Farjot, H. Priddle, S. Sancho, E. Peskett, et al., *Impaired B and T cell antigen receptor signaling in p110 delta PI 3-kinase mutant mice.* Science, 2002. **297**(5583): p. 1031-1034.
57. Sadhu, C., K. Dick, W. Tino, and D. Staunton, *Selective role of PI3K delta in neutrophil inflammatory responses.* Biochem Biophys Res Commun, 2003. **308**(4): p. 764-769.
58. Del Prete, A., W. Vermi, E. Dander, K. Otero, L. Barberis, W. Luini, et al., *Defective dendritic cell migration and activation of adaptive immunity in PI3K gamma-deficient mice.* EMBO J, 2004. **23**(17): p. 3505-3515.
59. Rodriguez-Borlado, L., D. Barber, C. Hernandez, M. Rodriguez-Marcos, A. Sanchez, E. Hirsch, et al., *Phosphatidylinositol 3-kinase regulates the CD4/CD8 T cell differentiation ratio.* J Immunol, 2003. **170**(9): p. 4475-4482.

60. Barbi, J., H. Cummings, B. Lu, S. Oghumu, T. Ruckle, C. Rommel, et al., *PI3Kgamma (PI3K gamma) is essential for efficient induction of CXCR3 on activated T cells*. Blood, 2008. **112**(8): p. 3048-3051.
61. Ji, H., F. Rintelen, C. Waltzinger, D. Meier, A. Bilancio, W. Pearce, et al., *Inactivation of PI3K gamma and PI3K delta distorts T-cell development and causes multiple organ inflammation*. Blood, 2007. **110**(8): p. 2940-2947.
62. Noble, M., J. Endicott, and L. Johnson, *Protein kinase inhibitors: Insights into drug design from structure*. Science, 2004. **303**(5665): p. 1800-1805.
63. Knight, Z. and K. Shokat, *Features of selective kinase inhibitors*. Chem Biol, 2005. **12**(6): p. 621-637.
64. Apsel, B., J. Blair, B. Gonzalez, T. Nazif, M. Feldman, B. Aizenstein, et al., *Targeted polypharmacology: discovery of dual inhibitors of tyrosine and phosphoinositide kinases*. Nat Chem Biol, 2008. **4**(11): p. 691-699.
65. Knight, Z., M. Feldman, A. Balla, T. Balla, and K. Shokat, *A membrane capture assay for lipid kinase activity*. Nat Protoc, 2007. **2**(10): p. 2459-2466.
66. Pomel, V., J. Klicic, D. Covini, D. Church, J. Shaw, K. Roulin, et al., *Furan-2-ylmethylene thiazolidinediones as novel, potent, and selective inhibitors of phosphoinositide 3-kinase gamma*. J Med Chem, 2006. **49**(13): p. 3857-3871.
67. Palanki, M., E. Dneprovskaia, J. Doukas, R. Fine, J. Hood, X. Kang, et al., *Discovery of 3,3-(2,4-Diaminopteridine-6,7-diyl)diphenol as an isozyme-selective inhibitor of PI3K for the treatment of ischemia reperfusion injury associated with myocardial infarction*. J Med Chem, 2007. **50**(18): p. 4279-4294.
68. Walker, E., M. Pacold, O. Perisic, L. Stephens, P. Hawkins, M. Wymann, et al., *Structural determinants of phosphoinositide 3-kinase inhibition by wortmannin, LY294002, quercetin, myricetin, and staurosporine*. Mol Cell, 2000. **6**(4): p. 909-919.
69. Wu, W.L., D.A. Burnett, R. Spring, W.J. Greenlee, M. Smith, L. Favreau, et al., *Dopamine D1/D5 receptor antagonists with improved pharmacokinetics: design, synthesis, and biological evaluation of phenol bioisosteric analogues of benzazepine D1/D5 antagonists*. J Med Chem, 2005. **48**(3): p. 680-93.
70. Bohm, H.J., D. Banner, S. Bendels, M. Kansy, B. Kuhn, K. Muller, et al., *Fluorine in medicinal chemistry*. Chembiochem, 2004. **5**(5): p. 637-43.
71. Muller, K., C. Faeh, and F. Diederich, *Fluorine in pharmaceuticals: looking beyond intuition*. Science, 2007. **317**(5846): p. 1881-6.
72. Purser, S., P.R. Moore, S. Swallow, and V. Gouverneur, *Fluorine in medicinal chemistry*. Chem Soc Rev, 2008. **37**(2): p. 320-30.
73. Walker, E., O. Perisic, C. Ried, L. Stephens, and R. Williams, *Structural insights into phosphoinositide 3-kinase catalysis and signalling*. Nature, 1999. **402**(6759): p. 313-320.
74. Berndt, A., S. Miller, O. Williams, D.D. Le, B.T. Houseman, J.I. Pacold, et al., *The p110 delta structure: mechanisms for selectivity and potency of new PI(3)K inhibitors*. Nat Chem Biol, 2010. **6**(2): p. 117-24.
75. Camps, M., T. Ruckle, H. Ji, V. Ardisson, F. Rintelen, J. Shaw, et al., *Blockade of PI3K gamma suppresses joint inflammation and damage in mouse models of rheumatoid arthritis*. Nat Med, 2005. **11**(9): p. 936-943.



76. Doukas, J., W. Wrasidlo, G. Noronha, E. Dneprovskaja, R. Fine, S. Weis, et al., *Phosphoinositide 3-kinase gamma/delta inhibition limits infarct size after myocardial ischemia/reperfusion injury*. Proc Natl Acad Sci USA, 2006. **103**(52): p. 19866-19871.
77. Williams, O., B.T. Houseman, E.J. Kunkel, B. Aizenstein, R. Hoffman, Z.A. Knight, et al., *Discovery of dual inhibitors of the immune cell PI3Ks p110delta and p110gamma: a prototype for new anti-inflammatory drugs*. Chem Biol, 2010. **17**(2): p. 123-34.
78. Jackson, S.P., S.M. Schoenwaelder, I. Goncalves, W.S. Nesbitt, C.L. Yap, C.E. Wright, et al., *PI 3-kinase p110beta: a new target for antithrombotic therapy*. Nat Med, 2005. **11**(5): p. 507-14.
79. Vanhaesebroeck, B., M. Welham, K. Kotani, R. Stein, P. Warne, M. Zvelebil, et al., *p110 delta, a novel phosphoinositide 3-kinase in leukocytes*. Proc Natl Acad Sci USA, 1997. **94**(9): p. 4330-4335.
80. Kelley, T., M. Graham, A. Doseff, R. Pomerantz, S. Lau, M. Ostrowski, et al., *Macrophage colony-stimulating factor promotes cell survival through Akt/protein kinase B*. J Biol Chem, 1999. **274**(37): p. 26393-26398.
81. Jones, G., E. Prigmore, R. Calvez, C. Hogan, G. Dunn, E. Hirsch, et al., *Requirement for PI 3-kinase gamma in macrophage migration to MCP-1 and CSF-1*. Exp Cell Res, 2003. **290**(1): p. 120-131.
82. Barber, D., A. Bartolome, C. Hernandez, J. Flores, C. Redondo, C. Fernandez-Arias, et al., *PI3K gamma inhibition blocks glomerulonephritis and extends lifespan in a mouse model of systemic lupus*. Nat Med, 2005. **11**(9): p. 933-935.
83. Chatham, W.W., R. Swaim, H. Frohsin, Jr., L.W. Heck, E.J. Miller, and W.D. Blackburn, Jr., *Degradation of human articular cartilage by neutrophils in synovial fluid*. Arthritis Rheum, 1993. **36**(1): p. 51-8.
84. Schon, M.P. and W.H. Boehncke, *Psoriasis*. N Engl J Med, 2005. **352**(18): p. 1899-912.
85. Witko-Sarsat, V., P. Rieu, B. Descamps-Latscha, P. Lesavre, and L. Halbwachs-Mecarelli, *Neutrophils: molecules, functions and pathophysiological aspects*. Lab Invest, 2000. **80**(5): p. 617-53.
86. Hayakawa, M., H. Kaizawa, K. Kawaguchi, N. Ishikawa, T. Koizumi, T. Ohishi, et al., *Synthesis and biological evaluation of imidazo[1,2-a]pyridine derivatives as novel PI3 kinase p110alpha inhibitors*. Bioorg Med Chem, 2007. **15**(1): p. 403-12.
87. Vlahos, C.J., W.F. Matter, K.Y. Hui, and R.F. Brown, *A specific inhibitor of phosphatidylinositol 3-kinase, 2-(4-morpholinyl)-8-phenyl-4H-1-benzopyran-4-one (LY294002)*. J Biol Chem, 1994. **269**(7): p. 5241-8.
88. Mukaida, N., A. Harada, and K. Matsushima, *Interleukin-8 (IL-8) and monocyte chemoattractant and activating factor (MCAF/MCP-1), chemokines essentially involved in inflammatory and immune reactions*. Cytokine Growth Factor Rev, 1998. **9**(1): p. 9-23.
89. Baggiolini, M. and I. Clark-Lewis, *Interleukin-8, a chemotactic and inflammatory cytokine*. FEBS Lett, 1992. **307**(1): p. 97-101.

90. Williams, D.L., C. Li, T. Ha, T. Ozment-Skelton, J.H. Kalbfleisch, J. Preiszner, et al., *Modulation of the phosphoinositide 3-kinase pathway alters innate resistance to polymicrobial sepsis*. J Immunol, 2004. **172**(1): p. 449-56.
91. Williams, D.L., T. Ozment-Skelton, and C. Li, *Modulation of the phosphoinositide 3-kinase signaling pathway alters host response to sepsis, inflammation, and ischemia/reperfusion injury*. Shock, 2006. **25**(5): p. 432-9.
92. Hua, F., T. Ha, J. Ma, Y. Li, J. Kelley, X. Gao, et al., *Protection against myocardial ischemia/reperfusion injury in TLR4-deficient mice is mediated through a phosphoinositide 3-kinase-dependent mechanism*. J Immunol, 2007. **178**(11): p. 7317-24.
93. Wrann, C.D., N.A. Tabriz, T. Barkhausen, A. Klos, M. van Griensven, H.C. Pape, et al., *The phosphatidylinositol 3-kinase signaling pathway exerts protective effects during sepsis by controlling C5a-mediated activation of innate immune functions*. J Immunol, 2007. **178**(9): p. 5940-8.
94. Berg, E., E. Kunkel, E. Hytopoulos, and I. Plavec, *Characterization of compound mechanisms and secondary activities by BioMAP analysis*. Journal of Pharmacological and Toxicological Methods, 2006. **53**(1): p. 67-74.
95. Kunkel, E., M. Dea, A. Ebens, E. Hytopoulos, J. Melrose, D. Nguyen, et al., *An integrative biology approach for analysis of drug action in models of human vascular inflammation*. Faseb J, 2004. **18**(9): p. 1279-1281.
96. Solberg, H., M. Ploug, G. Hoyer-Hansen, B. Nielsen, and L. Lund, *The murine receptor for urokinase-type plasminogen activator is primarily expressed in tissues actively undergoing remodeling*. J Histochem Cytochem, 2001. **49**(2): p. 237-246.
97. Kjoller, L. and A. Hall, *Rac mediates cytoskeletal rearrangements and increased cell motility induced by urokinase-type plasminogen activator receptor binding to vitronectin*. J Cell Biol, 2001. **152**(6): p. 1145-1157.
98. Rothbard, J., R. Lechler, K. Howland, V. Bal, D. Eckels, R. Sekaly, et al., *Structural Model of HLA-DR1 Restricted T-Cell Antigen Recognition*. Cell, 1988. **52**(4): p. 515-523.
99. McEver, R., *Selectins - Novel Receptors That Mediate Leukocyte Adhesion During Inflammation*. Thromb Haemostasis, 1991. **65**(3): p. 223-228.
100. Daly, C. and B. Rollins, *Monocyte chemoattractant protein-1 (CCL2) in inflammatory disease and adaptive immunity: Therapeutic opportunities and controversies*. Microcirculation, 2003. **10**(3-4): p. 247-257.
101. Plavec, I., O. Sirenko, S. Privat, Y. Wang, M. Dajee, J. Melrose, et al., *Method for analyzing signaling networks in complex cellular systems*. Proc Natl Acad Sci USA, 2004. **101**(5): p. 1223-1228.
102. Onishi, K., M. Higuchi, T. Asakura, N. Masuyama, and Y. Gotoh, *The PI3K-Akt pathway promotes microtubule stabilization in migrating fibroblasts*. Gene Cell, 2007. **12**(4): p. 535-546.
103. Calippe, B., V. Douin-Echinard, M. Laffargue, H. Laurell, V. Rana-Poussine, B. Pipy, et al., *Chronic estradiol administration in vivo promotes the proinflammatory response of macrophages to TLR4 activation: Involvement of the phosphatidylinositol 3-kinase pathway*. J Immunol, 2008. **180**(12): p. 7980-7988.

104. Simoncini, T., A. Hafezl-Moghadam, D. Brazil, K. Ley, W. Chin, and J. Liao, *Interaction of oestrogen receptor with the regulatory subunit of phosphatidylinositol-3-OH kinase*. *Nature*, 2000. **407**(6803): p. 538-541.
105. Schindler, U. and V. Baichwal, *3 NF-Kappa-B Binding Sites in the Human E-Selectin Gene Required for Maximal Tumor Necrosis Factor Alpha-Induced Expression*. *Mol Cell Biol*, 1994. **14**(9): p. 5820-5831.
106. Kerfant, B., D. Zhao, I. Lorenzen-Schmidt, L. Wilson, S. Cai, S. Chen, et al., *PI3K gamma is required for PDE4, not PDE3, activity in subcellular Microdomains containing the sarcoplasmic reticular calcium ATPase in cardiomyocytes*. *Circ Res*, 2007. **101**(4): p. 400-408.
107. Teixeira, M., R. Gristwood, N. Cooper, and P. Hellewell, *Phosphodiesterase (PDE)4 inhibitors: Anti-inflammatory drugs of the future?* *Trends Pharmacol Sci*, 1997. **18**(5): p. 164-170.
108. Souness, J., M. Griffin, C. Maslen, K. Ebsworth, L. Scott, K. Pollock, et al., *Evidence that cyclic AMP phosphodiesterase inhibitors suppress TNF alpha generation from human monocytes by interacting with a 'low-affinity' phosphodiesterase 4 conformer*. *Br J Pharmacol*, 1996. **118**(3): p. 649-658.
109. Lisby, S., A. Fauschou, and R. Gniadecki, *The autocrine TNF alpha signalling loop in keratinocytes requires atypical PKC species and NF-kappa B activation but is independent of cholesterol-enriched membrane microdomains*. *Biochem Pharmacol*, 2007. **73**(4): p. 526-533.
110. Frey, R., X. Gao, K. Javaid, S. Siddiqui, A. Rahman, and A. Malik, *Phosphatidylinositol 3-kinase gamma signaling through protein kinase C zeta induces NADPH oxidase-mediated oxidant generation and NF-kappa B activation in endothelial cells*. *J Biol Chem*, 2006. **281**(23): p. 16128-16138.
111. Li, X. and G. Stark, *NF kappa B-dependent signaling pathways*. *Exp Hematol*, 2002. **30**(4): p. 285-296.
112. Schaecke, H., M. Berger, H. Rehwinkel, and K. Asadullah, *Selective glucocorticoid receptor agonists (SEGRAs): Novel ligands with an improved therapeutic index*. *Mol Cell Endocrinol*, 2007. **275**(1-2): p. 109-117.
113. Carvalho, M., C. Benjamim, F. Santos, S. Ferreira, and F. Cunha, *Effect of mast cells depletion on the failure of neutrophil migration during sepsis*. *Eur J Pharmacol*, 2005. **525**(1-3): p. 161-9.
114. Mallen-St Clair, J., C.T. Pham, S.A. Villalta, G.H. Caughey, and P.J. Wolters, *Mast cell dipeptidyl peptidase I mediates survival from sepsis*. *J Clin Invest*, 2004. **113**(4): p. 628-34.
115. Ramos, C.D., N.E. Heluy-Neto, R.A. Ribeiro, S.H. Ferreira, and F.Q. Cunha, *Neutrophil migration induced by IL-8-activated mast cells is mediated by CINC-1*. *Cytokine*, 2003. **21**(5): p. 214-23.
116. Adib-Conquy, M. and J.M. Cavaillon, *Stress molecules in sepsis and systemic inflammatory response syndrome*. *FEBS Lett*, 2007. **581**(19): p. 3723-33.
117. Brown, K.A., S.D. Brain, J.D. Pearson, J.D. Edgeworth, S.M. Lewis, and D.F. Treacher, *Neutrophils in development of multiple organ failure in sepsis*. *Lancet*, 2006. **368**(9530): p. 157-69.
118. Guo, R.F. and P.A. Ward, *C5a, a therapeutic target in sepsis*. *Recent Pat Antiinfect Drug Discov*, 2006. **1**(1): p. 57-65.

119. Cohen, J., *The immunopathogenesis of sepsis*. Nature, 2002. **420**(6917): p. 885-91.
120. Galli, S.J., *New concepts about the mast cell*. N Engl J Med, 1993. **328**(4): p. 257-65.
121. Galli, S.J., J. Kalesnikoff, M.A. Grimbaldston, A.M. Piliponsky, C.M. Williams, and M. Tsai, *Mast cells as "tunable" effector and immunoregulatory cells: recent advances*. Annu Rev Immunol, 2005. **23**: p. 749-86.
122. Malaviya, R., T. Ikeda, E. Ross, and S.N. Abraham, *Mast cell modulation of neutrophil influx and bacterial clearance at sites of infection through TNF-alpha*. Nature, 1996. **381**(6577): p. 77-80.
123. Bischoff, S.C., *Role of mast cells in allergic and non-allergic immune responses: comparison of human and murine data*. Nat Rev Immunol, 2007. **7**(2): p. 93-104.
124. Record, R.D., L.L. Froelich, C.J. Vlahos, and B.L. Blazer-Yost, *Phosphatidylinositol 3-kinase activation is required for insulin-stimulated sodium transport in A6 cells*. Am J Physiol, 1998. **274**(4 Pt 1): p. E611-7.
125. Wang, J., P. Barbry, A.C. Maiyar, D.J. Rozansky, A. Bhargava, M. Leong, et al., *SGK integrates insulin and mineralocorticoid regulation of epithelial sodium transport*. Am J Physiol Renal Physiol, 2001. **280**(2): p. F303-13.
126. Wang, J., Z.A. Knight, D. Fiedler, O. Williams, K.M. Shokat, and D. Pearce, *Activity of the p110-alpha subunit of phosphatidylinositol-3-kinase is required for activation of epithelial sodium transport*. Am J Physiol Renal Physiol, 2008. **295**(3): p. F843-50.
127. Holinstat, M., A.M. Preininger, S.B. Milne, W.J. Hudson, H.A. Brown, and H.E. Hamm, *Irreversible platelet activation requires protease-activated receptor 1-mediated signaling to phosphatidylinositol phosphates*. Mol Pharmacol, 2009. **76**(2): p. 301-13.
128. Sly, L.M., M.J. Hamilton, E. Kuroda, V.W. Ho, F.L. Antignano, S.L. Omeis, et al., *SHIP prevents lipopolysaccharide from triggering an antiviral response in mice*. Blood, 2009. **113**(13): p. 2945-54.
129. Billottet, C., V.L. Grandage, R.E. Gale, A. Quattropiani, C. Rommel, B. Vanhaesebroeck, et al., *A selective inhibitor of the p110delta isoform of PI 3-kinase inhibits AML cell proliferation and survival and increases the cytotoxic effects of VP16*. Oncogene, 2006. **25**(50): p. 6648-59.
130. Sujobert, P., V. Bardet, P. Cornillet-Lefebvre, J.S. Hayflick, N. Prie, F. Verdier, et al., *Essential role for the p110delta isoform in phosphoinositide 3-kinase activation and cell proliferation in acute myeloid leukemia*. Blood, 2005. **106**(3): p. 1063-6.
131. Xu, Q., S.E. Simpson, T.J. Scialla, A. Bagg, and M. Carroll, *Survival of acute myeloid leukemia cells requires PI3 kinase activation*. Blood, 2003. **102**(3): p. 972-80.
132. Braun, B.S., J.A. Archard, J.A. Van Ziffle, D.A. Tuveson, T.E. Jacks, and K. Shannon, *Somatic activation of a conditional KrasG12D allele causes ineffective erythropoiesis in vivo*. Blood, 2006. **108**(6): p. 2041-4.
133. Hatzivassiliou, G., K. Song, I. Yen, B.J. Brandhuber, D.J. Anderson, R. Alvarado, et al., *RAF inhibitors prime wild-type RAF to activate the MAPK pathway and enhance growth*. Nature, 2010. **464**(7287): p. 431-5.

134. Poulidakos, P.I., C. Zhang, G. Bollag, K.M. Shokat, and N. Rosen, *RAF inhibitors transactivate RAF dimers and ERK signalling in cells with wild-type BRAF*. Nature, 2010. **464**(7287): p. 427-30.
135. Keiser, M.J., B.L. Roth, B.N. Armbruster, P. Ernsberger, J.J. Irwin, and B.K. Shoichet, *Relating protein pharmacology by ligand chemistry*. Nat Biotechnol, 2007. **25**(2): p. 197-206.
136. Keiser, M.J., V. Setola, J.J. Irwin, C. Laggner, A.I. Abbas, S.J. Hufeisen, et al., *Predicting new molecular targets for known drugs*. Nature, 2009. **462**(7270): p. 175-81.
137. Okkenhaug, K. and B. Vanhaesebroeck, *PI3K in lymphocyte development, differentiation and activation*. Nat Rev Immunol, 2003. **3**(4): p. 317-330.
138. Bilancio, A., K. Okkenhaug, M. Camps, J.L. Emery, T. Ruckle, C. Rommel, et al., *Key role of the p110delta isoform of PI3K in B-cell antigen and IL-4 receptor signaling: comparative analysis of genetic and pharmacologic interference with p110delta function in B cells*. Blood, 2006. **107**(2): p. 642-50.
139. Herman, S.E., A.L. Gordon, A.J. Wagner, N.A. Heerema, W. Zhao, J.M. Flynn, et al., *Phosphatidylinositol 3-kinase-delta inhibitor CAL-101 shows promising preclinical activity in chronic lymphocytic leukemia by antagonizing intrinsic and extrinsic cellular survival signals*. Blood, 2010. **116**(12): p. 2078-88.
140. Lannutti, B.J., S.A. Meadows, S.E. Herman, A. Kashishian, B. Steiner, A.J. Johnson, et al., *CAL-101, a p110{delta} selective phosphatidylinositol-3-kinase inhibitor (PI3K) for the treatment of B cell malignancies inhibits PI3K signaling and cellular viability*. Blood, 2010.
141. Park, S., N. Chapuis, V. Bardet, J. Tamburini, N. Gallay, L. Willems, et al., *PI-103, a dual inhibitor of Class IA phosphatidylinositide 3-kinase and mTOR, has antileukemic activity in AML*. Leukemia, 2008. **22**(9): p. 1698-706.
142. Wee, S., D. Wiederschain, S.M. Maira, A. Loo, C. Miller, R. deBeaumont, et al., *PTEN-deficient cancers depend on PIK3CB*. Proc Natl Acad Sci U S A, 2008. **105**(35): p. 13057-62.
143. Peng, C., Y.Y. Chen, Z.F. Yang, H.J. Zhang, L. Osterby, A.G. Rosmarin, et al., *PTEN is a tumor suppressor in CML stem cells and BCR-ABL-induced leukemias in mice*. Blood, 2010. **115**(3): p. 626-635.
144. Gronbaek, K., J. Zeuthen, P. Guldberg, E. Ralfkiaer, and K. Hou-Jensen, *Alterations of the MMAC1/PTEN gene in lymphoid malignancies*. Blood, 1998. **91**(11): p. 4388-90.
145. Miletic, A.V., A.N. Anzelon-Mills, D.M. Mills, S.A. Omori, I.M. Pedersen, D.M. Shin, et al., *Coordinate suppression of B cell lymphoma by PTEN and SHIP phosphatases*. J Exp Med, 2010. **207**(11): p. 2407-20.
146. Johnson, C., S.J. Marriott, and L.S. Levy, *Overexpression of p101 activates PI3K gamma signaling in T cells and contributes to cell survival*. Oncogene, 2007. **26**(49): p. 7049-7057.
147. McBride, W.H., *Phenotype and functions of intratumoral macrophages*. Biochim Biophys Acta, 1986. **865**(1): p. 27-41.
148. Bingle, L., N.J. Brown, and C.E. Lewis, *The role of tumour-associated macrophages in tumour progression: implications for new anticancer therapies*. J Pathol, 2002. **196**(3): p. 254-65.

149. Meng, Y., M.A. Beckett, H. Liang, H.J. Mauceri, N. van Rooijen, K.S. Cohen, et al., *Blockade of tumor necrosis factor alpha signaling in tumor-associated macrophages as a radiosensitizing strategy*. *Cancer Res*, 2010. **70**(4): p. 1534-43.
150. Qian, B., Y. Deng, J.H. Im, R.J. Muschel, Y. Zou, J. Li, et al., *A distinct macrophage population mediates metastatic breast cancer cell extravasation, establishment and growth*. *PLoS One*, 2009. **4**(8): p. e6562.
151. Qian, B.Z. and J.W. Pollard, *Macrophage diversity enhances tumor progression and metastasis*. *Cell*, 2010. **141**(1): p. 39-51.
152. Qualls, J.E. and P.J. Murray, *A double agent in cancer: stopping macrophages wounds tumors*. *Nat Med*, 2010. **16**(8): p. 863-4.
153. Dorsam, R.T. and J.S. Gutkind, *G-protein-coupled receptors and cancer*. *Nat Rev Cancer*, 2007. **7**(2): p. 79-94.
154. Guo, H., Y. Ma, B. Zhang, B. Sun, R. Niu, G. Ying, et al., *Pivotal Advance: PKCzeta is required for migration of macrophages*. *J Leukoc Biol*, 2009. **85**(6): p. 911-8.
155. Maus, U.A., M. Backi, C. Winter, M. Srivastava, M.K. Schwarz, T. Ruckle, et al., *Importance of phosphoinositide 3-kinase gamma in the host defense against pneumococcal infection*. *Am J Respir Crit Care Med*, 2007. **175**(9): p. 958-66.
156. Martin, E.L., D.G. Souza, C.T. Fagundes, F.A. Amaral, B. Assenzio, V. Puntorieri, et al., *Phosphoinositide-3 kinase gamma activity contributes to sepsis and organ damage by altering neutrophil recruitment*. *Am J Respir Crit Care Med*, 2010. **182**(6): p. 762-73.
157. Doi, T., K. Obayashi, T. Kadowaki, H. Fujii, and S. Koyasu, *PI3K is a negative regulator of IgE production*. *International Immunology*, 2008. **20**(4): p. 499-508.
158. Zhang, T.T., K. Okkenhaug, B.F. Nashed, K.D. Puri, Z.A. Knight, K.M. Shokat, et al., *Genetic or pharmaceutical blockade of p110delta phosphoinositide 3-kinase enhances IgE production*. *J Allergy Clin Immunol*, 2008. **122**(4): p. 811-819 e2.
159. Storey, J. and R. Tibshirani, *Statistical significance for genomewide studies*. *Proc Natl Acad Sci USA*, 2003. **100**(16): p. 9440-9445.

## Appendix

### Invitrogen Kinase Inhibitor Profiling Data. SW18, DL 01, DL06, DL07

Profiling Data for SW18 tested at 10 $\mu$ M against 219 Kinases

Compound	[ATP] $\mu$ M	Kinase	Percent Inhibition		
			Assay 1	Assay 2	Mean
SW18	10	ABL1	-3	0	-2
SW18	10	ABL1 E255K	5	6	6
SW18	10	ABL1 G250E	1	3	2
SW18	10	ABL1 T315I	1	1	1
SW18	10	ABL1 Y253F	1	2	1
SW18	10	ABL2 (Arg)	2	2	2
SW18	10	ACVR1B (ALK4)	-1	-2	-1
SW18	10	ADRBK1 (GRK2)	2	3	2
SW18	10	ADRBK2 (GRK3)	1	4	3
SW18	10	AKT1 (PKB alpha)	4	7	5
SW18	10	AKT2 (PKB beta)	-1	1	0
SW18	10	AKT3 (PKB gamma)	2	5	4
SW18	10	ALK	0	-3	-2
SW18	10	AMPK A1/B1/G1 (PRKA A1/B1/G1)	-3	-3	-3
SW18	10	AURKB (Aurora B)	-1	2	1
SW18	10	AURKC (Aurora C)	-3	1	-1
SW18	10	BLK	0	1	0
SW18	10	BMX	-4	-1	-3
SW18	100	BRAF	10	27	19
SW18	100	BRAF V599E	5	11	8
SW18	10	BRSK1 (SAD1)	-1	0	-1
SW18	10	BTK	-2	0	-1
SW18	10	CAMK1D (CaMKI delta)	3	11	7
SW18	10	CAMK2A (CaMKII alpha)	-11	-4	-7
SW18	10	CAMK2B (CaMKII beta)	2	3	2
SW18	10	CAMK2D (CaMKII delta)	2	2	2
SW18	10	CAMK4 (CaMKIV)	0	9	4
SW18	10	CDC42 BPA (MRCKA)	2	-1	1
SW18	10	CDC42 BPB (MRCKB)	1	-1	0

SW18	10	CDK1/cyclin B	2	4	3
SW18	10	CDK2/cyclin A	-5	3	-1
SW18	10	CDK5/p35	-4	3	0
SW18	10	CHEK1 (CHK1)	-5	3	-1
SW18	100	CLK1	-3	0	-1
SW18	10	CLK2	-1	1	0
SW18	100	CLK3	11	9	10
SW18	10	CSF1R (FMS)	2	0	1
SW18	10	CSK	-1	-1	-1
SW18	10	CSNK1A1 (CK1 alpha 1)	4	5	4
SW18	10	CSNK1D (CK1 delta)	7	6	7
SW18	10	CSNK1E (CK1 epsilon)	13	17	15
SW18	10	CSNK1G1 (CK1 gamma 1)	-5	0	-2
SW18	10	CSNK1G2 (CK1 gamma 2)	-5	2	-2
SW18	10	CSNK1G3 (CK1 gamma 3)	-6	-3	-5
SW18	10	CSNK2A1 (CK2 alpha 1)	-3	-1	-2
SW18	10	CSNK2A2 (CK2 alpha 2)	4	5	4
SW18	10	DAPK3 (ZIPK)	-4	-1	-2
SW18	100	DCAMKL2 (DCK2)	2	3	2
SW18	10	DYRK1A	8	10	9
SW18	10	DYRK1B	5	9	7
SW18	10	DYRK3	-8	-3	-5
SW18	10	DYRK4	0	0	0
SW18	10	EGFR (ErbB1)	-5	-3	-4
SW18	10	EGFR L858R (ErbB1 L858R)	-1	-3	-2
SW18	10	EGFR L861Q (ErbB1 L861Q)	-4	-1	-3
SW18	10	EPHA1	-6	-5	-5
SW18	10	EPHA2	4	3	4
SW18	10	EPHA3	4	-2	1
SW18	100	EPHA4	-4	-5	-4
SW18	10	EPHA5	0	1	0
SW18	10	EPHA8	4	5	5
SW18	10	EPHB1	2	0	1
SW18	10	EPHB2	4	2	3
SW18	10	EPHB3	2	-1	0
SW18	10	EPHB4	5	10	7
SW18	10	ERBB2 (HER2)	-5	-9	-7
SW18	10	ERBB4 (HER4)	-5	-2	-4
SW18	10	FER	1	1	1
SW18	10	FES (FPS)	19	19	19



SW18	10	FGFR1	3	3	3
SW18	10	FGFR2	0	4	2
SW18	10	FGFR3	6	6	6
SW18	10	FGFR3 K650E	-3	-3	-3
SW18	10	FGFR4	2	5	3
SW18	10	FGR	4	11	8
SW18	100	FLT1 (VEGFR1)	-1	-2	-1
SW18	10	FLT3	1	5	3
SW18	10	FLT3 D835Y	1	4	3
SW18	10	FLT4 (VEGFR3)	1	0	1
SW18	10	FRK (PTK5)	2	5	3
SW18	10	FYN	2	6	4
SW18	10	GRK4	-6	-5	-5
SW18	10	GRK5	-6	-6	-6
SW18	10	GRK6	3	-1	1
SW18	10	GRK7	6	7	6
SW18	10	GSK3A (GSK3 alpha)	5	6	6
SW18	10	GSK3B (GSK3 beta)	1	3	2
SW18	10	HCK	5	9	7
SW18	10	HIPK1 (Myak)	0	1	0
SW18	10	HIPK4	7	9	8
SW18	10	IGF1R	-2	0	-1
SW18	10	IKBKB (IKK beta)	1	0	1
SW18	10	INSR	0	-5	-2
SW18	100	INSRR (IRR)	0	-1	0
SW18	10	IRAK4	-7	-2	-5
SW18	10	ITK	-3	-7	-5
SW18	10	JAK2	2	0	1
SW18	100	JAK2 JH1 JH2	-2	-8	-5
SW18	10	JAK2 JH1 JH2 V617F	8	2	5
SW18	10	JAK3	1	0	0
SW18	10	KDR (VEGFR2)	-6	-8	-7
SW18	100	KIT	4	5	4
SW18	10	KIT T670I	-1	6	2
SW18	10	LCK	2	6	4
SW18	10	LTK (TYK1)	1	5	3
SW18	10	LYN A	1	7	4
SW18	10	LYN B	1	6	3
SW18	100	MAP2K1 (MEK1)	2	3	3
SW18	100	MAP2K2 (MEK2)	-1	1	0
SW18	100	MAP2K6 (MKK6)	-1	0	0
SW18	100	MAP3K8 (COT)	13	11	12
SW18	100	MAP3K9 (MLK1)	-6	-5	-5
SW18	10	MAP4K2 (GCK)	-6	1	-2
SW18	10	MAP4K4 (HGK)	-4	3	0
SW18	10	MAP4K5 (KHS1)	6	9	8

SW18	10	MAPK1 (ERK2)	2	3	3
SW18	100	MAPK11 (p38 beta)	7	6	6
SW18	10	MAPK12 (p38 gamma)	4	3	3
SW18	10	MAPK13 (p38 delta)	4	6	5
SW18	100	MAPK14 (p38 alpha)	0	2	1
SW18	10	MAPK3 (ERK1)	3	6	4
SW18	10	MAPKAPK2	-3	-2	-3
SW18	10	MAPKAPK3	0	1	1
SW18	10	MAPKAPK5 (PRAK)	4	4	4
SW18	10	MARK1 (MARK)	1	0	1
SW18	10	MARK2	-4	-1	-3
SW18	10	MATK (HYL)	-6	-8	-7
SW18	10	MERTK (cMER)	0	3	2
SW18	10	MET (cMet)	-13	5	-4
SW18	10	MET M1250T	-3	-2	-2
SW18	10	MINK1	4	9	7
SW18	10	MST1R (RON)	50	37	43
SW18	100	MST4	-4	-2	-3
SW18	100	MUSK	-6	-3	-5
SW18	100	MYLK2 (skMLCK)	2	5	3
SW18	10	NEK1	-11	0	-6
SW18	10	NEK2	-5	5	0
SW18	100	NEK4	-2	0	-1
SW18	10	NEK6	6	3	4
SW18	100	NEK7	3	4	4
SW18	10	NEK9	22	5	14
SW18	100	NTRK1 (TRKA)	17	17	17
SW18	10	NTRK2 (TRKB)	-3	-6	-4
SW18	10	NTRK3 (TRKC)	1	7	4
SW18	10	PAK2 (PAK65)	-2	-2	-2
SW18	10	PAK3	12	11	12
SW18	10	PAK4	8	4	6
SW18	10	PAK6	5	6	5
SW18	10	PAK7 (KIAA1264)	4	6	5
SW18	100	PASK	-2	0	-1
SW18	10	PDGFRA (PDGFR alpha)	-3	-8	-6
SW18	10	PDGFRA D842V	4	2	3
SW18	100	PDGFRA T674I	5	3	4
SW18	10	PDGFRB (PDGFR beta)	0	-2	-1
SW18	100	PDK1	1	3	2
SW18	10	PHKG1	-2	5	2

SW18	10	PHKG2	-1	5	2
SW18	10	PIM1	6	8	7
SW18	10	PIM2	4	8	6
SW18	10	PKN1 (PRK1)	-2	10	4
SW18	10	PLK1	-3	0	-2
SW18	10	PLK2	4	2	3
SW18	10	PLK3	-1	3	1
SW18	10	PRKACA (PKA)	-2	1	-1
SW18	10	PRKCA (PKC alpha)	-2	14	6
SW18	10	PRKCB1 (PKC beta I)	23	21	22
SW18	10	PRKCB2 (PKC beta II)	4	8	6
SW18	10	PRKCD (PKC delta)	-9	13	2
SW18	10	PRKCE (PKC epsilon)	10	14	12
SW18	10	PRKCG (PKC gamma)	12	14	13
SW18	10	PRKCH (PKC eta)	2	0	1
SW18	10	PRKCI (PKC iota)	-25	-1	-13
SW18	10	PRKCN (PKD3)	-9	-3	-6
SW18	10	PRKCQ (PKC theta)	-14	8	-3
SW18	10	PRKCZ (PKC zeta)	19	21	20
SW18	10	PRKD1 (PKC mu)	8	9	9
SW18	10	PRKD2 (PKD2)	8	8	8
SW18	10	PRKG1	5	6	6
SW18	10	PRKG2 (PKG2)	-1	-2	-2
SW18	10	PRKX	14	10	12
SW18	10	PTK2B (FAK2)	-4	-1	-2
SW18	100	PTK6 (Brk)	1	1	1
SW18	100	RAF1 (cRAF)	26	21	24
SW18	10	RET	0	4	2
SW18	10	RET V804L	-1	1	0
SW18	10	RET Y791F	-1	2	1
SW18	10	ROCK1	3	14	9
SW18	10	ROCK2	2	7	5
SW18	100	ROS1	-1	-3	-2
SW18	10	RPS6KA1 (RSK1)	1	1	1
SW18	10	RPS6KA2 (RSK3)	7	9	8
SW18	10	RPS6KA3 (RSK2)	0	1	0
SW18	10	RPS6KA4 (MSK2)	-4	1	-2
SW18	10	RPS6KA5 (MSK1)	-3	1	-1
SW18	10	RPS6KA6 (RSK4)	-3	-1	-2
SW18	10	RPS6KB1 (p70S6K)	-10	-6	-8
SW18	10	SGK (SGK1)	-3	1	-1

SW18	10	SGK2	0	2	1
SW18	10	SGKL (SGK3)	-3	-1	-2
SW18	10	SRC	5	4	4
SW18	10	SRC N1	3	5	4
SW18	100	SRMS (Srm)	-4	-2	-3
SW18	10	SRPK1	3	6	4
SW18	10	SRPK2	0	8	4
SW18	10	STK22B (TSSK2)	-3	-1	-2
SW18	10	STK22D (TSSK1)	3	5	4
SW18	100	STK23 (MSSK1)	0	2	1
SW18	100	STK24 (MST3)	3	15	9
SW18	10	STK25 (YSK1)	8	4	6
SW18	10	STK3 (MST2)	0	1	0
SW18	10	STK4 (MST1)	-6	-6	-6
SW18	10	STK6 (Aurora A)	-4	-6	-5
SW18	10	SYK	-1	3	1
SW18	100	TAOK2 (TAO1)	-8	0	-4
SW18	10	TBK1	5	5	5
SW18	10	TEK (Tie2)	-5	-4	-4
SW18	10	TYRO3 (RSE)	-4	-9	-7
SW18	10	YES1	7	11	9
SW18	10	ZAP70	16	18	17

## Profiling Data for DL01 tested at 10 $\mu$ M against 246 Kinases

Compound	[ATP] $\mu$ M	Kinase	Percent Inhibition		
			Assay 1	Assay 2	Mean
DL01	Km app	ABL1	38	41	40
DL01	Km app	ABL1 E255K	56	55	55
DL01	Km app	ABL1 G250E	42	43	43
DL01	Km app	ABL1 T315I	44	42	43
DL01	Km app	ABL1 Y253F	56	55	56
DL01	Km app	ABL2 (Arg)	43	44	43
DL01	Km app	ACVR1B (ALK4)	18	17	18
DL01	Km app	ADRBK1 (GRK2)	4	1	2
DL01	Km app	ADRBK2 (GRK3)	0	23	11
DL01	Km app	AKT1 (PKB alpha)	-2	-6	-4
DL01	Km app	AKT2 (PKB beta)	-1	-2	-2
DL01	Km app	AKT3 (PKB gamma)	4	2	3
DL01	Km app	ALK	10	19	15
DL01	Km app	AMPK A1/B1/G1	27	23	25
DL01	Km app	AMPK A2/B1/G1	18	16	17
DL01	Km app	AURKA (Aurora A)	57	58	58
DL01	Km app	AURKB (Aurora B)	24	24	24
DL01	Km app	AURKC (Aurora C)	27	23	25
DL01	Km app	AXL	5	3	4
DL01	Km app	BLK	62	62	62
DL01	Km app	BMX	25	28	26
DL01	100	BRAF	21	14	18
DL01	100	BRAF V599E	28	37	33
DL01	Km app	BRSK1 (SAD1)	32	30	31
DL01	Km app	BTK	29	25	27
DL01	Km app	CAMK1D (CaMKI delta)	14	14	14
DL01	Km app	CAMK2A (CaMKII alpha)	2	0	1
DL01	Km app	CAMK2B (CaMKII beta)	16	16	16
DL01	Km app	CAMK2D (CaMKII delta)	33	35	34
DL01	Km app	CAMK4 (CaMKIV)	2	1	2
DL01	Km app	CDC42 BPA (MRCKA)	16	15	15
DL01	Km app	CDC42 BPB (MRCKB)	-3	-4	-4
DL01	Km app	CDK1/cyclin B	15	13	14
DL01	Km app	CDK2/cyclin A	32	31	32
DL01	Km app	CDK5/p25	18	17	17
DL01	Km app	CDK5/p35	28	30	29

DL01	Km app	CHEK1 (CHK1)	13	17	15
DL01	Km app	CHEK2 (CHK2)	4	-2	1
DL01	Km app	CLK1	34	34	34
DL01	Km app	CLK2	71	70	70
DL01	Km app	CLK3	27	29	28
DL01	Km app	CSF1R (FMS)	57	55	56
DL01	Km app	CSK	33	39	36
DL01	Km app	CSNK1A1 (CK1 alpha 1)	21	18	19
DL01	Km app	CSNK1D (CK1 delta)	51	50	50
DL01	Km app	CSNK1E (CK1 epsilon)	53	54	54
DL01	Km app	CSNK1G1 (CK1 gamma 1)	20	23	21
DL01	Km app	CSNK1G2 (CK1 gamma 2)	29	28	29
DL01	Km app	CSNK1G3 (CK1 gamma 3)	29	43	36
DL01	Km app	CSNK2A1 (CK2 alpha 1)	-6	-6	-6
DL01	Km app	CSNK2A2 (CK2 alpha 2)	8	7	8
DL01	Km app	DAPK3 (ZIPK)	18	18	18
DL01	Km app	DCAMKL2 (DCK2)	5	3	4
DL01	Km app	DNA-PK	45	42	43
DL01	Km app	DYRK1A	13	12	12
DL01	Km app	DYRK1B	23	34	29
DL01	Km app	DYRK3	73	74	73
DL01	Km app	DYRK4	5	5	5
DL01	Km app	EEF2K	9	9	9
DL01	Km app	EGFR (ErbB1)	9	3	6
DL01	Km app	EGFR (ErbB1) L858R	11	10	11
DL01	Km app	EGFR (ErbB1) L861Q	2	3	2
DL01	Km app	EGFR (ErbB1) T790M	15	15	15
DL01	Km app	EGFR (ErbB1) T790M L858R	33	30	32
DL01	Km app	EPHA1	57	55	56
DL01	Km app	EPHA2	21	19	20
DL01	Km app	EPHA4	23	24	24
DL01	Km app	EPHA5	35	33	34
DL01	Km app	EPHA8	22	21	22
DL01	Km app	EPHB1	38	41	40
DL01	Km app	EPHB2	29	28	28
DL01	Km app	EPHB3	52	52	52
DL01	Km app	EPHB4	29	30	29
DL01	Km app	ERBB2 (HER2)	-2	-8	-5
DL01	Km app	ERBB4 (HER4)	24	17	20
DL01	Km app	FER	30	30	30
DL01	Km app	FES (FPS)	21	25	23

DL01	Km app	FGFR1	32	34	33
DL01	Km app	FGFR2	36	36	36
DL01	Km app	FGFR3	17	16	16
DL01	Km app	FGFR3 K650E	37	34	36
DL01	Km app	FGFR4	23	23	23
DL01	Km app	FGR	72	72	72
DL01	Km app	FLT1 (VEGFR1)	18	19	18
DL01	Km app	FLT3	66	67	66
DL01	Km app	FLT3 D835Y	100	94	97
DL01	Km app	FLT4 (VEGFR3)	66	65	66
DL01	Km app	FRAP1 (mTOR)	54	49	51
DL01	Km app	FRK (PTK5)	29	26	28
DL01	Km app	FYN	40	38	39
DL01	Km app	GRK4	15	11	13
DL01	Km app	GRK5	-1	2	0
DL01	Km app	GRK6	2	1	2
DL01	Km app	GRK7	9	6	8
DL01	Km app	GSK3A (GSK3 alpha)	47	45	46
DL01	Km app	GSK3B (GSK3 beta)	35	32	33
DL01	Km app	HCK	27	27	27
DL01	Km app	HIPK1 (Myak)	23	26	24
DL01	Km app	HIPK2	21	24	22
DL01	Km app	HIPK3 (YAK1)	6	24	15
DL01	Km app	HIPK4	22	22	22
DL01	Km app	IGF1R	13	12	13
DL01	Km app	IKBKB (IKK beta)	13	11	12
DL01	Km app	IKBKE (IKK epsilon)	-7	-8	-8
DL01	Km app	INSR	-3	-9	-6
DL01	Km app	INSRR (IRR)	7	7	7
DL01	Km app	IRAK4	46	39	43
DL01	Km app	ITK	3	-2	0
DL01	Km app	JAK1	9	9	9
DL01	Km app	JAK2	25	24	24
DL01	Km app	JAK2 JH1 JH2	6	3	4
DL01	Km app	JAK2 JH1 JH2 V617F	0	1	1
DL01	Km app	JAK3	17	15	16
DL01	Km app	KDR (VEGFR2)	72	72	72
DL01	Km app	KIT	16	17	16
DL01	Km app	KIT T670I	6	11	8
DL01	Km app	LCK	59	64	62
DL01	Km app	LTK (TYK1)	8	7	8

DL01	Km app	LYN A	50	52	51
DL01	Km app	LYN B	55	57	56
DL01	100	MAP2K1 (MEK1)	2	3	2
DL01	100	MAP2K2 (MEK2)	11	12	11
DL01	100	MAP2K6 (MKK6)	-1	-1	-1
DL01	100	MAP3K8 (COT)	4	5	4
DL01	Km app	MAP3K9 (MLK1)	6	5	6
DL01	Km app	MAP4K2 (GCK)	58	61	60
DL01	Km app	MAP4K4 (HGK)	29	27	28
DL01	Km app	MAP4K5 (KHS1)	35	31	33
DL01	Km app	MAPK1 (ERK2)	4	3	4
DL01	100	MAPK10 (JNK3)	-2	16	7
DL01	Km app	MAPK11 (p38 beta)	9	8	8
DL01	Km app	MAPK12 (p38 gamma)	11	14	12
DL01	Km app	MAPK13 (p38 delta)	0	-1	0
DL01	100	MAPK14 (p38 alpha)	4	0	2
DL01	Km app	MAPK14 (p38 alpha) Direct	11	9	10
DL01	Km app	MAPK3 (ERK1)	8	11	9
DL01	100	MAPK8 (JNK1)	16	17	16
DL01	100	MAPK9 (JNK2)	8	7	7
DL01	Km app	MAPKAPK2	14	11	12
DL01	Km app	MAPKAPK3	4	5	4
DL01	Km app	MAPKAPK5 (PRAK)	7	7	7
DL01	Km app	MARK1 (MARK)	12	8	10
DL01	Km app	MARK2	6	5	5
DL01	Km app	MARK3	37	35	36
DL01	Km app	MARK4	18	26	22
DL01	Km app	MATK (HYL)	4	8	6
DL01	Km app	MELK	101	103	102
DL01	Km app	MERTK (cMER)	12	18	15
DL01	Km app	MET (cMet)	-1	-1	-1
DL01	Km app	MET M1250T	6	6	6
DL01	Km app	MINK1	30	28	29
DL01	Km app	MKNK1 (MNK1)	13	12	13
DL01	Km app	MST1R (RON)	20	20	20
DL01	Km app	MST4	25	16	21
DL01	Km app	MUSK	22	22	22
DL01	Km app	MYLK2 (skMLCK)	2	5	3
DL01	Km app	NEK1	19	22	20
DL01	Km app	NEK2	-12	-10	-11
DL01	Km app	NEK4	14	11	13



DL01	Km app	NEK6	4	-2	1
DL01	Km app	NEK7	11	6	9
DL01	Km app	NEK9	-5	-2	-3
DL01	Km app	NTRK1 (TRKA)	45	55	50
DL01	Km app	NTRK2 (TRKB)	74	75	74
DL01	Km app	NTRK3 (TRKC)	73	73	73
DL01	Km app	PAK1	8	12	10
DL01	Km app	PAK2 (PAK65)	0	1	1
DL01	Km app	PAK3	-4	1	-1
DL01	Km app	PAK4	41	54	48
DL01	Km app	PAK6	-4	1	-1
DL01	Km app	PAK7 (KIAA1264)	34	34	34
DL01	Km app	PASK	14	14	14
DL01	Km app	PDGFRA (PDGFR alpha)	27	26	26
DL01	Km app	PDGFRA D842V	30	27	28
DL01	Km app	PDGFRA T674I	16	14	15
DL01	Km app	PDGFRA V561D	55	57	56
DL01	Km app	PDGFRB (PDGFR beta)	14	13	13
DL01	100	PDK1	12	12	12
DL01	Km app	PDK1 Direct	9	4	7
DL01	Km app	PHKG1	4	13	9
DL01	Km app	PHKG2	9	14	11
DL01	Km app	PIM1	5	3	4
DL01	Km app	PIM2	4	-1	2
DL01	Km app	PKN1 (PRK1)	8	20	14
DL01	Km app	PLK1	-1	2	1
DL01	Km app	PLK2	10	12	11
DL01	Km app	PLK3	-2	11	5
DL01	Km app	PRKACA (PKA)	10	11	10
DL01	Km app	PRKCA (PKC alpha)	24	17	21
DL01	Km app	PRKCB1 (PKC beta I)	14	15	14
DL01	Km app	PRKCB2 (PKC beta II)	8	4	6
DL01	Km app	PRKCD (PKC delta)	5	4	5
DL01	Km app	PRKCE (PKC epsilon)	20	16	18
DL01	Km app	PRKCG (PKC gamma)	30	28	29
DL01	Km app	PRKCH (PKC eta)	21	33	27
DL01	Km app	PRKCI (PKC iota)	-1	-3	-2
DL01	Km app	PRKCN (PKD3)	52	54	53
DL01	Km app	PRKCQ (PKC theta)	1	-1	0
DL01	Km app	PRKCZ (PKC zeta)	-3	-8	-5
DL01	Km app	PRKD1 (PKC mu)	44	41	42

DL01	Km app	PRKD2 (PKD2)	55	55	55
DL01	Km app	PRKG1	9	8	9
DL01	Km app	PRKG2 (PKG2)	20	21	21
DL01	Km app	PRKX	6	8	7
DL01	Km app	PTK2 (FAK)	12	12	12
DL01	Km app	PTK2B (FAK2)	5	10	8
DL01	Km app	PTK6 (Brk)	59	47	53
DL01	100	RAF1 (cRAF) Y340D Y341D	29	27	28
DL01	Km app	RET	92	94	93
DL01	Km app	RET V804L	81	82	82
DL01	Km app	RET Y791F	93	94	93
DL01	Km app	ROCK1	12	8	10
DL01	Km app	ROCK2	25	27	26
DL01	Km app	ROS1	40	42	41
DL01	Km app	RPS6KA1 (RSK1)	9	9	9
DL01	Km app	RPS6KA2 (RSK3)	9	15	12
DL01	Km app	RPS6KA3 (RSK2)	9	6	7
DL01	Km app	RPS6KA4 (MSK2)	61	63	62
DL01	Km app	RPS6KA5 (MSK1)	29	32	30
DL01	Km app	RPS6KA6 (RSK4)	38	35	37
DL01	Km app	RPS6KB1 (p70S6K)	11	6	9
DL01	Km app	SGK (SGK1)	27	19	23
DL01	Km app	SGK2	22	30	26
DL01	Km app	SGKL (SGK3)	25	18	22
DL01	Km app	SNF1LK2	29	31	30
DL01	Km app	SRC	38	38	38
DL01	Km app	SRC N1	44	48	46
DL01	Km app	SRMS (Srm)	24	23	23
DL01	Km app	SRPK1	3	1	2
DL01	Km app	SRPK2	7	8	8
DL01	Km app	STK22B (TSSK2)	3	5	4
DL01	Km app	STK22D (TSSK1)	14	14	14
DL01	Km app	STK23 (MSSK1)	6	8	7
DL01	Km app	STK24 (MST3)	26	23	24
DL01	Km app	STK25 (YSK1)	30	30	30
DL01	Km app	STK3 (MST2)	25	28	26
DL01	Km app	STK4 (MST1)	34	37	36
DL01	Km app	SYK	5	8	7
DL01	Km app	TAOK2 (TAO1)	8	4	6
DL01	Km app	TBK1	-5	-6	-6
DL01	Km app	TEK (Tie2)	8	10	9

DL01	Km app	TXK	65	66	66
DL01	Km app	TYK2	18	19	18
DL01	Km app	TYRO3 (RSE)	21	16	19
DL01	Km app	YES1	60	58	59
DL01	Km app	ZAP70	3	1	2

## Profiling Data for DL06 tested at 10 $\mu$ M against 243 Kinases

Compound	[ATP] $\mu$ M	Kinase	Percent Inhibition		
			Assay 1	Assay 2	Mean
DL06	Km app	ABL1	61	68	65
DL06	Km app	ABL1 E255K	69	68	68
DL06	Km app	ABL1 G250E	60	63	62
DL06	Km app	ABL1 T315I	35	46	41
DL06	Km app	ABL1 Y253F	73	73	73
DL06	Km app	ABL2 (Arg)	38	39	39
DL06	Km app	ACVR1B (ALK4)	14	14	14
DL06	Km app	ADRBK1 (GRK2)	2	0	1
DL06	Km app	ADRBK2 (GRK3)	1	0	0
DL06	Km app	AKT1 (PKB alpha)	-8	-8	-8
DL06	Km app	AKT2 (PKB beta)	7	6	7
DL06	Km app	AKT3 (PKB gamma)	2	0	1
DL06	Km app	ALK	11	17	14
DL06	Km app	AMPK A1/B1/G1	7	9	8
DL06	Km app	AMPK A2/B1/G1	33	31	32
DL06	Km app	AURKA (Aurora A)	32	32	32
DL06	Km app	AURKB (Aurora B)	26	27	26
DL06	Km app	AURKC (Aurora C)	23	22	22
DL06	Km app	AXL	11	8	9
DL06	Km app	BLK	29	33	31
DL06	Km app	BMX	38	39	39
DL06	100	BRAF	58	48	53
DL06	100	BRAF V599E	83	81	82
DL06	Km app	BRSK1 (SAD1)	14	14	14
DL06	Km app	BTK	54	57	56
DL06	Km app	CAMK1D (CaMKI delta)	11	0	5
DL06	Km app	CAMK2A (CaMKII alpha)	15	13	14
DL06	Km app	CAMK2B (CaMKII beta)	17	10	14
DL06	Km app	CAMK2D (CaMKII delta)	21	23	22
DL06	Km app	CAMK4 (CaMKIV)	7	3	5
DL06	Km app	CDC42 BPA (MRCKA)	5	4	4
DL06	Km app	CDC42 BPB (MRCKB)	5	-3	1
DL06	Km app	CDK1/cyclin B	11	12	12
DL06	Km app	CDK2/cyclin A	0	-1	-1
DL06	Km app	CDK5/p25	10	9	10
DL06	Km app	CDK5/p35	8	6	7
DL06	Km app	CHEK1 (CHK1)	-14	-12	-13
DL06	Km app	CHEK2 (CHK2)	0	-2	-1
DL06	Km app	CLK1	12	16	14
DL06	Km app	CLK2	24	26	25
DL06	Km app	CLK3	16	17	17
DL06	Km app	CSF1R (FMS)	52	56	54

DL06	Km app	CSK	20	19	19
DL06	Km app	CSNK1A1 (CK1 alpha 1)	1	2	2
DL06	Km app	CSNK1D (CK1 delta)	44	47	46
DL06	Km app	CSNK1E (CK1 epsilon)	93	93	93
DL06	Km app	CSNK1G1 (CK1 gamma 1)	-9	-15	-12
DL06	Km app	CSNK1G2 (CK1 gamma 2)	9	11	10
DL06	Km app	CSNK1G3 (CK1 gamma 3)	4	9	7
DL06	Km app	CSNK2A1 (CK2 alpha 1)	0	9	4
DL06	Km app	CSNK2A2 (CK2 alpha 2)	0	0	0
DL06	Km app	DAPK3 (ZIPK)	1	1	1
DL06	Km app	DCAMKL2 (DCK2)	2	2	2
DL06	Km app	DYRK1A	3	5	4
DL06	Km app	DYRK1B	-4	-3	-4
DL06	Km app	DYRK3	4	6	5
DL06	Km app	DYRK4	0	1	1
DL06	Km app	EEF2K	12	12	12
DL06	Km app	EGFR (ErbB1)	10	9	9
DL06	Km app	EGFR (ErbB1) L858R	10	8	9
DL06	Km app	EGFR (ErbB1) L861Q	10	10	10
DL06	Km app	EGFR (ErbB1) T790M	6	11	9
DL06	Km app	EGFR (ErbB1) T790M L858R	6	14	10
DL06	Km app	EPHA1	75	77	76
DL06	Km app	EPHA2	22	22	22
DL06	Km app	EPHA3	3	7	5
DL06	Km app	EPHA4	39	41	40
DL06	Km app	EPHA5	26	29	28
DL06	Km app	EPHA8	53	56	54
DL06	Km app	EPHB1	52	51	52
DL06	Km app	EPHB2	53	56	55
DL06	Km app	EPHB3	31	29	30
DL06	Km app	EPHB4	27	32	30
DL06	Km app	ERBB2 (HER2)	11	11	11
DL06	Km app	ERBB4 (HER4)	20	18	19
DL06	Km app	FER	15	15	15
DL06	Km app	FES (FPS)	7	12	10
DL06	Km app	FGFR1	19	15	17
DL06	Km app	FGFR2	62	63	63
DL06	Km app	FGFR3	30	24	27
DL06	Km app	FGFR3 K650E	49	47	48
DL06	Km app	FGFR4	18	16	17
DL06	Km app	FGR	76	76	76
DL06	Km app	FLT1 (VEGFR1)	12	6	9
DL06	Km app	FLT3	58	60	59
DL06	Km app	FLT3 D835Y	20	20	20
DL06	Km app	FLT4 (VEGFR3)	48	46	47
DL06	Km app	FRAP1 (mTOR)	70	73	72
DL06	Km app	FRK (PTK5)	39	44	41

DL06	Km app	FYN	56	56	56
DL06	Km app	GRK4	-4	1	-2
DL06	Km app	GRK5	-2	-1	-1
DL06	Km app	GRK6	0	2	1
DL06	Km app	GRK7	-2	2	0
DL06	Km app	GSK3A (GSK3 alpha)	11	12	11
DL06	Km app	GSK3B (GSK3 beta)	0	-1	-1
DL06	Km app	HCK	58	53	55
DL06	Km app	HIPK1 (Myak)	5	5	5
DL06	Km app	HIPK2	12	13	12
DL06	Km app	HIPK4	16	16	16
DL06	Km app	IGF1R	4	3	4
DL06	Km app	IKBKB (IKK beta)	7	10	8
DL06	Km app	IKBKE (IKK epsilon)	-2	-1	-2
DL06	Km app	INSR	1	1	1
DL06	Km app	INSRR (IRR)	22	21	22
DL06	Km app	IRAK4	5	2	4
DL06	Km app	ITK	7	15	11
DL06	Km app	JAK1	4	3	4
DL06	Km app	JAK2	-1	3	1
DL06	Km app	JAK2 JH1 JH2	1	1	1
DL06	Km app	JAK2 JH1 JH2 V617F	9	7	8
DL06	Km app	JAK3	0	0	0
DL06	Km app	KDR (VEGFR2)	49	50	49
DL06	Km app	KIT	4	3	3
DL06	Km app	KIT T670I	8	9	8
DL06	Km app	LCK	54	55	54
DL06	Km app	LTK (TYK1)	12	14	13
DL06	Km app	LYN A	61	64	63
DL06	Km app	LYN B	60	60	60
DL06	100	MAP2K1 (MEK1)	6	5	6
DL06	100	MAP2K2 (MEK2)	14	6	10
DL06	100	MAP2K6 (MKK6)	-1	-3	-2
DL06	100	MAP3K8 (COT)	28	28	28
DL06	Km app	MAP3K9 (MLK1)	9	5	7
DL06	Km app	MAP4K2 (GCK)	9	12	11
DL06	Km app	MAP4K4 (HGK)	7	5	6
DL06	Km app	MAP4K5 (KHS1)	23	29	26
DL06	Km app	MAPK1 (ERK2)	0	0	0
DL06	100	MAPK10 (JNK3)	11	10	11
DL06	Km app	MAPK11 (p38 beta)	10	10	10
DL06	Km app	MAPK12 (p38 gamma)	13	6	9
DL06	Km app	MAPK13 (p38 delta)	11	9	10
DL06	100	MAPK14 (p38 alpha)	38	36	37
DL06	Km app	MAPK14 (p38 alpha) Direct	-4	-4	-4
DL06	Km app	MAPK3 (ERK1)	8	5	7
DL06	100	MAPK8 (JNK1)	25	25	25

DL06	100	MAPK9 (JNK2)	33	29	31
DL06	Km app	MAPKAPK2	3	2	2
DL06	Km app	MAPKAPK3	5	5	5
DL06	Km app	MAPKAPK5 (PRAK)	-1	0	0
DL06	Km app	MARK1 (MARK)	-1	4	1
DL06	Km app	MARK2	16	16	16
DL06	Km app	MARK3	6	7	6
DL06	Km app	MARK4	3	6	5
DL06	Km app	MATK (HYL)	6	7	6
DL06	Km app	MELK	20	29	24
DL06	Km app	MERTK (cMER)	30	30	30
DL06	Km app	MET (cMet)	7	5	6
DL06	Km app	MET M1250T	7	3	5
DL06	Km app	MINK1	41	42	42
DL06	Km app	MST1R (RON)	0	-1	-1
DL06	Km app	MST4	-4	-6	-5
DL06	Km app	MUSK	17	25	21
DL06	Km app	MYLK2 (skMLCK)	5	5	5
DL06	Km app	NEK1	14	15	14
DL06	Km app	NEK2	7	2	5
DL06	Km app	NEK4	9	9	9
DL06	Km app	NEK6	3	4	3
DL06	Km app	NEK7	18	20	19
DL06	Km app	NEK9	6	-1	2
DL06	Km app	NTRK1 (TRKA)	31	28	30
DL06	Km app	NTRK2 (TRKB)	66	62	64
DL06	Km app	NTRK3 (TRKC)	84	88	86
DL06	Km app	PAK1	21	22	22
DL06	Km app	PAK2 (PAK65)	6	6	6
DL06	Km app	PAK3	6	-1	2
DL06	Km app	PAK4	13	12	13
DL06	Km app	PAK6	13	13	13
DL06	Km app	PAK7 (KIAA1264)	16	16	16
DL06	Km app	PASK	19	19	19
DL06	Km app	PDGFRA (PDGFR alpha)	18	22	20
DL06	Km app	PDGFRA D842V	7	9	8
DL06	Km app	PDGFRA T674I	76	80	78
DL06	Km app	PDGFRA V561D	62	58	60
DL06	Km app	PDGFRB (PDGFR beta)	1	1	1
DL06	100	PDK1	19	15	17
DL06	Km app	PDK1 Direct	0	-2	-1
DL06	Km app	PHKG1	4	18	11
DL06	Km app	PHKG2	8	7	8
DL06	Km app	PIM1	15	9	12
DL06	Km app	PIM2	-7	-7	-7
DL06	Km app	PKN1 (PRK1)	11	-3	4
DL06	Km app	PLK1	0	3	2

DL06	Km app	PLK2	-1	7	3
DL06	Km app	PLK3	-2	-2	-2
DL06	Km app	PRKACA (PKA)	0	-1	-1
DL06	Km app	PRKCA (PKC alpha)	0	1	1
DL06	Km app	PRKCB1 (PKC beta I)	11	3	7
DL06	Km app	PRKCB2 (PKC beta II)	11	9	10
DL06	Km app	PRKCD (PKC delta)	2	3	3
DL06	Km app	PRKCE (PKC epsilon)	13	23	18
DL06	Km app	PRKCG (PKC gamma)	15	15	15
DL06	Km app	PRKCH (PKC eta)	18	16	17
DL06	Km app	PRKCI (PKC iota)	15	4	10
DL06	Km app	PRKCN (PKD3)	12	12	12
DL06	Km app	PRKCQ (PKC theta)	17	17	17
DL06	Km app	PRKCZ (PKC zeta)	8	-2	3
DL06	Km app	PRKD1 (PKC mu)	23	15	19
DL06	Km app	PRKD2 (PKD2)	12	7	9
DL06	Km app	PRKG1	9	8	8
DL06	Km app	PRKG2 (PKG2)	13	13	13
DL06	Km app	PRKX	1	3	2
DL06	Km app	PTK2 (FAK)	12	15	14
DL06	Km app	PTK2B (FAK2)	3	2	3
DL06	Km app	PTK6 (Brk)	6	4	5
DL06	100	RAF1 (cRAF) Y340D Y341D	79	80	79
DL06	Km app	RET	98	96	97
DL06	Km app	RET V804L	23	24	23
DL06	Km app	RET Y791F	101	98	100
DL06	Km app	ROCK1	7	4	6
DL06	Km app	ROCK2	-5	-13	-9
DL06	Km app	ROS1	89	89	89
DL06	Km app	RPS6KA1 (RSK1)	7	9	8
DL06	Km app	RPS6KA2 (RSK3)	-3	0	-2
DL06	Km app	RPS6KA3 (RSK2)	11	11	11
DL06	Km app	RPS6KA4 (MSK2)	8	13	10
DL06	Km app	RPS6KA5 (MSK1)	15	13	14
DL06	Km app	RPS6KA6 (RSK4)	11	14	12
DL06	Km app	RPS6KB1 (p70S6K)	4	3	4
DL06	Km app	SGK (SGK1)	-8	-8	-8
DL06	Km app	SGK2	6	0	3
DL06	Km app	SGKL (SGK3)	3	6	4
DL06	Km app	SNF1LK2	12	20	16
DL06	Km app	SRC	31	33	32
DL06	Km app	SRC N1	56	55	55
DL06	Km app	SRMS (Srm)	19	3	11
DL06	Km app	SRPK1	13	15	14
DL06	Km app	SRPK2	4	-1	2
DL06	Km app	STK22B (TSSK2)	1	3	2
DL06	Km app	STK22D (TSSK1)	1	4	2



DL06	Km app	STK23 (MSSK1)	5	15	10
DL06	Km app	STK24 (MST3)	8	7	8
DL06	Km app	STK25 (YSK1)	3	-12	-4
DL06	Km app	STK3 (MST2)	1	-1	0
DL06	Km app	STK4 (MST1)	18	15	17
DL06	Km app	SYK	-3	-2	-3
DL06	Km app	TAOK2 (TAO1)	2	-1	0
DL06	Km app	TBK1	7	10	9
DL06	Km app	TEK (Tie2)	11	8	10
DL06	Km app	TYK2	10	24	17
DL06	Km app	TYRO3 (RSE)	23	23	23
DL06	Km app	YES1	57	60	59
DL06	Km app	ZAP70	11	11	11

Profiling Data for DL07 tested at 10 $\mu$ M against 243 Kinases

Compound	[ATP] $\mu$ M	Kinase	Percent Inhibition		
			Assay 1	Assay 2	Mean
DL07	Km app	ABL1	101	100	100
DL07	Km app	ABL1 E255K	100	102	101
DL07	Km app	ABL1 G250E	103	105	104
DL07	Km app	ABL1 T315I	100	100	100
DL07	Km app	ABL1 Y253F	99	97	98
DL07	Km app	ABL2 (Arg)	95	93	94
DL07	Km app	ACVR1B (ALK4)	102	104	103
DL07	Km app	ADRBK1 (GRK2)	30	24	27
DL07	Km app	ADRBK2 (GRK3)	0	4	2
DL07	Km app	AKT1 (PKB alpha)	6	5	6
DL07	Km app	AKT2 (PKB beta)	4	10	7
DL07	Km app	AKT3 (PKB gamma)	39	42	40
DL07	Km app	ALK	103	104	104
DL07	Km app	AMPK A1/B1/G1	97	98	98
DL07	Km app	AMPK A2/B1/G1	92	93	92
DL07	Km app	AURKA (Aurora A)	59	55	57
DL07	Km app	AURKB (Aurora B)	74	81	77
DL07	Km app	AURKC (Aurora C)	77	85	81
DL07	Km app	AXL	78	78	78
DL07	Km app	BLK	100	99	99
DL07	Km app	BMX	100	100	100
DL07	100	BRAF	99	101	100
DL07	100	BRAF V599E	99	102	100
DL07	Km app	BRSK1 (SAD1)	97	95	96
DL07	Km app	BTB	99	102	100
DL07	Km app	CAMK1D (CaMKI delta)	70	60	65
DL07	Km app	CAMK2A (CaMKII alpha)	48	48	48
DL07	Km app	CAMK2B (CaMKII beta)	30	40	35
DL07	Km app	CAMK2D (CaMKII delta)	83	85	84
DL07	Km app	CAMK4 (CaMKIV)	19	22	20
DL07	Km app	CDC42 BPA (MRCKA)	3	7	5
DL07	Km app	CDC42 BPB (MRCKB)	5	6	5
DL07	Km app	CDK1/cyclin B	65	71	68
DL07	Km app	CDK2/cyclin A	57	54	56
DL07	Km app	CDK5/p25	71	76	73
DL07	Km app	CDK5/p35	73	75	74
DL07	Km app	CHEK1 (CHK1)	-8	-9	-8
DL07	Km app	CHEK2 (CHK2)	80	81	81
DL07	Km app	CLK1	38	39	39
DL07	Km app	CLK2	83	84	84
DL07	Km app	CLK3	45	46	46
DL07	Km app	CSF1R (FMS)	96	98	97

DL07	Km app	CSK	96	100	98
DL07	Km app	CSNK1A1 (CK1 alpha 1)	43	41	42
DL07	Km app	CSNK1D (CK1 delta)	95	97	96
DL07	Km app	CSNK1E (CK1 epsilon)	101	100	101
DL07	Km app	CSNK1G1 (CK1 gamma 1)	44	46	45
DL07	Km app	CSNK1G2 (CK1 gamma 2)	50	52	51
DL07	Km app	CSNK1G3 (CK1 gamma 3)	55	57	56
DL07	Km app	CSNK2A1 (CK2 alpha 1)	5	10	8
DL07	Km app	CSNK2A2 (CK2 alpha 2)	3	3	3
DL07	Km app	DAPK3 (ZIPK)	99	101	100
DL07	Km app	DCAMKL2 (DCK2)	29	34	32
DL07	Km app	DYRK1A	66	72	69
DL07	Km app	DYRK1B	76	76	76
DL07	Km app	DYRK3	94	92	93
DL07	Km app	DYRK4	12	14	13
DL07	Km app	EEF2K	9	11	10
DL07	Km app	EGFR (ErbB1)	90	90	90
DL07	Km app	EGFR (ErbB1) L858R	90	92	91
DL07	Km app	EGFR (ErbB1) L861Q	93	90	92
DL07	Km app	EGFR (ErbB1) T790M	96	94	95
DL07	Km app	EGFR (ErbB1) T790M L858R	86	88	87
DL07	Km app	EPHA1	101	102	101
DL07	Km app	EPHA2	97	97	97
DL07	Km app	EPHA3	73	72	73
DL07	Km app	EPHA4	101	100	101
DL07	Km app	EPHA5	101	99	100
DL07	Km app	EPHA8	101	104	102
DL07	Km app	EPHB1	100	102	101
DL07	Km app	EPHB2	99	99	99
DL07	Km app	EPHB3	97	98	98
DL07	Km app	EPHB4	100	100	100
DL07	Km app	ERBB2 (HER2)	87	91	89
DL07	Km app	ERBB4 (HER4)	96	97	96
DL07	Km app	FER	72	72	72
DL07	Km app	FES (FPS)	52	56	54
DL07	Km app	FGFR1	96	96	96
DL07	Km app	FGFR2	103	104	103
DL07	Km app	FGFR3	89	90	90
DL07	Km app	FGFR3 K650E	101	105	103
DL07	Km app	FGFR4	94	96	95
DL07	Km app	FGR	100	102	101
DL07	Km app	FLT1 (VEGFR1)	93	93	93
DL07	Km app	FLT3	88	88	88
DL07	Km app	FLT3 D835Y	98	98	98
DL07	Km app	FLT4 (VEGFR3)	102	101	101
DL07	Km app	FRAP1 (mTOR)	100	100	100
DL07	Km app	FRK (PTK5)	95	95	95

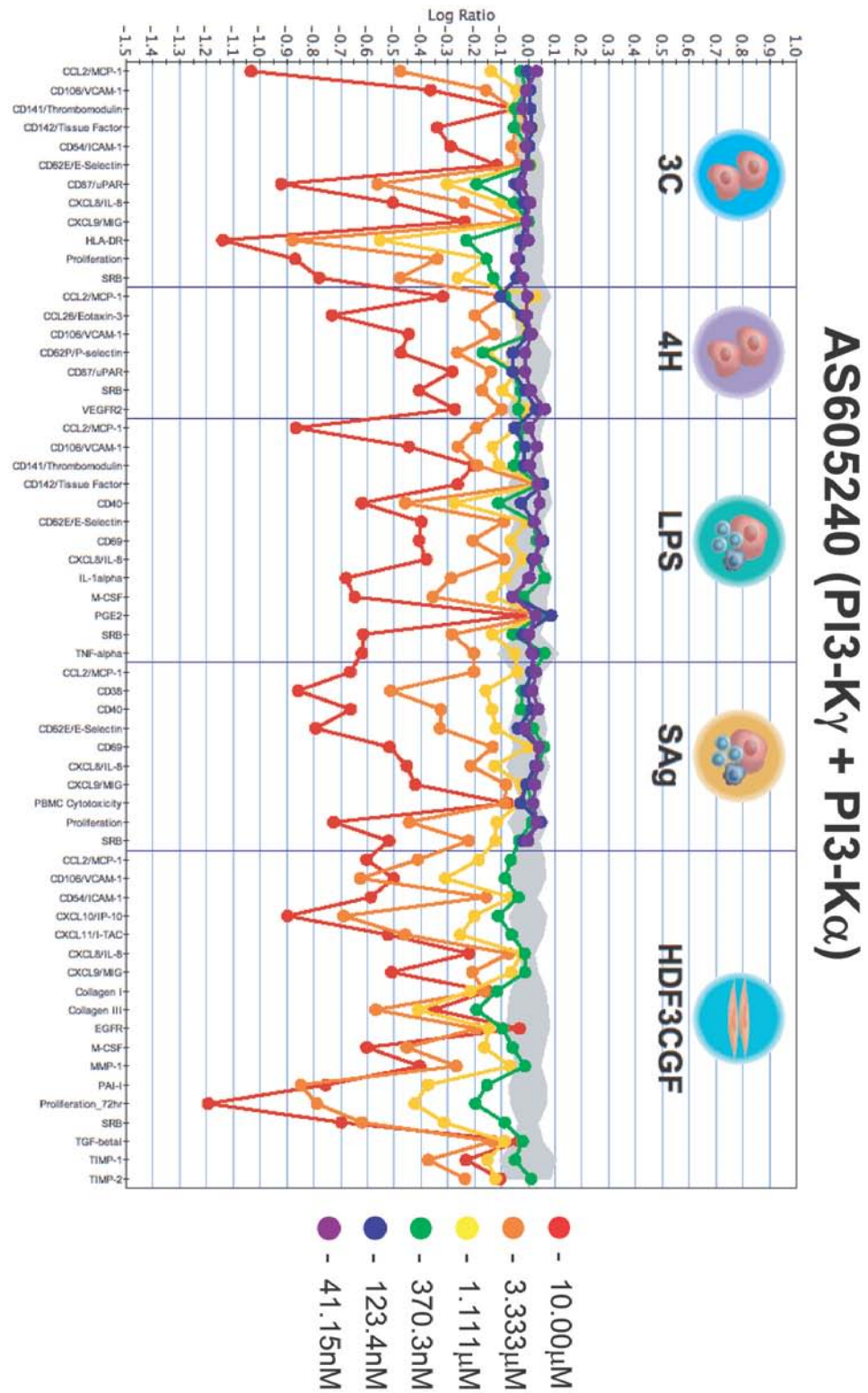
DL07	Km app	FYN	100	101	101
DL07	Km app	GRK4	48	51	49
DL07	Km app	GRK5	68	66	67
DL07	Km app	GRK6	89	87	88
DL07	Km app	GRK7	87	88	87
DL07	Km app	GSK3A (GSK3 alpha)	94	96	95
DL07	Km app	GSK3B (GSK3 beta)	89	90	90
DL07	Km app	HCK	102	98	100
DL07	Km app	HIPK1 (Myak)	61	60	60
DL07	Km app	HIPK2	59	61	60
DL07	Km app	HIPK4	39	42	41
DL07	Km app	IGF1R	30	30	30
DL07	Km app	IKBKB (IKK beta)	26	33	30
DL07	Km app	IKBKE (IKK epsilon)	15	1	8
DL07	Km app	INSR	23	20	22
DL07	Km app	INSRR (IRR)	43	43	43
DL07	Km app	IRAK4	26	30	28
DL07	Km app	ITK	99	101	100
DL07	Km app	JAK1	87	90	89
DL07	Km app	JAK2	94	94	94
DL07	Km app	JAK2 JH1 JH2	94	95	95
DL07	Km app	JAK2 JH1 JH2 V617F	97	98	98
DL07	Km app	JAK3	94	93	93
DL07	Km app	KDR (VEGFR2)	100	101	100
DL07	Km app	KIT	44	45	45
DL07	Km app	KIT T670I	17	21	19
DL07	Km app	LCK	99	99	99
DL07	Km app	LYN A	101	101	101
DL07	Km app	LYN B	99	100	100
DL07	100	MAP2K1 (MEK1)	37	44	40
DL07	100	MAP2K2 (MEK2)	35	44	40
DL07	100	MAP2K6 (MKK6)	27	32	29
DL07	100	MAP3K8 (COT)	43	57	50
DL07	Km app	MAP3K9 (MLK1)	66	73	70
DL07	Km app	MAP4K2 (GCK)	100	101	101
DL07	Km app	MAP4K4 (HGK)	90	89	90
DL07	Km app	MAP4K5 (KHS1)	97	97	97
DL07	Km app	MAPK1 (ERK2)	8	8	8
DL07	100	MAPK10 (JNK3)	40	48	44
DL07	Km app	MAPK11 (p38 beta)	48	50	49
DL07	Km app	MAPK12 (p38 gamma)	14	17	16
DL07	Km app	MAPK13 (p38 delta)	14	14	14
DL07	100	MAPK14 (p38 alpha)	70	73	71
DL07	Km app	MAPK14 (p38 alpha) Direct	18	19	19
DL07	Km app	MAPK3 (ERK1)	25	23	24
DL07	100	MAPK8 (JNK1)	38	39	38

DL07	100	MAPK9 (JNK2)	89	89	89
DL07	Km app	MAPKAPK2	4	8	6
DL07	Km app	MAPKAPK3	1	2	2
DL07	Km app	MAPKAPK5 (PRAK)	0	3	2
DL07	Km app	MARK1 (MARK)	100	99	99
DL07	Km app	MARK2	102	98	100
DL07	Km app	MARK3	99	97	98
DL07	Km app	MARK4	98	97	98
DL07	Km app	MATK (HYL)	19	13	16
DL07	Km app	MELK	103	104	103
DL07	Km app	MERTK (cMER)	76	78	77
DL07	Km app	MET (cMet)	8	9	9
DL07	Km app	MET M1250T	11	13	12
DL07	Km app	MINK1	99	103	101
DL07	Km app	MST1R (RON)	7	10	8
DL07	Km app	MST4	83	83	83
DL07	Km app	MUSK	61	70	65
DL07	Km app	MYLK2 (skMLCK)	74	74	74
DL07	Km app	NEK1	46	50	48
DL07	Km app	NEK2	3	21	12
DL07	Km app	NEK4	24	28	26
DL07	Km app	NEK6	-2	6	2
DL07	Km app	NEK7	9	25	17
DL07	Km app	NEK9	14	28	21
DL07	Km app	NTRK1 (TRKA)	82	81	82
DL07	Km app	NTRK2 (TRKB)	98	105	102
DL07	Km app	NTRK3 (TRKC)	104	103	104
DL07	Km app	PAK1	24	38	31
DL07	Km app	PAK2 (PAK65)	22	23	22
DL07	Km app	PAK3	23	19	21
DL07	Km app	PAK4	91	96	94
DL07	Km app	PAK6	68	75	72
DL07	Km app	PAK7 (KIAA1264)	90	91	91
DL07	Km app	PASK	98	99	98
DL07	Km app	PDGFRA (PDGFR alpha)	99	98	98
DL07	Km app	PDGFRA D842V	100	99	99
DL07	Km app	PDGFRA T674I	76	81	78
DL07	Km app	PDGFRA V561D	100	103	102
DL07	Km app	PDGFRB (PDGFR beta)	77	84	81
DL07	100	PDK1	21	20	20
DL07	Km app	PDK1 Direct	20	19	20
DL07	Km app	PHKG1	99	102	100
DL07	Km app	PHKG2	64	69	66
DL07	Km app	PIM1	63	72	68
DL07	Km app	PIM2	92	90	91
DL07	Km app	PKN1 (PRK1)	54	69	62
DL07	Km app	PLK1	6	10	8

DL07	Km app	PLK2	8	24	16
DL07	Km app	PLK3	3	-2	0
DL07	Km app	PRKACA (PKA)	68	67	67
DL07	Km app	PRKCA (PKC alpha)	15	16	15
DL07	Km app	PRKCB1 (PKC beta I)	38	41	40
DL07	Km app	PRKCB2 (PKC beta II)	33	26	29
DL07	Km app	PRKCD (PKC delta)	17	19	18
DL07	Km app	PRKCE (PKC epsilon)	57	62	60
DL07	Km app	PRKCG (PKC gamma)	47	52	50
DL07	Km app	PRKCH (PKC eta)	19	29	24
DL07	Km app	PRKCI (PKC iota)	52	52	52
DL07	Km app	PRKCN (PKD3)	77	72	75
DL07	Km app	PRKCQ (PKC theta)	25	36	31
DL07	Km app	PRKCZ (PKC zeta)	49	56	52
DL07	Km app	PRKD1 (PKC mu)	79	81	80
DL07	Km app	PRKD2 (PKD2)	86	85	85
DL07	Km app	PRKG1	40	42	41
DL07	Km app	PRKG2 (PKG2)	99	101	100
DL07	Km app	PRKX	21	29	25
DL07	Km app	PTK2 (FAK)	37	39	38
DL07	Km app	PTK2B (FAK2)	40	38	39
DL07	Km app	PTK6 (Brk)	13	3	8
DL07	100	RAF1 (cRAF) Y340D Y341D	99	102	100
DL07	Km app	RET	101	102	101
DL07	Km app	RET V804L	98	99	98
DL07	Km app	RET Y791F	103	103	103
DL07	Km app	ROCK1	10	8	9
DL07	Km app	ROCK2	-4	-7	-5
DL07	Km app	ROS1	85	87	86
DL07	Km app	RPS6KA1 (RSK1)	79	84	81
DL07	Km app	RPS6KA2 (RSK3)	81	79	80
DL07	Km app	RPS6KA3 (RSK2)	89	94	92
DL07	Km app	RPS6KA4 (MSK2)	80	80	80
DL07	Km app	RPS6KA5 (MSK1)	45	51	48
DL07	Km app	RPS6KA6 (RSK4)	91	92	91
DL07	Km app	RPS6KB1 (p70S6K)	58	64	61
DL07	Km app	SGK (SGK1)	8	9	8
DL07	Km app	SGK2	26	33	29
DL07	Km app	SGKL (SGK3)	21	22	22
DL07	Km app	SNF1LK2	99	100	100
DL07	Km app	SRC	91	91	91
DL07	Km app	SRC N1	99	101	100
DL07	Km app	SRMS (Srm)	96	95	95
DL07	Km app	SRPK1	36	38	37
DL07	Km app	SRPK2	63	66	65
DL07	Km app	STK22B (TSSK2)	23	27	25
DL07	Km app	STK22D (TSSK1)	95	96	96

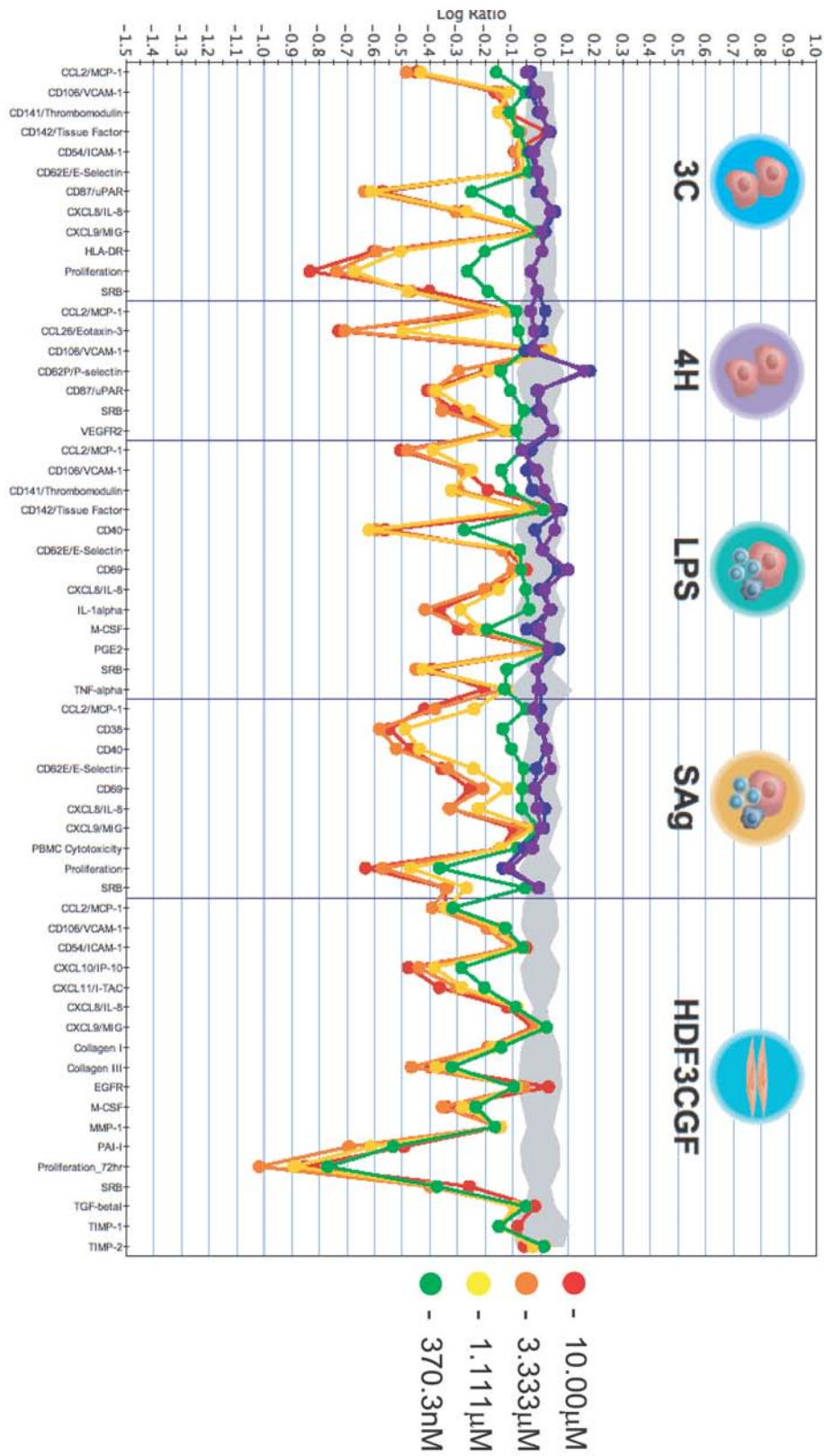
DL07	Km app	STK23 (MSSK1)	47	51	49
DL07	Km app	STK24 (MST3)	85	91	88
DL07	Km app	STK25 (YSK1)	91	94	92
DL07	Km app	STK3 (MST2)	94	94	94
DL07	Km app	STK4 (MST1)	97	99	98
DL07	Km app	SYK	66	68	67
DL07	Km app	TAOK2 (TAO1)	53	49	51
DL07	Km app	TBK1	15	15	15
DL07	Km app	TEK (Tie2)	89	88	89
DL07	Km app	TYK2	99	99	99
DL07	Km app	TYRO3 (RSE)	97	99	98
DL07	Km app	YES1	102	103	102
DL07	Km app	ZAP70	12	5	8

## BioMAP Profiles of PI3K Inhibitors.

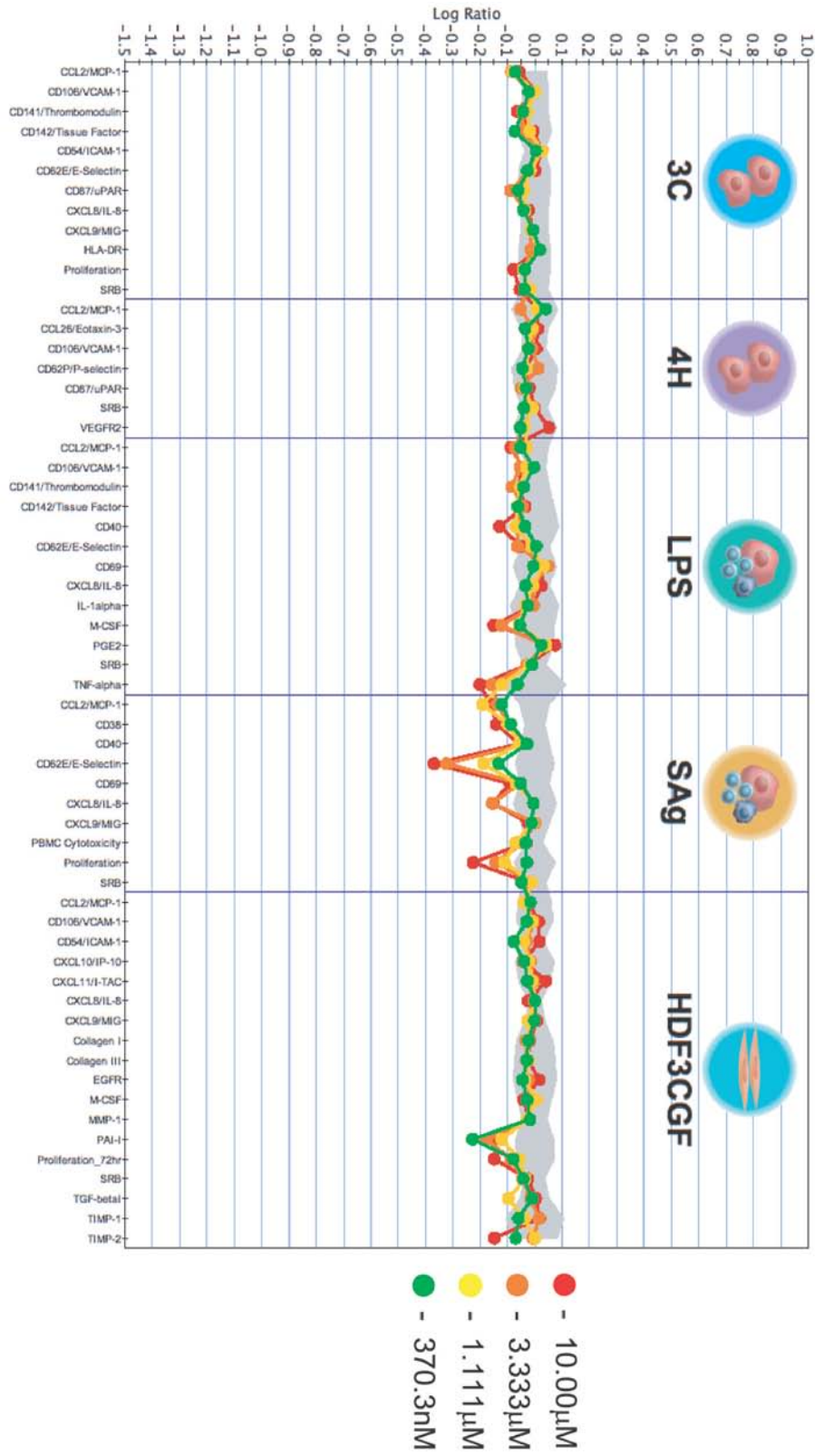




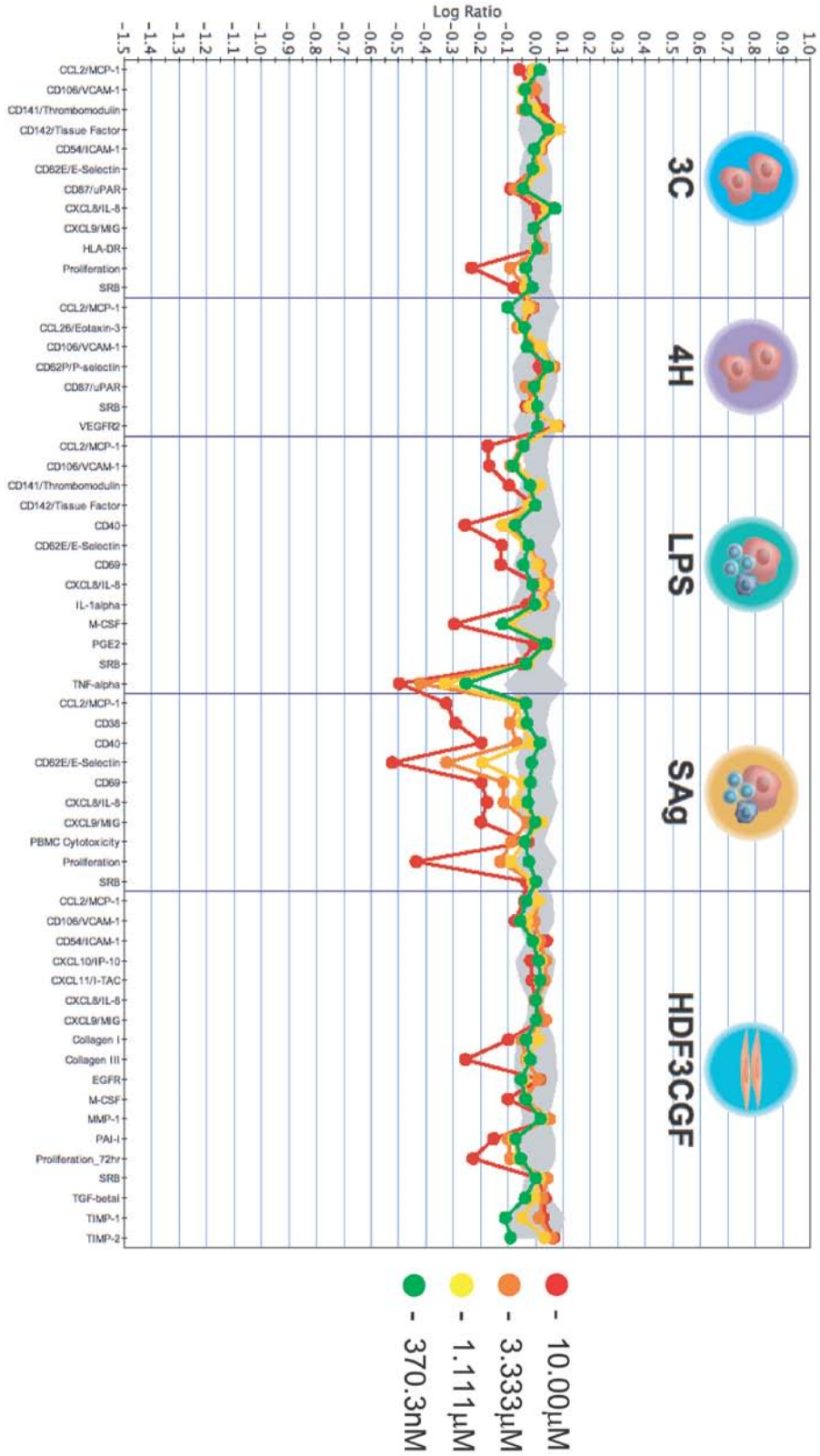
# PI-103 (pan-PI3-K + mTOR)



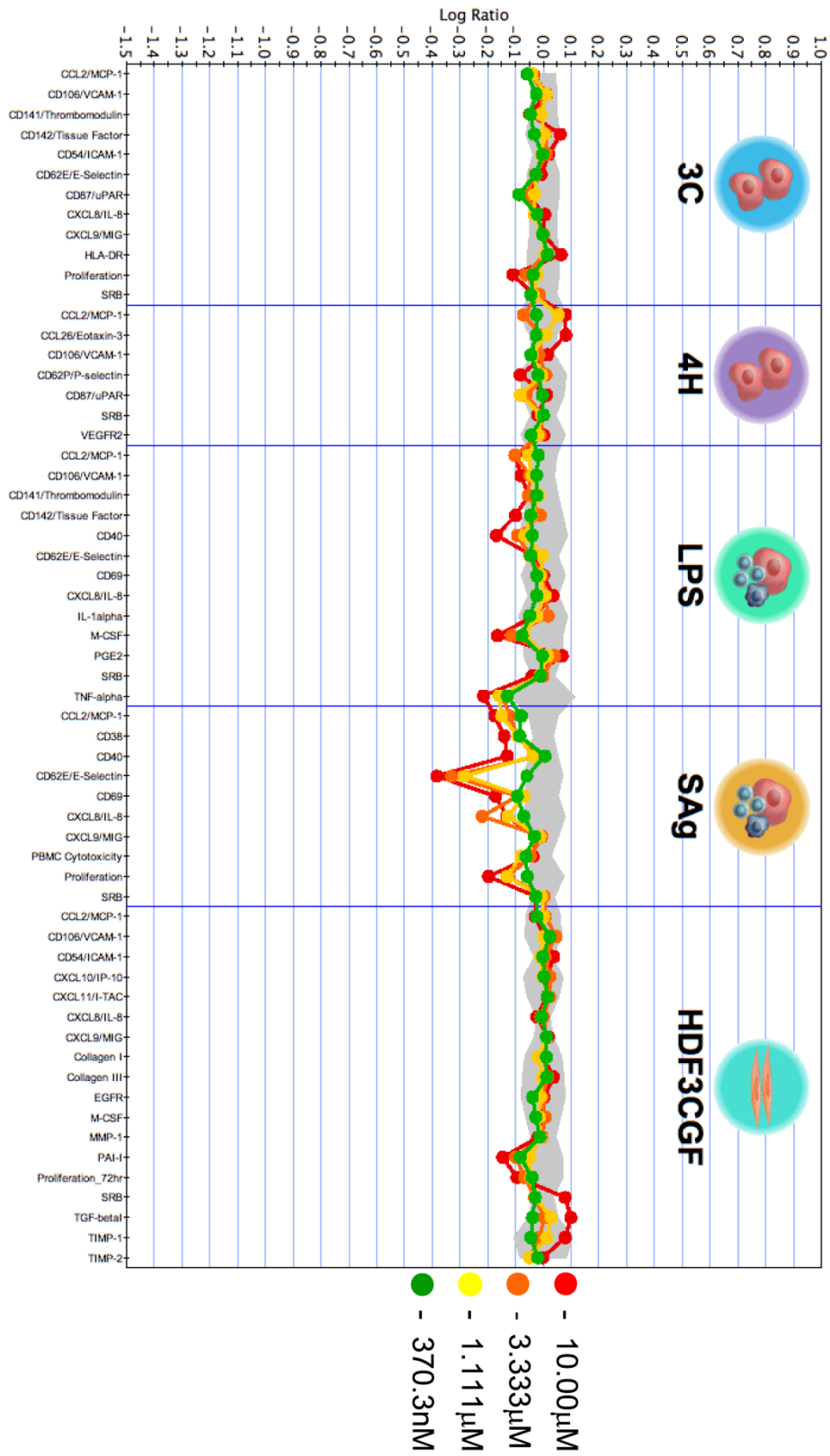
# IC87114 (P13-K8)



# SW19 (PI3-K $\delta/\gamma$ )



# SW24 (PI3-K $\delta$ )



## Synthetic Data and Characterization

### Detailed Syntheses:

Abbreviations:

DME (dimethoxyethane), EtOH (ethanol), EtOAc (ethyl acetate), MeCN acetonitrile), TFA (trifluoroacetic acid), THF (tetrahydrofuran)

### Detailed Syntheses:

#### General Procedures for the synthesis of Series 1

2-((4-amino-3-iodo-1H-pyrazolo[3,4-d]pyrimidin-1-yl)methyl)-5-methyl-3-o-tolylquinazolin-4(3H)-one (**SW3**) (60 mg, 0.115 mmol, 1 equiv), relevant boronic acid (2.0 equiv) and tetrakis(triphenylphosphine) palladium (28mg, 0.023 mmol, 0.2 equiv) were dissolved in a solution of DME (3.5 mL), EtOH (0.6 mL) and saturated aqueous Na<sub>2</sub>CO<sub>3</sub> (0.9 mL). The reaction was heated to reflux overnight under an argon atmosphere. The reaction was then poured into water, and the aqueous phase extracted three times with CH<sub>2</sub>Cl<sub>2</sub>. The organic extract was concentrated in vacuo and purified by RP-HPLC (MeCN:H<sub>2</sub>O:0.1% TFA).

#### General Procedure for the synthesis of Series 2

2-((4-amino-3-iodo-1H-pyrazolo[3,4-d]pyrimidin-1-yl)methyl)-5-methyl-3-o-tolylquinazolin-4(3H)-one (**SW3**) (60 mg, 0.115 mmol, 1 equiv), relevant terminal alkyne (4.0 equiv), tetrakis(triphenylphosphine) palladium (28mg, 0.023 mmol, 0.2 equiv), CuI (11mg, .575mmol, 0.5equiv), were dissolved in 4mL of THF. 162μL (1.15mmol, 10 equiv) of diisopropyl amine was then added. The reaction was stirred under an argon atmosphere at room temperature overnight. The THF was then removed in vacuo. The resultant solid was dissolved in CH<sub>2</sub>Cl<sub>2</sub>, and run through a silica plug. The relevant fractions were combined, concentrated in vacuo and further purified by RP-HPLC (MeCN:H<sub>2</sub>O:0.1% TFA).

**Synthesis of 2-(chloromethyl)-5-methyl-3-o-tolylquinazolin-4(3H)-one** was carried out as shown previously<sup>16</sup> with 23% yield. LR-ESI MS (M+H)<sup>+</sup> *m/z* calcd 299.1, found 298.8.

<sup>1</sup>H NMR (400 MHz, CDCl<sub>3</sub>):δ 7.670- 7.614(m, 2H), 7.455- 7.363(m,3H), 7.307-7.249 (m, 2H), 4.28 (d, *J* = 11.73 Hz, 1H), 4.11 (d, *J* = 11.73 Hz, 1H), 2.841 (s, 3H), 2.167 (s, 3H).

<sup>13</sup>C NMR (100 MHz, CDCl<sub>3</sub>):δ 161.845, 151.192, 148.672, 141.800, 136.198, 135.322, 133.853, 131.444, 130.531, 129.881, 128.712, 127.359, 125.906, 119.645, 43.406, 22.939, 17.780.

**Synthesis of 3-iodo-1H-pyrazolo[3,4-d]pyrimidin-4-amine** was carried out as shown previously<sup>16, 64</sup> with 100% yield LC-ESI-MS (M+H)<sup>+</sup> *m/z* calcd 262.0, found 262.0

**Synthesis of 2-((4-amino-1H-pyrazolo[3,4-d]pyrimidin-1-yl)methyl)-5-methyl-3-o-tolylquinazolin-4(3H)-one (PIK-293)** was carried out as shown previously<sup>16</sup>

LC-ESI-MS [MH]<sup>+</sup> *m/z* calculated for C<sub>22</sub>H<sub>20</sub>N<sub>7</sub>O, 398.17239; found, 398.17250.

#### Synthesis of Tolyl Quinazolinone Precursor SW3

2-(chloromethyl)-5-methyl-3-o-tolylquinazolin-4(3H)-one (3 g, 10.0 mmol) and 3-iodo-1H-pyrazolo[3,4-d]pyrimidin-4-amine (3.91 g, 15.05 mmol) were added to DMF (50 mL) and K<sub>2</sub>CO<sub>3</sub> (2.77 g, 20 mmol) and allowed to stir at RT in the dark for 24 hours. The product was precipitated by addition of water (900 mL) and collected by filtration. The precipitate, **SW3**, was further purified by silica gel chromatography (2% MeOH/CH<sub>2</sub>Cl<sub>2</sub>) to yield a brown solid (3.01g, 57% yield).

<sup>1</sup>H NMR (400 MHz, DMSO-*d*<sub>6</sub>):δ 8.157 (s, 1H), 7.65 (t, *J* = 7.78, 7.78 Hz, 2H), 7.350-7.266 (m, 7H), 5.21 (d, *J* = 16.45 Hz, 1H), 5.14 (d, *J* = 16.49 Hz, 1H), 2.720(s, 3H), 2.012 (s, 3H).

<sup>13</sup>C NMR (100 MHz, DMSO-*d*<sub>6</sub>):δ 160.868, 155.448, 153.076, 153.037, 150.207, 148.051, 140.509, 135.273, 134.778, 133.908, 130.814, 129.789, 129.168, 128.181, 127.326, 125.489, 118.903, 102.761, 91.135, 49.510, 22.445, 16.931.

LC-ESI-MS [MH]<sup>+</sup> *m/z* calculated for C<sub>22</sub>H<sub>19</sub>IN<sub>7</sub>O, 524.06904; found, 524.06900.

**Synthesis of SW4 (PIK 294) 2-[4-Amino-3-(3-hydroxy-phenyl)-pyrazolo[3,4-d]pyrimidin-1-ylmethyl]-5-methyl-3-o-tolyl-3H-quinazolin-4-one.**

**PIK294** (9.1 mg) was synthesized according to General Series 1 procedure in 16.2% yield.

<sup>1</sup>HNMR (400 MHz, DMSO-*d*<sub>6</sub>): δ 8.069 (s, 1H), 7.67 (t, *J* = 7.70, 7.70 Hz, 1H), 7.397-7.226 (m, 8H), 7.050-7.031 (m, 2H), 6.875-6.849 (m, 1H), 5.225 (s, 2H), 2.726 (s, 3H), 1.979 (s, 3H).

<sup>13</sup>C NMR (100 MHz, DMSO-*d*<sub>6</sub>): δ 161.697, 158.523, 156.971, 154.611, 154.276, 154.254, 151.286, 148.881, 145.756, 141.242, 135.588, 134.679, 134.002, 131.492, 131.103, 130.523, 129.820, 128.874, 127.956, 126.234, 119.646, 119.424, 116.810, 115.471, 97.576, 50.171, 23.175, 17.612.

LC-ESI-MS [MH]<sup>+</sup> m/z calculated for C<sub>28</sub>H<sub>24</sub>N<sub>7</sub>O<sub>2</sub>, 490.19860; found, 490.19860.

**Synthesis of SW10**

**SW10** (33.2 mg) was synthesized according to General Series 1 procedure in 54.3% yield

<sup>1</sup>HNMR (400 MHz, DMSO-*d*<sub>6</sub>): δ 8.16 (s, 1H), 7.66 (t, *J* = 7.79, 7.79 Hz, 1H), 7.40-7.26 (m, 7H), 7.16 (ddd, *J* = 23.73, 11.81, 5.06 Hz, 4H), 5.27 (d, *J* = 16.36 Hz, 1H), 5.20 (d, *J* = 16.33 Hz, 1H), 3.82 (s, 3H), 3.81 (s, 3H), 2.73 (s, 3H), 2.01 (s, 3H)

<sup>13</sup>C NMR (100 MHz, DMSO-*d*<sub>6</sub>): δ 161.010, 150.574, 149.524, 149.045, 148.198, 140.587, 136.130, 135.390, 134.961, 134.029, 133.115, 130.898, 130.092, 129.856, 129.217, 128.299, 127.382, 125.562, 124.228, 120.701, 119.065, 118.981, 117.105, 112.213, 111.439, 96.838, 55.549, 55.452, 22.557, 16.990.

LC-ESI-MS [MH]<sup>+</sup> m/z calculated for C<sub>30</sub>H<sub>28</sub>N<sub>7</sub>O<sub>3</sub>, 534.22481; found, 534.22490.

**Synthesis of SW11**

**SW11** (25 mg) was synthesized according to General Series 1 procedure in 38.6% yield.

<sup>1</sup>HNMR (400 MHz, DMSO-*d*<sub>6</sub>): δ 8.15 (s, 1H), 7.66 (dd, *J* = 16.20, 8.20 Hz, 3H), 7.46-7.23 (m, 9H), 7.203-7.103 (m, 5H), 5.28 (d, *J* = 16.26 Hz, 1H), 5.23 (d, *J* = 16.25 Hz, 1H), 2.73 (s, 3H), 1.99 (s, 3H).

<sup>13</sup>C NMR (100 MHz, DMSO-*d*<sub>6</sub>): δ 160.924, 157.341, 156.064, 155.871, 153.755, 152.827, 152.311, 152.265, 152.050, 150.456, 148.133, 144.708, 140.485, 135.759, 135.273, 134.860, 133.894, 130.763, 130.041, 129.948, 129.750, 129.074, 128.156, 127.909, 127.215, 126.902, 125.492, 123.776, 118.952, 96.809, 49.498, 22.430, 16.873.

LC-ESI-MS [MH]<sup>+</sup> m/z calculated for C<sub>34</sub>H<sub>28</sub>N<sub>7</sub>O<sub>2</sub>, 566.22990; found, 566.23000.

**Synthesis of SW13**

**SW13** (15.2 mg) was synthesized according to General Series 1 procedure in 26.3% yield.

<sup>1</sup>HNMR (400 MHz, DMSO-*d*<sub>6</sub>): δ 8.213 (s, 1H), 7.67 (t, *J* = 7.80, 7.80 Hz, 2H), 7.391-7.261 (m, 7H), 6.880-6.828 (m, 2H), 6.68 (td, *J* = 10.80, 2.00, 2.00 Hz, 1H), 5.29 (d, *J* = 16.29 Hz, 1H), 5.24 (d, *J* = 16.33 Hz, 1H), 2.724 (s, 3H), 1.989 (s, 3H).

<sup>13</sup>C NMR (100 MHz, DMSO-*d*<sub>6</sub>): δ 164.389, 161.972, 160.915, 159.493, 155.275, 153.543, 152.241, 150.325, 148.109, 144.445, 140.507, 135.281, 134.837, 133.929, 130.787, 129.799, 129.116, 128.195, 127.261, 125.507, 118.922, 111.336, 105.717, 105.486, 103.383, 103.144, 96.727, 49.588, 22.440, 16.882.

LC-ESI-MS [MH]<sup>+</sup> m/z calculated for C<sub>28</sub>H<sub>23</sub>FN<sub>7</sub>O<sub>2</sub>, 508.18918; found, 508.18920.

**Synthesis of SW14**

**SW14** (21.7mg) was synthesized according to General Series 1 procedure in 37.3% yield.

<sup>1</sup>HNMR (400 MHz, DMSO-*d*<sub>6</sub>): δ 8.205 (s, 1H), 7.67 (t, *J* = 7.79, 7.79 Hz, 2H), 7.394-7.260 (m, 9H), 7.10 (t, *J* = 8.68, 8.68 Hz, 1H), 5.28 (d, *J* = 16.34 Hz, 1H), 5.22 (d, *J* = 16.25 Hz, 1H), 2.726 (s, 3H), 1.992 (s, 3H).

<sup>13</sup>C NMR (100 MHz, DMSO-*d*<sub>6</sub>): δ 161.657, 155.950, 154.152, 152.965, 151.096, 150.558, 148.855, 146.569, 145.376, 141.234, 136.029, 135.590, 134.648, 131.530, 130.515, 129.826, 128.928, 127.983, 126.245, 125.464, 123.632, 119.668, 119.125, 119.088, 116.843, 116.644, 97.392, 50.280, 23.179, 17.620.

LC-ESI-MS [MH]<sup>+</sup> m/z calculated for C<sub>28</sub>H<sub>23</sub>FN<sub>7</sub>O<sub>2</sub>, 508.18918; found, 508.18920.

### Synthesis of SW15

**SW15** (24.7 mg) was synthesized according to General Series 1 procedure in 42.8% yield.

<sup>1</sup>HNMR (400 MHz, DMSO-*d*<sub>6</sub>): δ 8.17 (s, 1H), 7.70-7.54 (m, 6H), 7.395-7.260 (m, 6H), 7.10 (d, *J* = 8.42 Hz, 2H), 5.28 (d, *J* = 16.28 Hz, 1H), 5.23 (d, *J* = 16.39 Hz, 1H), 3.82 (s, 3H), 2.73 (s, 3H), 1.99 (s, 3H).

<sup>13</sup>CNMR (100 MHz, DMSO-*d*<sub>6</sub>): δ 161.712, 160.468, 157.197, 154.672, 151.322, 148.870, 145.520, 141.237, 135.997, 135.579, 134.678, 132.771, 132.168, 131.503, 130.515, 129.816, 129.494, 129.376, 128.855, 127.953, 126.217, 125.142, 119.632, 97.622, 55.915, 50.124, 46.464, 23.165, 17.590.

LC-ESI-MS [MH]<sup>+</sup> *m/z* calculated for C<sub>29</sub>H<sub>26</sub>N<sub>7</sub>O<sub>2</sub>, 504.21425; found, 504.21430.

### Synthesis of SW18

2-(chloromethyl)-5-methyl-3-*o*-tolylquinazolin-4(3H)-one (400mg, 1.34 mmol) and PP367<sup>16</sup> (from Z.A.K.) (672mg, 2 mmol) were added to DMF (10 mL) and K<sub>2</sub>CO<sub>3</sub> (369mg, 2.68 mmol) and allowed to stir at RT in the dark for 24 hours. The product was precipitated by addition of water (200 mL) and collected by filtration. The crude precipitate (300 mg), was deprotected with 90% formic acid, 10% conc. HCl, purified by silica gel chromatography (4% MeOH/CH<sub>2</sub>Cl<sub>2</sub>) to yield a beige solid which was further purified by RP-HPLC (MeCN:H<sub>2</sub>O:0.1% TFA) (100.4mg 14.8% yield).

<sup>1</sup>HNMR (400 MHz, DMSO-*d*<sub>6</sub>): δ 8.197 (s, 1H), 7.67 (t, *J* = 7.79, 7.79 Hz, 2H), 7.400-7.192 (m, 9H), 7.051-7.014 (m, 1H) 5.29 (d, *J* = 16.40 Hz, 1H), 5.24 (d, *J* = 16.39 Hz, 1H), 2.728 (s, 3H), 1.985 (s, 3H).

<sup>13</sup>CNMR (100 MHz, DMSO-*d*<sub>6</sub>): δ 161.661, 154.225, 151.135, 148.862, 146.207, 146.084, 145.464, 141.247, 136.010, 135.583, 134.675, 131.498, 130.541, 129.833, 129.078, 128.919, 127.988, 126.245, 120.062, 119.656, 118.140, 118.108, 117.727, 117.544, 97.418, 50.279, 23.180, 17.631.

LC-ESI-MS [MH]<sup>+</sup> *m/z* calculated for C<sub>28</sub>H<sub>23</sub>FN<sub>7</sub>O<sub>2</sub>, 508.18918; found, 508.18910.

### Synthesis of SW19

**SW19** (12.1 mg) was synthesized according to General Series 1 procedure in 41.3% yield.

<sup>1</sup>HNMR (400 MHz, DMSO-*d*<sub>6</sub>): δ 11.386 (s, 1H), 8.121 (s, 1H), 7.677-7.638 (m, 2H), 7.548-7.163 (m, 11H), 6.467 (m, 1H), 5.30 (d, *J* = 16.23 Hz, 1H), 5.22 (d, *J* = 16.25 Hz, 1H), 2.722 (s, 3H), 2.023 (s, 3H).

<sup>13</sup>CNMR (100 MHz, DMSO-*d*<sub>6</sub>): δ 161.722, 157.789, 155.492, 154.877, 151.584, 148.959, 144.887, 141.215, 136.956, 136.064, 135.706, 134.624, 131.618, 130.413, 129.918, 128.948, 127.944, 127.184, 126.802, 126.171, 124.510, 122.017, 120.354, 119.646, 113.111, 101.279, 98.800, 49.847, 23.184, 17.655.

LC-ESI-MS [MH]<sup>+</sup> *m/z* calculated for C<sub>30</sub>H<sub>25</sub>N<sub>8</sub>O, 513.2151; found, 513.2150.

### Synthesis of SW20

**SW20** (26.8 mg) was synthesized according to General Series 1 procedure in 45.6% yield.

<sup>13</sup>CNMR (100 MHz, DMSO-*d*<sub>6</sub>): δ 161.697, 156.502, 154.356, 153.193, 151.311, 148.911, 147.429, 141.231, 136.673, 136.047, 135.639, 134.648, 132.693, 131.495, 130.495, 129.820, 128.928, 128.901, 127.974, 127.657, 126.253, 125.178, 121.514, 119.660, 112.148, 101.918, 97.559, 50.221, 23.186, 17.649.

LC-ESI-MS [MH]<sup>+</sup> *m/z* calculated for C<sub>30</sub>H<sub>25</sub>N<sub>8</sub>O, 513.2151; found, 513.2151.

### Synthesis of SW23

**SW23** (22.6 mg) was synthesized according to General Series 1 procedure in 32.4% yield.

<sup>13</sup>CNMR (100 MHz, DMSO-*d*<sub>6</sub>): δ 161.664, 158.686, 158.031, 155.596, 151.221, 148.872, 142.537, 141.223, 136.071, 135.681, 134.619, 131.694, 131.572, 131.371, 131.039, 130.468, 129.893, 129.386, 129.097, 128.000, 126.245, 125.546, 125.275, 122.890, 119.661, 98.113, 50.309, 23.176, 17.597.

LC-ESI-MS [MH]<sup>+</sup> *m/z* calculated for C<sub>30</sub>H<sub>22</sub>F<sub>6</sub>N<sub>7</sub>O, 610.17830; found, 610.17845.

### Synthesis of SW24

**SW24** (41.2 mg) was synthesized according to General Series 2 procedure in 77.8% yield.

<sup>1</sup>HNMR (400 MHz, DMSO-*d*<sub>6</sub>): δ 8.07 (s, 1H), 7.65 (t, *J* = 7.79, 7.79 Hz, 1H), 7.37-7.22 (m, 6H), 5.15 (d, *J* = 16.39 Hz, 1H), 5.03 (d, *J* = 16.38 Hz, 1H), 2.73 (s, 3H), 2.03 (s, 3H), 1.68 (tt, *J* = 8.27, 8.27, 5.10, 5.10 Hz, 1H), 0.97-0.89 (m, 2H), 0.89-0.82 (m, 2H).

<sup>13</sup>CNMR (100 MHz, DMSO-*d*<sub>6</sub>): δ 160.862, 156.423, 154.839, 152.933, 150.327, 148.061, 140.465, 135.272, 134.801, 133.885, 133.146, 132.127, 130.893, 129.735, 129.245, 128.174, 127.269, 125.450, 118.873, 100.034, 99.530, 66.906, 49.191, 22.426, 16.856, 8.479, -0.112.

LC-ESI-MS [MH]<sup>+</sup> *m/z* calculated for C<sub>27</sub>H<sub>24</sub>N<sub>7</sub>O, 462.2042; found, 462.2042.

### Synthesis of SW25

**SW25** (25.6 mg) was synthesized according to General Series 2 procedure in 43.5% yield.

<sup>13</sup>CNMR (100 MHz, DMSO-*d*<sub>6</sub>): δ 161.641, 157.958, 155.813, 153.985, 151.065, 148.838, 141.256, 136.091, 135.587, 134.670, 132.711, 131.717, 130.792, 130.494, 130.069, 129.009, 128.101, 127.329, 126.251, 123.927, 123.413, 122.611, 118.946, 117.783, 100.838, 94.655, 80.594, 50.120, 23.203, 17.672.  
LC-ESI-MS [MH]<sup>+</sup> m/z calculated for C<sub>30</sub>H<sub>24</sub>N<sub>7</sub>O<sub>2</sub>, 514.1991; found, 514.1989.

### Synthesis of SW26

**SW26** (4.1 mg) was synthesized according to General Series 2 procedure in 6.98% yield.

<sup>1</sup>HNMR (400 MHz, DMSO-*d*<sub>6</sub>): δ 8.13 (s, 1H), 7.66 (t, *J* = 7.81, 7.81 Hz, 2H), 7.42-7.24 (m, 8H), 7.19-7.11 (m, 1H), 6.82-6.75 (m, 1H), 6.64-6.56 (m, 1H), 5.24 (d, *J* = 16.44 Hz, 1H), 5.10 (d, *J* = 16.54 Hz, 1H), 2.74 (s, 3H), 2.08 (s, 3H).

<sup>13</sup>CNMR (100 MHz, DMSO-*d*<sub>6</sub>): δ 161.645, 157.684, 156.061, 151.145, 150.626, 148.848, 141.245, 136.083, 135.601, 134.654, 133.192, 131.698, 131.350, 130.501, 130.030, 128.996, 128.064, 127.845, 126.215, 119.661, 116.979, 116.326, 115.331, 100.844, 92.461, 85.740, 50.046, 23.195, 17.680.  
LC-ESI-MS [MH]<sup>+</sup> m/z calculated for C<sub>30</sub>H<sub>25</sub>N<sub>8</sub>O, 513.2151; found, 513.2152.

### Synthesis of SW27

**SW27** (32.6 mg) was synthesized according to General Series 2 procedure in 57% yield.

<sup>1</sup>HNMR (400 MHz, DMSO-*d*<sub>6</sub>): δ 8.95 (s, 1H), 8.69-8.63 (m, 1H), 8.23-8.18 (m, 1H), 8.17 (s, 1H), 7.70-7.63 (m, 1H), 7.58-7.51 (m, 1H), 7.42-7.23 (m, 6H), 5.27 (d, *J* = 16.59 Hz, 1H), 5.13 (d, *J* = 16.43 Hz, 1H), 2.74 (s, 3H), 2.08 (s, 3H).

<sup>13</sup>CNMR (100 MHz, DMSO-*d*<sub>6</sub>): δ 161.620, 157.008, 155.628, 154.000, 152.419, 150.973, 149.764, 148.810, 141.254, 140.431, 136.081, 135.552, 134.666, 131.716, 130.538, 130.078, 128.989, 128.087, 126.840, 126.235, 124.319, 119.656, 119.305, 100.834, 91.119, 84.116, 50.216, 23.175, 17.653.  
LC-ESI-MS [MH]<sup>+</sup> m/z calculated for C<sub>29</sub>H<sub>23</sub>N<sub>8</sub>O, 499.1995; found, 499.1993.

### Synthesis of SW28

**SW28** (18.7 mg) was synthesized according to General Series 2 procedure in 32.7% yield.

<sup>1</sup>HNMR (400 MHz, DMSO-*d*<sub>6</sub>): δ 8.68-8.64 (m, 1H), 8.16 (s, 1H), 7.95-7.84 (m, 2H), 7.68-7.62 (m, 2H), 7.51-7.46 (m, 1H), 7.39-7.28 (m, 7H), 5.27 (d, *J* = 16.46 Hz, 1H), 5.13 (d, *J* = 16.48 Hz, 1H), 2.74 (s, 3H), 2.08 (s, 3H).

<sup>13</sup>CNMR (100 MHz, DMSO-*d*<sub>6</sub>): δ 161.631, 157.593, 156.457, 154.197, 151.046, 150.843, 148.831, 141.967, 141.239, 137.601, 136.075, 135.590, 134.657, 131.699, 130.513, 130.060, 129.009, 128.530, 128.091, 126.348, 126.241, 124.955, 119.655, 101.267, 93.799, 80.198, 50.191, 23.182, 17.657.  
LC-ESI-MS [MH]<sup>+</sup> m/z calculated for C<sub>29</sub>H<sub>23</sub>N<sub>8</sub>O, 499.1995; found, 499.1993.

### Synthesis of SW29

**SW29** (17.4 mg) was synthesized according to General Series 1 procedure in 28.9% yield.

<sup>1</sup>HNMR (400 MHz, DMSO-*d*<sub>6</sub>): δ 9.08-9.02 (m, 1H), 8.70-8.65 (m, 1H), 8.35-8.31 (m, 1H), 8.26-8.18 (m, 2H), 8.10-8.05 (m, 1H), 7.76-7.64 (m, 3H), 7.42-7.26 (m, 7H), 5.35 (d, *J* = 16.38 Hz, 1H), 5.30 (d, *J* = 16.33 Hz, 1H), 2.73 (s, 3H), 2.01 (s, 3H).

<sup>13</sup>CNMR (100 MHz, DMSO-*d*<sub>6</sub>): δ 161.675, 159.257, 158.908, 156.681, 154.716, 153.742, 151.170, 150.788, 148.879, 146.356, 145.167, 141.245, 139.396, 136.032, 135.603, 134.661, 131.552, 131.195, 130.957, 130.527, 129.843, 128.958, 128.859, 128.014, 126.264, 122.767, 119.683, 97.838, 50.392, 23.175, 17.657.

LC-ESI-MS [MH]<sup>+</sup> m/z calculated for C<sub>31</sub>H<sub>25</sub>N<sub>8</sub>O, 525.2151; found, 525.2151.



### Synthesis of SW30

**SW30** (5.4 mg) was synthesized according to General Series 2 procedure in 10.4% yield.

<sup>1</sup>HNMR (400 MHz, DMSO-*d*<sub>6</sub>): δ 8.06 (s, 1H), 7.65 (t, *J* = 7.78, 7.78 Hz, 1H), 7.41-7.22 (m, 6H), 5.43 (t, *J* = 6.03, 6.03 Hz, 1H), 5.18 (d, *J* = 16.40 Hz, 1H), 5.05 (d, *J* = 16.41 Hz, 1H), 4.37 (d, *J* = 6.02 Hz, 2H), 2.78-2.69 (m, 3H), 2.04 (s, 3H).

<sup>13</sup>CNMR (100 MHz, DMSO-*d*<sub>6</sub>): δ 160.879, 157.375, 156.317, 153.477, 150.436, 148.089, 140.440, 135.273, 134.843, 133.862, 130.882, 129.695, 129.244, 128.192, 127.254, 126.106, 125.446, 118.864, 100.262, 94.921, 75.235, 49.579, 49.132, 22.417, 16.856.

LC-ESI-MS [MH]<sup>+</sup> *m/z* calculated for C<sub>25</sub>H<sub>22</sub>N<sub>7</sub>O<sub>2</sub>, 452.1835; found, 452.1834.

### Synthesis of SW31

**SW31** (10 mg) was synthesized according to General Series 2 procedure in 18.8% yield.

<sup>1</sup>HNMR (400 MHz, DMSO-*d*<sub>6</sub>): δ 9.03 (s, 1H), 8.11 (s, 1H), 7.65 (t, *J* = 7.77, 7.77 Hz, 1H), 7.40-7.20 (m, 6H), 5.21 (d, *J* = 16.41 Hz, 1H), 5.08 (d, *J* = 16.41 Hz, 1H), 4.22 (s, 2H), 2.73 (s, 3H), 2.67 (s, 3H), 2.04 (s, 3H)

<sup>13</sup>CNMR (100 MHz, DMSO-*d*<sub>6</sub>): δ 161.607, 157.912, 157.134, 154.309, 151.090, 148.812, 141.254, 136.021, 135.565, 134.665, 131.665, 130.518, 130.053, 128.960, 128.048, 126.167, 125.603, 119.620, 101.205, 86.462, 79.001, 50.067, 38.750, 32.754, 23.173, 17.621.

LC-ESI-MS [MH]<sup>+</sup> *m/z* calculated for C<sub>26</sub>H<sub>25</sub>N<sub>8</sub>O, 465.2151; found, 465.2151.

### Synthesis of SW34

**SW34** (22.4 mg) was synthesized according to General Series 2 procedure in 43.4% yield.

<sup>1</sup>HNMR (400 MHz, DMSO-*d*<sub>6</sub>): δ 8.34 (s, 2H), 8.11 (s, 1H), 7.65 (t, *J* = 7.79, 7.79 Hz, 1H), 7.39-7.24 (m, 6H), 5.21 (d, *J* = 16.45 Hz, 1H), 5.06 (d, *J* = 16.42 Hz, 1H), 4.09 (s, 1H), 4.08 (s, 1H), 2.73 (s, 3H), 2.04 (s, 3H)

<sup>13</sup>C NMR (100 MHz, DMSO-*d*<sub>6</sub>): δ 160.661, 156.843, 156.010, 153.326, 150.141, 147.864, 140.298, 135.080, 134.621, 133.714, 130.736, 129.558, 129.130, 128.014, 127.099, 125.215, 124.918, 118.662, 100.159, 87.416, 76.732, 49.076, 29.155, 22.234, 16.67.

LC-ESI-MS [MH]<sup>+</sup> *m/z* calculated for C<sub>25</sub>H<sub>23</sub>N<sub>8</sub>O, 451.1995; found, 451.1994.

### Synthesis of SW35

**SW35** (14.4 mg) was synthesized according to General Series 2 procedure in 26.2% yield

<sup>13</sup>CNMR (100 MHz, DMSO-*d*<sub>6</sub>): δ 161.616, 157.901, 156.995, 154.266, 151.049, 148.803, 141.250, 136.020, 135.544, 134.667, 131.654, 130.671, 130.529, 130.019, 129.472, 128.941, 128.054, 126.191, 119.627, 85.040, 80.277, 50.143, 47.471, 42.605, 34.940, 23.175, 17.630.

LC-ESI-MS [MH]<sup>+</sup> *m/z* calculated for C<sub>27</sub>H<sub>27</sub>N<sub>8</sub>O, 479.2308; found, 479.2306.

### Synthesis of SW36

**SW36** (2 mg) was synthesized according to General Series 2 procedure in 3.75% yield.

<sup>1</sup>HNMR (400 MHz, DMSO-*d*<sub>6</sub>): δ 8.07 (s, 1H), 7.68-7.61 (m, 1H), 7.38-7.26 (m, 6H), 5.17 (d, *J* = 16.39 Hz, 1H), 5.04 (d, *J* = 16.48 Hz, 1H), 4.67 (dd, *J* = 13.19, 6.57 Hz, 1H), 2.73 (s, 3H), 2.04 (s, 3H), 1.40 (d, *J* = 6.62 Hz, 3H).

LC-ESI-MS [MH]<sup>+</sup> *m/z* calculated for C<sub>26</sub>H<sub>24</sub>N<sub>7</sub>O<sub>2</sub>, 466.1991; found, 466.1990.

### Synthesis of SW37

**SW37** (10.6 mg) was synthesized according to General Series 2 procedure in 19.9% yield.

<sup>1</sup>HNMR (400 MHz, DMSO-*d*<sub>6</sub>): δ 8.10 (s, 1H), 7.65 (t, *J* = 7.75, 7.75 Hz, 1H), 7.37-7.24 (m, 6H), 5.18 (d, *J* = 16.47 Hz, 1H), 5.04 (d, *J* = 16.41 Hz, 1H), 4.67 (dd, *J* = 13.10, 6.51 Hz, 1H), 2.73 (s, 3H), 2.05 (s, 3H), 1.41 (d, *J* = 6.55 Hz, 3H).

<sup>13</sup>CNMR (100 MHz, DMSO-*d*<sub>6</sub>): δ 161.627, 157.665, 156.420, 154.025, 151.109, 148.831, 141.219, 136.044, 135.583, 134.639, 131.677, 130.482, 130.041, 128.965, 128.050, 127.046, 126.218, 119.627, 99.041, 74.567, 57.458, 49.937, 46.396, 24.523, 23.185, 17.619.

LC-ESI-MS [MH]<sup>+</sup> *m/z* calculated for C<sub>26</sub>H<sub>24</sub>N<sub>7</sub>O<sub>2</sub>, 466.1991; found, 466.1991.

### Synthesis of SW38

**SW38** (11.4 mg) was synthesized according to General Series 2 procedure in 20.1% yield.

<sup>1</sup>HNMR (400 MHz, DMSO-*d*<sub>6</sub>): δ 8.10 (s, 1H), 7.64 (t, *J* = 7.79, 7.79 Hz, 1H), 7.37-7.26 (m, 6H), 5.18 (d, *J* = 16.47 Hz, 1H), 5.04 (d, *J* = 16.47 Hz, 1H), 4.04 (s, 2H), 2.73 (s, 3H), 2.05 (s, 3H).

<sup>13</sup>CNMR (100 MHz, DMSO-*d*<sub>6</sub>): δ 161.627, 159.364, 157.331, 156.014, 153.931, 151.086, 148.829, 141.197, 136.051, 135.588, 134.630, 131.677, 130.474, 130.057, 128.989, 128.063, 127.372, 126.244, 119.619, 101.276, 95.312, 73.313, 49.942, 30.759, 23.184, 17.625.

LC-ESI-MS [MH]<sup>+</sup> m/z calculated for C<sub>26</sub>H<sub>24</sub>N<sub>9</sub>O<sub>2</sub>, 494.2053; found, 494.2051.

### Synthesis of SW40

**SW40** (3.1 mg) was synthesized according to General Series 2 procedure in 5.81% yield.

<sup>1</sup>HNMR (400 MHz, DMSO-*d*<sub>6</sub>): δ 8.08 (s, 1H), 7.65 (t, *J* = 7.78, 7.78 Hz, 1H), 7.37-7.25 (m, 6H), 5.19 (d, *J* = 16.42 Hz, 1H), 5.08 (d, *J* = 16.46 Hz, 1H), 4.42 (s, 2H), 3.34 (s, 3H), 2.73 (s, 3H), 2.04 (s, 3H).

<sup>13</sup>CNMR (100 MHz, DMSO-*d*<sub>6</sub>): δ 160.868, 157.131, 156.073, 150.393, 148.085, 140.460, 135.275, 134.823, 133.920, 133.886, 130.873, 129.720, 129.233, 128.207, 127.286, 125.459, 118.875, 100.311, 93.881, 91.356, 76.996, 59.699, 57.163, 49.227, 22.432, 16.873.

LC-ESI-MS [MH]<sup>+</sup> m/z calculated for C<sub>26</sub>H<sub>24</sub>N<sub>7</sub>O<sub>2</sub>, 466.1991; found, 466.1991.

### Synthesis of SW41

**SW41** (15 mg) was synthesized according to General Series 2 procedure in 28.1% yield.

<sup>1</sup>HNMR (400 MHz, DMSO-*d*<sub>6</sub>): δ 8.11 (s, 1H), 7.65 (t, *J* = 7.78, 7.78 Hz, 1H), 7.41-7.22 (m, 6H), 5.18 (d, *J* = 16.45 Hz, 1H), 5.04 (d, *J* = 16.44 Hz, 1H), 3.65 (t, *J* = 6.16, 6.16 Hz, 2H), 2.73 (s, 3H), 2.67 (t, *J* = 6.13, 6.13 Hz, 2H), 2.05 (s, 3H).

<sup>13</sup>CNMR (100 MHz, DMSO-*d*<sub>6</sub>): δ 161.628, 157.234, 155.693, 155.665, 153.762, 151.105, 148.829, 141.214, 136.053, 135.589, 134.633, 131.677, 130.479, 130.041, 128.979, 128.054, 126.223, 119.623, 101.145, 96.402, 73.364, 59.901, 49.922, 23.987, 23.183, 17.622.

LC-ESI-MS [MH]<sup>+</sup> m/z calculated for C<sub>26</sub>H<sub>24</sub>N<sub>7</sub>O<sub>2</sub>, 466.1991; found, 466.1990.

### Synthesis of SW44

**SW44** (4.7 mg) was synthesized according to General Series 2 procedure in 8.37% yield.

<sup>13</sup>C NMR (100 MHz, DMSO-*d*<sub>6</sub>): δ 161.627, 157.733, 156.308, 153.915, 151.162, 148.831, 141.219, 136.032, 135.582, 134.637, 131.656, 130.473, 130.007, 128.945, 128.037, 127.763, 126.218, 119.633, 101.007, 100.833, 72.306, 49.867, 33.693, 30.784, 25.315, 23.186, 17.618.

LC-ESI-MS [MH]<sup>+</sup> m/z calculated for C<sub>29</sub>H<sub>28</sub>N<sub>7</sub>O, 490.2355; found, 490.2353.

### Synthesis of SW46

**SW46** (15.6 mg) was synthesized according to General Series 1 procedure in 27.7% yield.

<sup>1</sup>HNMR (400 MHz, DMSO-*d*<sub>6</sub>): δ 8.17 (s, 1H), 7.70-7.25 (m, 13H), 5.29 (d, *J* = 16.28 Hz, 1H), 5.23 (d, *J* = 16.39 Hz, 1H), 2.73 (s, 3H), 2.00 (s, 3H).

<sup>13</sup>CNMR (100 MHz, DMSO-*d*<sub>6</sub>): δ 164.267, 161.835, 161.681, 157.162, 154.883, 154.489, 151.231, 148.887, 144.437, 141.232, 136.024, 135.626, 134.636, 131.535, 130.489, 129.838, 128.942, 127.979, 126.250, 125.044, 119.677, 116.526, 116.318, 115.815, 115.590, 97.713, 50.232, 23.187, 17.622.

LC-ESI-MS [MH]<sup>+</sup> m/z calculated for C<sub>28</sub>H<sub>23</sub>FN<sub>7</sub>O, 492.1948; found, 492.1947.

### Synthesis of SW47

**SW47** (12.6 mg) was synthesized according to General Series 1 procedure in 22.4% yield.

<sup>1</sup>HNMR (400 MHz, DMSO-*d*<sub>6</sub>): δ 8.14 (s, 1H), 7.66 (t, *J* = 7.10, 7.10 Hz, 3H), 7.40-7.24 (m, 8H), 5.28 (d, *J* = 16.43 Hz, 1H), 5.22 (d, *J* = 16.39 Hz, 1H), 2.72 (s, 3H), 1.99 (s, 3H).

<sup>13</sup>CNMR (100 MHz, DMSO-*d*<sub>6</sub>): δ 164.383, 161.936, 161.673, 157.346, 154.856, 154.673, 151.297, 148.886, 144.648, 141.213, 135.996, 135.618, 134.620, 131.490, 131.113, 131.028, 130.464, 129.800, 129.379, 129.348, 128.901, 127.944, 126.230, 119.656, 116.888, 116.670, 97.697, 50.151, 23.175, 17.609.

LC-ESI-MS [MH]<sup>+</sup> m/z calculated for C<sub>28</sub>H<sub>23</sub>FN<sub>7</sub>O, 492.1948; found, 492.1946.

### Synthesis of SW49

**SW49** (17 mg) was synthesized according to General Series 1 procedure in 29.1% yield.

<sup>1</sup>HNMR (400 MHz, DMSO-*d*<sub>6</sub>): δ 8.20 (s, 1H), 7.74-7.52 (m, 6H), 7.52-7.24 (m, 7H), 5.29 (d, *J* = 16.50 Hz, 1H), 5.22 (d, *J* = 16.17 Hz, 1H), 2.72 (s, 3H), 2.00 (s, 3H)

<sup>13</sup>CNMR (100 MHz, DMSO-*d*<sub>6</sub>): δ 161.648, 156.466, 154.539, 153.658, 151.068, 148.843, 141.217, 136.012, 135.578, 134.630, 132.679, 131.540, 130.500, 129.842, 128.939, 127.967, 126.240, 119.660, 119.068, 118.894, 118.381, 118.201, 97.666, 50.280, 23.160, 17.600.

LC-ESI-MS [MH]<sup>+</sup> *m/z* calculated for C<sub>28</sub>H<sub>23</sub>F<sub>2</sub>N<sub>7</sub>O, 510.1854; found, 510.1852.

### Synthesis of SW50

**SW50** (24.1 mg) was synthesized according to General Series 1 procedure in 41.3% yield.

<sup>1</sup>HNMR (400 MHz, DMSO-*d*<sub>6</sub>): δ 8.23 (s, 1H), 7.70-7.52 (m, 4H), 7.42-7.25 (m, 9H), 5.31 (d, *J* = 16.40 Hz, 1H), 5.23 (d, *J* = 16.31 Hz, 1H), 2.73 (s, 3H), 2.01 (s, 3H).

<sup>13</sup>CNMR (100 MHz, DMSO-*d*<sub>6</sub>): δ 164.529, 162.206, 162.074, 161.638, 156.324, 154.581, 153.493, 150.986, 148.829, 141.218, 136.023, 135.685, 135.572, 134.621, 132.675, 131.563, 130.504, 129.855, 128.962, 127.985, 126.245, 119.666, 112.445, 112.179, 105.381, 105.121, 97.675, 50.352, 23.156, 17.592.

LC-ESI-MS [MH]<sup>+</sup> *m/z* calculated for C<sub>28</sub>H<sub>23</sub>F<sub>2</sub>N<sub>7</sub>O, 510.1854; found, 510.1853.

HPLC was conducted on a Varian Star with a Dynamax Solvent Delivery system with an Agilent Zorbax SB-C18 21.2 x 250mm 7μm column. The method used a gradient ranging from 5% MeCN (95% H<sub>2</sub>O) to 95% (5% H<sub>2</sub>O). The total TFA in all solvents was 0.1%.

LC-MS was conducted with a Waters2695 Separation Module and Waters micromass ZQ mass spectrometer on a Waters Xterra MS-C18 3.5μm 2.1x120mm IS column. The methods used a gradient ranging from 5% MeCN (95% H<sub>2</sub>O) to 95% (5% H<sub>2</sub>O). The total formic acid in all solvents was 0.1%.

### In vitro Kinase Assays.

IC<sub>50</sub>s were determined as previously described<sup>65</sup>. Purified kinase domains were incubated with inhibitors at two-fold dilutions over a concentration range of 100 μM to 0.006 μM or with vehicle (0.1% DMSO) in the presence of 10 μM ATP, 2.5 μCi of [γ-<sup>32</sup>P]ATP and substrate. Reactions were terminated by spotting onto nitrocellulose membranes; membrane was then washed four times to remove unbound radioactivity and dried. Transferred radioactivity was quantitated by phosphorimaging, and IC<sub>50</sub> values were calculated by fitting the data to a sigmoidal dose-response using Prism (GraphPad).

### THP-1 Cell Culture

THP-1 monocytes (ATCC) were grown in RPMI-1640 media with 10% Fetal Bovine Serum (FBS), 0.004% beta mercaptoethanol (BME), and under 5% CO<sub>2</sub> at 300,000-500,000 cells/mL.

### THP-1 Signaling Assays

THP-1 monocytes were grown in serum-free RPMI-1640 with 0.004% BME under 5% CO<sub>2</sub> at 1,000,000 cells/mL for 4 hours, incubated with inhibitors or DMSO for 10 minutes and stimulated with 100nM MCP-1 (R&D) for 5 minutes or 50ng/mL CSF-1 (Peprotec) for 7 minutes. Cells were fixed with paraformaldehyde; 1mL of cold methanol was added and cells were stored at -20°C overnight. 2mL of PBS was added, and cells were spun, resuspended in 1mL PBS with 5% FBS (FACS Buffer), and stored at 4°C. Buffer was aspirated, and 10μL of block solution was added. After 10 minutes, 30μL of Alexa conjugated antibody in FACS buffer (1/5 dilution) was added to cells. After 30 minutes, cells were resuspended in 2mL of PBS and spun. PBS was removed; cells were resuspended in 100μL of FACS buffer and read on the FACS.

**Cell Culture.** Human umbilical vein endothelial cells (HUVEC) were pooled from multiple donors, cultured according to standard methods, and plated into microtiter plates at passage 4. Peripheral blood mononuclear cells (PBMC) were prepared from buffy coats from normal human donors according to standard methods. Concentrations of agents added to confluent microtiter plates to build each system: cytokines (IL-1 $\beta$ , 1 ng/ml; TNF $\alpha$ , 5 ng/ml; IFN- $\gamma$ , 20 ng/ml; IL-4, 5 ng/ml), activators (SAg, 20 ng/ml; histamine, 10  $\mu$ M; or LPS, 2 ng/ml), and leukocytes (PBMC, 75,000 cells/well).

**Compounds.** Compounds were tested at the indicated concentrations. Compounds were added 1 hour before stimulation of the cells, and were present during the whole 24 hour stimulation period (or longer for proliferation assays).

**Readout Measurements.** The expression of many readouts was measured by cell-based ELISAs. For the ELISAs, microtiter plates are treated, blocked, and then incubated with primary antibodies or isotype control antibodies (0.01-0.5  $\mu$ g/ml) for 1 hr. After washing, plates were incubated with a peroxidase-conjugated anti-mouse IgG secondary antibody or a biotin-conjugated anti-mouse IgG antibody for 1 hr followed by streptavidin-HRP for 30 min. Plates were washed and developed with TMB substrate and the absorbance (OD) was read at 450 nm (subtracting the background absorbance at 650 nm). Quantitation of TNF- $\alpha$  and PGE2 was done using commercially available kits according to the manufacturer's directions. Proliferation of PBMCs (T cells) was quantified by Alamar blue reduction. Proliferation of adherent cell types was quantified by SRB staining.

#### **Proliferation and Toxicity Assessments.**

Proliferation of PBMC (T cells) was quantified by Alamar blue reduction. Proliferation of adherent cell types was quantified by SRB staining.

Adverse effects of compounds on cells were determined by 1) measuring alterations in total protein (SRB assay), and 2) measuring the viability of PBMCs (reduction of Alamar blue). SRB was performed by staining cells with 0.1% sulforhodamine B after fixation with 10% TCA, and reading wells at 560 nm. PBMC viability was assessed by adding 10% Alamar blue to PBMC that had been cultured for 16 hours in the presence of activators and measuring the amount of dye reduced over the next 8 h.

#### **Data analysis.**

The mean value (or single well OD value) for each parameter in a treated sample was divided by the mean value from an appropriate control to generate a ratio. All ratios were then log<sub>10</sub> transformed. 95% significance prediction envelopes (grey shading in Figs) were calculated for historical controls. Analysis of profile data to determine the significance of profile similarities (assessed by Pearson's correlation) and for generating function similarity maps (e.g. Fig 5) was performed as described previously<sup>101</sup>, applying an approach based on false discovery rate<sup>159</sup>.

This was done by 1) creating a set of null distributions of Pearson correlations using randomized data made from permuting the empirical profiles, 2) creating an empirical distribution of Pearson correlations by pairwise correlation of all the profiles selected for analysis, 3) selecting a Pearson correlation that minimizes the FDR (the FDR is the ratio of correlations called significant in the null distributions for a given Pearson correlation level, to those called significant for the same Pearson correlation in the empirical distribution), and 4) applying this cut-off Pearson correlation value to the correlations between experimental profiles. This ensures that for a 5% FDR, at the selected Pearson correlation threshold, 5% of the correlations deemed significant might have reached this level of significance by chance, allowing one to have high confidence that the selected connections represent true biological effects. Correlations were visualized in two dimensions by multidimensional scaling using AT&T GraphViz software (<http://www.research.att.com/sw/tools/graphviz/>). Distances between compounds are representative of their similarities and lines are drawn between compounds whose profiles are similar at a level not due to chance (as defined above).

**Publishing Agreement**

*It is the policy of the University to encourage the distribution of all theses and dissertations. Copies of all UCSF theses and dissertations will be routed to the library via the Graduate Division. The library will make all theses and dissertations accessible to the public and will preserve these to the best of their abilities, in perpetuity.*

***Please sign the following statement:***

*I hereby grant permission to the Graduate Division of the University of California, San Francisco to release copies of my thesis or dissertation to the Campus Library to provide access and preservation, in whole or in part, in perpetuity.*

  
\_\_\_\_\_  
Author Signature

01/28/2011  
Date